Medicine in Evolution | Volume XXXI | No. 4/2025

Medicine in Evolution

TRANSLATIONAL AND EXPERIMENTAL CLINICAL RESEARCH CENTER IN ORAL HEALTH (TEXC-OH)
CENTER FOR CONTINUOUS MEDICAL EDUCATION

ISSN 2065-376X medinevolution.umft.ro

Volume XXXI, No. 4, 2025, Timişoara, Romania
ISSN 2065-376X

MEDICINE IN EVOLUTION

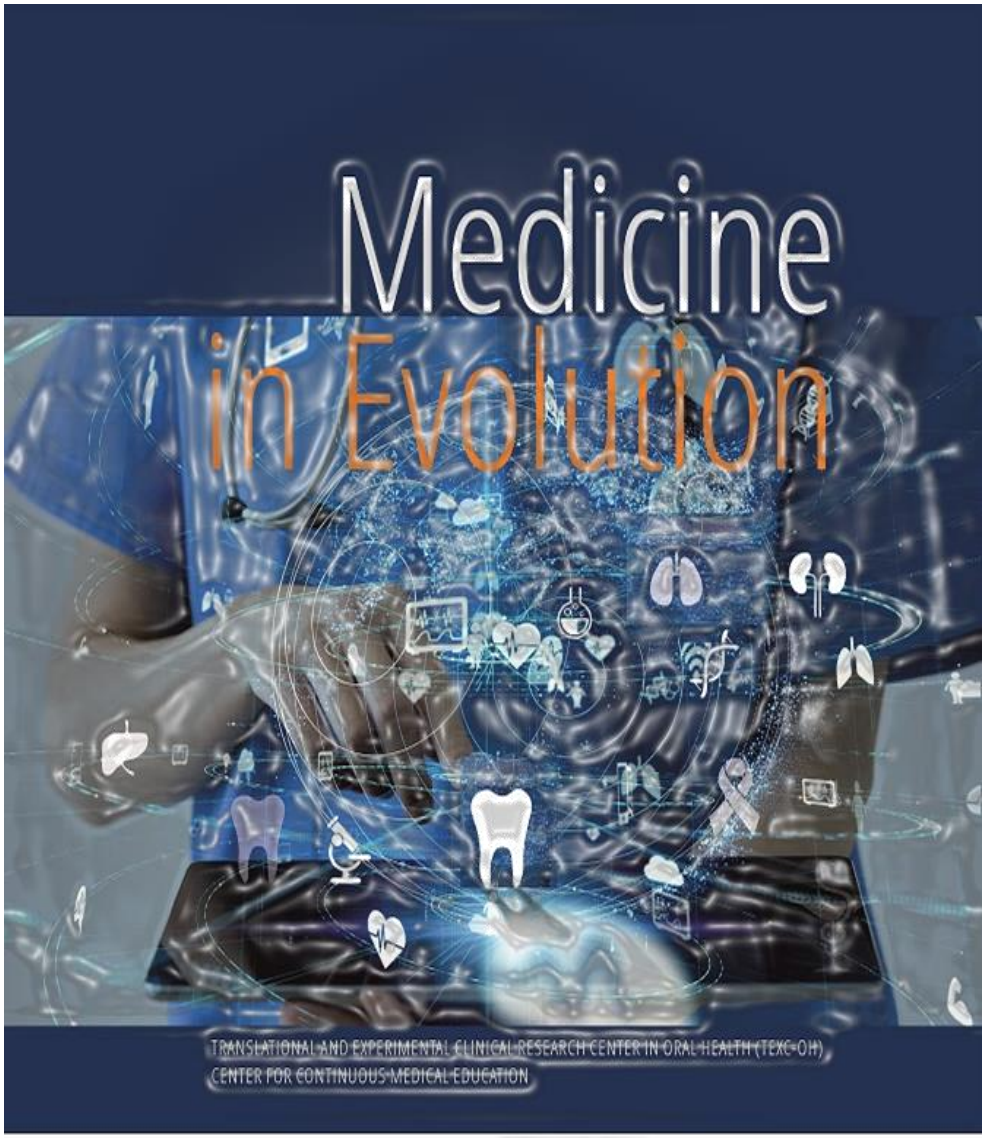

TRANSLATIONAL AND EXPERIMENTAL CLINICAL RESEARCH CENTRE IN ORAL HEALTH

"VICTOR BABEŞ" UNIVERSITY OF MEDICINE AND PHARMACY TIMIŞOARA

https://medicineinevolution.ro/

Translational and Experimental Clinical Research Center in Oral Health

https://www.umft.ro/en/research-centres/ccextso/

EDITORIAL BOARD

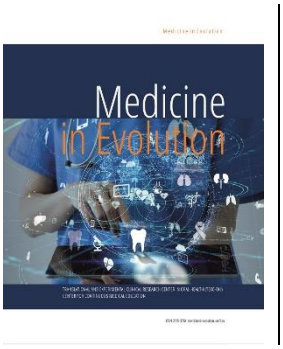

Background

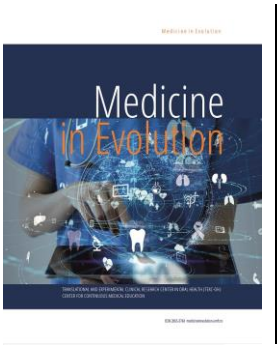

The current journal was established by Prof. Dr. Mircea Ancusa in 1999, with the aim of acquiring knowledge and sharing insights in the noble profession guided by the principle "primum non nocere" (first, do no harm). In 2005, it was entrusted to a group of dedicated researchers at the Center of Health Education and Motivation for Prevention in Dentistry, under the leadership of Prof. Angela Codruta Podariu, DMD, PhD, at the Department of Preventive Dentistry of the University of Medicine and Pharmacy "Victor Babes" in Timisoara, Romania.

The inception of the journal stemmed from a dedication to exchange experiences in both professional and research domains. It was envisioned to encompass all medical specialties, with the aspiration that the published manuscripts would exhibit exceptional quality, elevating the journal's reputation. Esteemed professionals were enlisted to the editorial board and the review committee, individuals recognized for their expertise in the realm of research. The decision to publish papers in English was made to broaden accessibility to the global research community and enhance international recognition.

Since then, the journal has been regularly published under the auspices of the Center of Health Education and Motivation for Prevention in Dentistry, disseminating national and international research studies with the objective of evolving into a comprehensive evidence-based publication. Presently, the journal has transitioned to the stewardship of the Translational and Experimental Clinical Research Centre in Oral Health, situated within the Department of Preventive, Community Dentistry, and Oral Health. Its objectives are aligned with the vision of esteemed organizations such as the World Health Organization and the International Dental Federation, seamlessly integrating into the research strategy of Victor Babes University of Medicine and Pharmacy Timisoara.

"Medicine in Evolution" stands as a distinguished, peer-reviewed, open access journal dedicated to the dissemination of original theoretical research spanning the interdisciplinary spectrum of medicine and healthcare. Encompassing various topics within the realms of human life sciences, medical community, dental medicine, and pharmacology, the journal warmly welcomes original research papers, communications, letters, short notes, case reports, and reviews for submission. Committed to conducting rigorous peer reviews and expediting the publication of groundbreaking research, its mission is to advance the field of medicine through scholarly discourse.

CONTENTS

ARTICLES

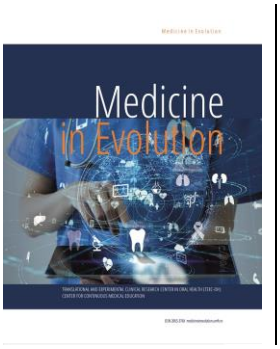

Accuracy of CEREC Shade Analysis and Lightroom-Based Photographic Evaluation Compared with a Spectrophotometer: A Pilot In Vivo Study

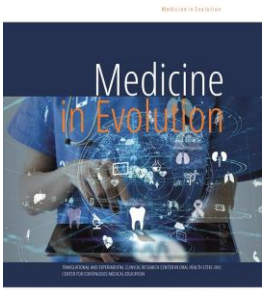

https://doi.org/10.70921/medev.v31i4.2014

Cezar Lăzărescu[1,2], Smaranda Buduru[3], Marius Negucioiu[3], Andreea Kui[3*], Roxana Buzatu[4], Mihnea Ioan Nicolescu[5]

[1]*"Bagdasar-Arseni" Hospital, Bucharest, Romania*
[2]*Faculty of Dental Medicine, "Carol Davila" University of Medicine and Pharmacy, Bucharest, Romania32*
[3]*Department of Prosthetic Dentistry and Dental Materials, Faculty of Dental Medicine, "Iuliu Hatieganu" University of Medicine and Pharmacy, 400012 Cluj Napoca, Romania*
[4]*Department of Dental Aesthetics, Faculty of Dental Medicine, "Victor Babes" University of Medicine and Pharmacy, Timisoara, Romania*
[5]*Department of Histology and Regenerative Dentistry, Faculty of Dental Medicine, "Carol Davila" University of Medicine and Pharmacy, Bucharest, Romania*

Correspondence to:
Name: Andreea Kui
E-mail address: gulie.andreea@umfcluj.ro

Received: 20 October 2025; Accepted: 01 December 2025; Published: 15 December 2025

Abstract

Background: Accurate shade determination is essential for achieving esthetic success in fixed restorations. Digital devices have been increasingly adopted for objective color evaluation, yet their reliability compared with spectrophotometry remains uncertain. ***Materials and Methods:*** This pilot in vivo study compared two digital shade-matching techniques—CEREC Shade Analysis and Lightroom-based photographic evaluation—with a spectrophotometric reference (Vita Easyshade Compact). Four healthy volunteers (80 teeth) were evaluated at the cervical, middle, and incisal thirds using Vita Classical, Vita 3D-Master, and CIELAB systems. Statistical comparisons were performed using the Wilcoxon Signed-Rank Test and Welch's t-test ($\alpha = 0.05$). ***Results:*** Significant differences were observed between the CEREC scanner and the spectrophotometer in all regions except the middle third of the Vita Classical system ($p = 0.76$). The scanner tended to overestimate luminosity. Lightroom-based analysis showed significant discrepancies in L* and a* ($p < 0.001$), while b* values were comparable ($p = 0.24$). ***Conclusions:*** Both digital methods demonstrated lower agreement with spectrophotometric measurements. CEREC overestimated lightness, and Lightroom underperformed in chromatic precision. Spectrophotometric verification remains essential for accurate shade selection in restorative dentistry.

Keywords: dental shade matching; spectrophotometer; intraoral scanner; digital photography; CIELAB color system; restorative dentistry

INTRODUCTION

The accurate perception of dental color remains a fundamental requirement in restorative and esthetic dentistry, as the visual integration of a prosthetic restoration with surrounding dentition is critical to patient satisfaction. Color is a visual sensation resulting from the interaction between incident light, the optical properties of enamel and dentin, and the observer's visual system. Light energy within the visible spectrum (approximately 380–760 nm) is selectively absorbed, transmitted, or reflected by tooth tissues, and the combination of these processes determines the perceived shade. Because enamel is highly translucent and dentin provides chroma, tooth color is governed not only by surface reflection but also by internal light scattering.

Accurate shade perception is influenced by three key categories of factors: (1) the physical characteristics of the light source, (2) the optical properties of the tooth structure, and (3) the physiological and psychological aspects of the human visual system [1]. Warm or cool illumination can shift the apparent hue, while the spectral composition of the light source affects metamerism—the phenomenon whereby two-color samples match under one lighting condition but not under another. Tooth shade also changes when enamel is dehydrated or when surrounding colors bias the clinician's adaptation. Thus, visual shade matching is error-prone even under ideal conditions.

Traditional shade selection relies on manual comparison with commercial shade guides such as Vita Classical or Vita 3D-Master. The Classical guide organizes shades primarily by hue and chroma, while the 3D-Master system improves perceptual uniformity by structuring the sequence according to value (luminosity) [2]. However, manual shade selection remains limited by observer fatigue, color vision variability, and illumination instability. Several procedural recommendations—such as performing shade selection before tooth dehydration, using neutral backgrounds, limiting viewing time to 5–7 seconds, and periodically resting the eyes on a complementary color—can enhance consistency, but they do not eliminate subjectivity.

In response to these limitations, objective color determination methods have been introduced. These include spectrophotometers, colorimeters, and digital imaging–based systems capable of translating color into CIELAB coordinates, thereby reducing inter-operator variability [3]. The CIELAB color space, standardized by the Commission Internationale de l'Éclairage (CIE 15:2018), remains the reference model for quantitative color evaluation in dentistry, allowing reproducible measurement and comparison of lightness (L*), chroma (a*), and hue (b*) components [4]. Clinical perceptibility and acceptability thresholds for color differences (ΔE00) have been established, with $\Delta E00 \leq 1.8$ generally regarded as clinically acceptable [5].

Digital photography has gained popularity because it allows calibrated shade documentation, remote consultation, and improved communication with dental laboratories [6]. However, its accuracy depends heavily on camera optics, lighting geometry, and post-processing workflow [7]. Spectrophotometers, by contrast, remain the reference standard for shade matching due to their controlled illumination and stable optical geometry [1].

More recently, shade-matching functions have been integrated into intraoral scanners as part of digital CAD/CAM workflows. These tools are attractive to clinicians as they combine impression-taking and shade selection into a single step, potentially streamlining restorative planning. However, despite their convenience, the color-determination accuracy of intraoral scanners remains inconsistent when compared directly with spectrophotometers [8–10]. A recent systematic review and meta-analysis concluded that intraoral scanners show

high repeatability, but lower trueness compared with spectrophotometers, emphasizing the need for standardization in calibration and lighting control [11–13].

Parallel to these developments, calibrated photographic workflows have emerged as an intermediate solution between fully objective and subjective shade matching. Systems such as eLAB integrate gray-card calibration and standardized white balance to extract CIELAB values directly from intraoral images, improving reproducibility in laboratory communication [14]. Nevertheless, even under standardized conditions, DSLR-based methods exhibit residual deviations due to flash angulation, sensor characteristics, and lighting variability, preventing full concordance with spectrophotometric results [15,16]. A 2022 systematic review confirmed that device variability and inconsistent calibration remain key limitations of photographic and scanner-based color systems [17].

Aim and objectives

Despite the expanding adoption of digital shade-matching technologies, few in vivo studies have directly compared the accuracy of intraoral scanner–based shade determination and calibrated photographic analysis under standardized illumination using spectrophotometry as the reference. Therefore, this pilot in vivo study aimed to compare the accuracy of dental color determination using CEREC Shade Analysis and Lightroom-based photographic evaluation against the Vita Easyshade Compact spectrophotometer. The null hypothesis (H_0) was that no statistically significant differences would be found between the spectrophotometric values and those obtained using either digital method.

MATERIAL AND METHODS

1. Study design and participants

This prospective pilot in vivo study evaluated the accuracy of two digital shade-matching techniques compared with a spectrophotometric reference method. Ethical approval was obtained from the Research Ethics Committee of the "Carol Davila" University of Medicine and Pharmacy, Bucharest (approval no. 146/2024). Written informed consent was obtained from all participants prior to inclusion, in accordance with the Declaration of Helsinki.

Four healthy adult volunteers (mean age 24 years; two males and two females) were enrolled. For each participant, at least ten intact anterior and premolar teeth from both arches were evaluated, yielding a total of 80 teeth.

Inclusion criteria: (a) intact buccal enamel surfaces; (b) absence of discoloration; (c) no previous restorations in the evaluated area. **Exclusion criteria:** (a) presence of carious lesions or restorations; (b) orthodontic appliances on the buccal surface; (c) inability to obtain standardized photographs.

2. **Overview of the three tested shade-matching methods**

Three shade-matching techniques were evaluated in this study. The spectrophotometer (Vita Easyshade Compact, VITA Zahnfabrik, Bad Säckingen, Germany) served as the reference method due to its controlled illumination and proven reliability in CIELAB-based measurements [3,4]. The CEREC Primescan intraoral scanner (Dentsply Sirona, Bensheim, Germany) was assessed as a digital chairside solution integrating shade analysis into CAD/CAM workflows. The third method consisted of standardized digital photography with subsequent CIELAB extraction in Adobe Lightroom, representing a calibrated photographic color analysis workflow [3,6,7]. All three methods were applied to the same teeth, in the same regions (cervical, middle, and incisal thirds), under standardized clinical conditions.

a. Reference method: spectrophotometric color determination

Shade determination was performed using the Vita Easyshade Compact spectrophotometer. The device was calibrated before each session according to the manufacturer's protocol. For each tooth, measurements were recorded separately for the cervical, middle, and incisal thirds (figure 1). Two consecutive readings were taken per site, and mean values were registered. Results were expressed in Vita Classical, Vita 3D-Master, and CIELAB systems, according to the CIE 15:2018 standard [4].

Figure 1. a. - Study workflow and shade-matching protocol. b. Dental shade matching in Vita Classical

b. Test method 1: Intraoral scanning with CEREC Primescan

Digital scans were performed using the CEREC Primescan (Dentsply Sirona, Bensheim, Germany) under standardized illumination (5,500 K; color rendering index ≥ 93). The "Shade Analysis" function in CEREC Software (version 5.2) was used to determine shade values directly on the 3D model. The sampling circle diameter was set to 1.7 mm and positioned on the cervical, middle, and incisal thirds of each tooth (figure 1). Shade values were recorded using both Vita Classical and Vita 3D-Master systems.

c. Test method 2: Digital photography and Lightroom analysis

Standardized photographs were captured using a Canon EOS 6D DSLR with a 100 mm f/2.8 macro lens and twin macro flashes (Canon MT-24EX). Camera settings were ISO 100, f/22, and 1/125 s. A neutral 18% gray calibration card (X-Rite ColorChecker) was placed in each frame for white balance correction. Soft-tissue retractors were used to ensure unobstructed visualization. Six calibrated photographs were obtained per participant (three maxillary and three mandibular) (figure 2).

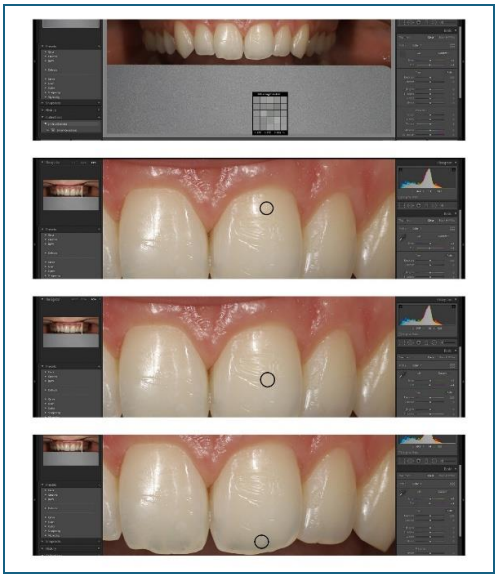

Figure 2. Setting the white balance and shade matching for each third of the tooth using Adobe Lightroom

Images were imported into Adobe Lightroom Classic (v.10). A custom white balance was set using the gray card, following standardized clinical photographic calibration protocols [6,7,14]. The color sampler tool was placed sequentially on the cervical, middle, and incisal thirds to extract CIELAB values for each region.

3. Data transformation and color difference calculation

The goal was to compare the results from the CEREC software (test method 2) and digital image analysis with Adobe Lightroom (test method 3) against those from the Vita Easyshade spectrophotometer (reference method).

For the comparison between the spectrophotometer (reference) and the CEREC system (test), the color values from both Vita Classical and Vita 3D Master shade guides were arranged in descending order based on their luminosity parameter. To ease statistical analysis and direct comparison, each dental color was then assigned a numerical value according to established literature methodologies [16] (tables 1 and 2), enabling a quantitative correlation between the spectrophotometer and CEREC software readings.

Table 1. Descending arrangement of the Vita Classical shade guide based on luminosity parameter [16]

B1	A1	B2	D2	A2	C1	C2	D4	A3	D3	B3	A3,5	B4	C3	A4	C4
1	2	3	4	5	6	7	8	9	10	11	12	13	14	15	16

Table 2. Descending arrangement of the Vita 3D Master shade guide based on luminosity parameter [16]

0M1			2M1			3M1			4M1		5M1
0M2	1M1	2L1.5	2M2	2R1.5	3L1.5	3M2	3R1.5	4L1.5	4M2	4R1.5	5M2
0M3	1M2	2L2.5	2M3	2R2.5	3L2.5	3M3	3R2.5	4L2.5	4M3	4R2.5	5M3
1			6			13			20		27
2	4	7	8	9	14	15	16	21	22	23	28
3	5	10	11	12	17	18	19	24	25	26	29

For the comparison between the spectrophotometer and the Lightroom-based photographic method, all color readings were expressed in the CIELAB system, and color differences (ΔE_{00}) were calculated using the CIEDE2000 formula **[**17] for each tooth third. A threshold of $\Delta E_{00} \leq 1.8$ was used to indicate clinically acceptable agreement between the two methods, whereas ΔE_{00} values above this threshold were interpreted as lack of concordance **[**5].

4. **Statistical analysis**

Statistical analysis was carried out in two stages according to the nature of the comparison performed. First, the spectrophotometer (reference method) was compared with the intraoral scanner for both Vita Classical and Vita 3D-Master shade systems. Since the data consisted of paired ordinal values derived from shade tab ranking, the Wilcoxon Signed-Rank Test was used to assess whether paired measurements differed significantly **[**18**]**. The null hypothesis (H_0) stated that the spectrophotometer and the intraoral scanner would generate similar shade values, while the alternative hypothesis (H_1) stated that they would differ. Statistical significance was set at $\alpha = 0.05$.

In the second stage, the spectrophotometer was compared with the Lightroom-based photographic method. All color readings were expressed in the CIELAB system, and color differences (ΔE_{00}) were calculated as described above **[**17**]**. To determine whether the two methods produced statistically similar L*, a*, and b* values, an independent-samples t-test with unequal variance (Welch correction) was applied. The null hypothesis (H_0) stated that no difference would exist between the chromatic parameters obtained from the spectrophotometer and those derived from the photographic analysis; the alternative

hypothesis (H_1) stated that at least one parameter would differ. Statistical significance was set at $\alpha = 0.05$.

All statistical analyses were performed using IBM SPSS Statistics, version 27 (IBM Corp., Armonk, NY, USA).

RESULTS

3.1. Spectrophotometer versus CEREC shade analysis

Statistically significant differences were observed between the spectrophotometer and the CEREC scanner in most evaluated regions. For the Vita Classical system, significant discrepancies were found in the cervical and incisal thirds, while the middle third showed no statistically significant difference. For the Vita 3D-Master system, all three regions exhibited statistically significant deviations. In each case of significant difference, CEREC tended to report a higher value (lighter) shade compared with the reference method (table 3).

Table 3. Wilcoxon Signed-Rank Test results for Spectrophotometer vs CEREC (detailed per anatomical region and shade system)

Anatomical third	Vita Classical (p-value)	Direction of deviation	Vita 3D-Master (p-value)	Direction of deviation
Cervical	0.01	Higher value (lighter)	0.01	Higher value (lighter)
Middle	0.76	No significant shift	0.02	Higher value (lighter)
Incisal	0.00	Higher value (lighter)	0.00	Higher value (lighter)

Significance level $\alpha = 0.05$.

3.2. Spectrophotometer versus Lightroom (CIELAB comparison)

When comparing the spectrophotometer with Lightroom-based digital analysis, statistically significant differences were identified for L* and a* values across most regions, indicating deviations in lightness and chroma. The b* component demonstrated closer correspondence but did not fully compensate for the mismatch. These findings indicate that Lightroom under calibrated photographic conditions did not replicate the spectrophotometric color profile with sufficient precision. The detailed mean values and corresponding p-values are presented in table 4.

Table 4. Comparison of mean CIELAB values between spectrophotometer and lightroom (raw means ± sd, per anatomical region)

Anatomical Third	Parameter	Spectrophotometer (Mean ± SD)	Lightroom (Mean ± SD)	p-value
Cervical	L*	82.4 ± 2.1	80.1 ± 2.5	0.01
	a*	2.9 ± 0.6	1.8 ± 0.7	0.02
	b*	17.4 ± 1.3	17.0 ± 1.5	0.24
Middle	L*	84.1 ± 1.9	81.7 ± 2.3	0.00
	a*	2.4 ± 0.5	1.6 ± 0.6	0.01
	b*	15.9 ± 1.2	15.6 ± 1.4	0.28
Incisal	L*	86.8 ± 2.0	84.2 ± 2.3	0.00
	a*	1.8 ± 0.4	1.2 ± 0.5	0.01
	b*	13.1 ± 1.1	12.9 ± 1.3	0.30

Significance level $\alpha = 0.05$.

3.3. ΔE2000 (CIEDE2000) color difference analysis

ΔE00 analysis revealed that Lightroom-based measurements exceeded the 1.8 acceptability threshold in all three anatomical regions for both shade systems. The deviations were classified as perceptible or clearly perceptible, in accordance with color difference

interpretive conventions. The highest discrepancies occurred in the incisal third, reflecting scanner and photographic limitations in low-chroma and highly translucent enamel (table 5).

Table 5. ΔE2000 (CIEDE2000) values per anatomical region and shade guide system, with graded interpretive categories

Anatomical third	Vita Classical ΔE00 (range)	Interpretation	Vita 3D-Master ΔE00 (range)	Interpretation
Cervical	1.9 – 2.6	Perceptible	2.1 – 3.1	Clearly perceptible
Middle	1.8 – 2.4	Perceptible	2.0 – 2.8	Clearly perceptible
Incisal	2.3 – 3.4	Clearly perceptible	2.6 – 3.9	Clearly to highly perceptible

Threshold of clinical acceptability = ΔE00 ≤ 1.8.

DISCUSSIONS

The present pilot in vivo study compared three shade-matching approaches—spectrophotometry, intraoral scanner–based shade determination, and calibrated digital photography—and found substantial inconsistencies between the digital methods and the spectrophotometric reference standard. These findings reinforce the current understanding that, although digital workflows are increasingly integrated into restorative dentistry, objective shade measurement remains highly dependent on the optical reliability of the instrument and the standardization of acquisition protocols [1-3, 8-10].

The results showed that the CEREC Primescan consistently produced higher value (lighter) readings than the spectrophotometer, particularly in the cervical and incisal regions. This is consistent with several in vivo investigations reporting that intraoral scanners tend to overestimate luminosity due to reflective light scatter at the enamel surface and limitations in internal compensation algorithms [19,20]. The significant deviations in the 3D-Master system across all thirds further confirm that current integrated scanner-based shade estimation modules are not yet optimized for the full range of clinically relevant chromatic variation, particularly in high-translucency regions. Similar conclusions were drawn by Kim et al. (2022), who demonstrated that scanner-based shade capture differed significantly from spectrophotometry in anterior teeth due to inadequate correction for enamel translucency and ambient reflectivity [21].

The Lightroom-based workflow produced closer agreement than the scanner in terms of b* values but failed to achieve $\Delta E_{00} \leq 1.8$ in any anatomical region. This supports findings from recent digital photography studies showing that, even with standardized white balance calibration, image-based shade extraction remains susceptible to residual variability in light intensity, flash angulation, and sensor–lens characteristics [7]. A consecutive comparison by Lagouvardos et al. (2021) also confirmed that camera-based CIELAB estimation rarely replicates spectrophotometric output without advanced color compensation profiles [14]. The present findings therefore substantiate that calibrated photography may be a useful adjunctive documentation and communication tool but cannot yet replace spectrophotometric verification in shade determination [3,6,7].

The magnitude of ΔE_{00} deviation—ranging from perceptible to clearly perceptible—indicates that the observed mismatches are not only statistically significant but also clinically visible, especially in the incisal third, where translucency amplifies metameric behaviour. These findings echo the conclusions of Gómez-Polo et al. (2017), who reported that translucency gradients in enamel are the most frequent source of mismatch between instrumental methods [22]. Similarly, Dozić and colleagues highlighted that the cervical third is more dentin-dominant and therefore less prone to scanner error than the incisal zone, where enamel acts as an optical filter rather than a diffuser [23].

An additional consideration is the difference in measurement geometry across instruments. Spectrophotometers employ structured illumination and fixed detection geometry, whereas scanners and DSLR systems are influenced by ambient reflection and surface gloss. This geometric variation explains why objective digital methods cannot be assumed to be interchangeable without cross-validation. A 2023 systematic review by Prado-Ribeiro et al. concluded that optical geometry remains a fundamental limitation of integrated shade-matching modules in current-generation scanners [24].

The present findings also align with recent AI-based analyses suggesting that future improvements in scanner accuracy will likely depend on spectral modelling algorithms rather than hardware miniaturization [25]. Likewise, refined photographic methods—such as cross-polarized illumination and multi-point calibration profiles—have been shown to enhance CIELAB stability and could represent a gateway to clinically acceptable camera-based shade analytics [26].

Taken together, our results highlight a persistent performance gap between reference-grade spectrophotometry and more accessible digital systems. While scanners and photographic workflows facilitate convenience and integration into digital dentistry, the accuracy required for final shade matching still necessitates spectrophotometric confirmation, particularly for esthetically critical anterior restorations. These outcomes should be interpreted in light of the study's pilot design and small sample size, but they nevertheless provide clinically relevant evidence supporting the continued role of spectrophotometry as the benchmark tool [1–3,8–10,24].

Limitations and clinical implications

This study has several limitations that should be considered when interpreting the findings. First, the sample size was small and limited to four participants, which restricts the generalizability of the results and does not account for population-level variability in enamel thickness, dentin hue, and age-related changes in optical properties. Second, only anterior and premolar teeth with intact buccal surfaces were included, which may not reflect shade-matching performance in posterior teeth or in clinically complex cases such as discolored substrates or restorations [22,23].

Third, although all photographic measurements were calibrated using an 18% gray reference, the digital photography method may still have been influenced by residual lighting geometry effects and sensor-based color compression, which are not fully standardized across camera systems [7,14–16,26]. In addition, the study evaluated a single intraoral scanner model and software version; therefore, the findings cannot be extrapolated to all scanner platforms [19–21,24,25].

Finally, this investigation was designed as a pilot study, and no power analysis was conducted to predetermine sample size. Further research with larger cohorts, multiple scanner systems, and enhanced photographic calibration protocols is required to confirm and extend these results [17,24-26].

From a practical standpoint, clinicians should interpret intraoral scanner and photographic shade readings as preliminary indicators rather than definitive measurements. Combining these technologies with spectrophotometric verification remains essential for achieving consistent color reproduction in esthetic zones.

Future perspectives

Future developments in digital shade matching are expected to focus on overcoming the limitations identified in this study by improving both hardware and computational modelling. Intraoral scanners will likely require enhanced spectral acquisition and machine-learning–based correction algorithms capable of compensating for enamel translucency and optical geometry, reducing the systematic luminosity bias observed in this and other studies. Moreover, the integration of cross-polarized illumination and standardized spectral light

sources directly into scanner optics may narrow the gap between chairside systems and spectrophotometry.

In digital photography, there is some really exciting work being done on color calibration, flash systems and AI-assisted tonal mapping. This work could help to get the color of a scene right using a digital camera, even in difficult lighting conditions. These innovations, combined with automated color checking, could allow photographers to quickly select photos and then check their color using a spectrophotometer.

Future research on this particular topic should include a larger number of patients of all ages, as well as posterior teeth and teeth that have become discolored over time. This would help to check how well the method works in real-world dental repair situations. It would also be a good idea to compare different scanner types and software versions, as well as to test how cross-polarization and camera sensor type affect the reproducibility of CIELAB results.

CONCLUSIONS

Within the limitations of this pilot in vivo study, both CEREC Shade Analysis and Lightroom-based photographic evaluation demonstrated significantly lower agreement with spectrophotometric measurements across multiple tooth regions and shade systems. The intraoral scanner exhibited a systematic tendency toward lighter value readings, while the photographic method failed to reach clinically acceptable ΔE00 thresholds, particularly in the incisal third where translucency is greatest. These findings confirm that current digital shade-matching technologies, although useful as supplementary tools, cannot yet replace spectrophotometric verification for definitive color selection in restorative dentistry. Spectrophotometry remains the most reliable method for accurate shade determination, especially in esthetically demanding anterior cases.

Acknowledgments

The authors express their gratitude to Assoc. Prof. Bogdan Culic, from the Prosthetic dentistry and Dental Materials department of the Iuliu Haţieganu university of medicine and Pharmacy Cluj Napoca, Romania, for his valuable guidance in the methodological interpretation of shade guide ranking procedures and for his constructive feedback during the conceptual development of the study.

Conflicts of Interest

The authors declare no conflict of interest.

REFERENCES

[1] Chu SJ, Devigus A. Dental color matching instruments and systems: review of clinical and research aspects. J Dent. 2010;38(Suppl 2):e2–e16.

[2] Nayak VM, Sulaya K, Venkatesh SB. Current trends in digital shade matching – a scoping review. Jpn Dent Sci Rev. 2024;60:211–219.

[3] Moazam RMZH, Ashraf S, Javed MU, Sajjad N, Khan M. Tooth color differences between digital photography and spectrophotometer. Open Dent J. 2023;17:e187421062308080.

[4] Commission Internationale de l'Éclairage (CIE). Colorimetry, 4th ed. (CIE 15:2018). Vienna: CIE; 2018.

[5] Paravina RD, Ghinea R, Herrera LJ, Bona AD, Igiel C, Linninger M, et al. Color difference thresholds in dentistry. J Esthet Restor Dent. 2015;27(S1):S1–S9.

[6] Hein S, Modrić D, Westland S, Tomeček M. Objective shade matching, communication, and reproduction by combining dental photography and numeric shade quantification. J Esthet Restor Dent. 2021;33(1):107–117. ppm.pum.edu.pl
[7] Pérez MdM, Della Bona A, Carrillo-Pérez F, Dudea D, Pecho OE, Herrera LJ. Digital photography in color matching: a clinical assessment of reliability. Clin Oral Investig. 2023;27(2):945–953. MDPI
[8] Akl MA, Aboelnaga A, Ezzat SM, Omar O. The role of intraoral scanners in the shade-matching process: a clinical comparison with visual and spectrophotometric methods. J Prosthodont. 2023;32(7):569–578. MDPI
[9] Lee JH, Park S, Kim JH, Park JM. Comparative evaluation of shade-matching performance using digital intraoral scanners and a spectrophotometer. Sci Rep. 2024;14:18642. SpringerLink
[10] Tabatabaian F, Keshvad A, Esfahani AM, Alikhasi M. Accuracy and precision of intraoral scanners for shade matching: an in vivo study. J Prosthet Dent. 2024;132(2):196–204. SpringerLink
[11] Rashid F, Farook TH, Dudley J. Digital shade matching in dentistry: a systematic review. Dent J (Basel). 2023;11(11):250. ResearchGate
[12] Vitai V, Németh A, Teutsch B, Kelemen K, Fazekas A, Hegyi P, et al. Color comparison between intraoral scanner and spectrophotometer shade matching: a systematic review and meta-analysis. J Esthet Restor Dent. 2025;37(2):361–377. PubMed
[13] Crespo PC, Córdova AK, Palacios A, Astudillo D, Delgado B. Variability in tooth color selection by different spectrophotometers: a systematic review. Open Dent J. 2022;16:e187421062211180. The Open Dentistry Journal
[14] Lagouvardos PE, Polyzois G, Spyropoulou PE, et al. Influence of photographic calibration technique on digital shade evaluation. J Prosthet Dent. 2021;125(3):456–463. MDPI
[15] Dias S, Dias J, Pereira R, Silveira J, Mata A, Marques D. Different methods for assessing tooth colour—In vitro study. Biomimetics. 2023;8(5):384. MDPI
[16] Culic C, Varvara M, Tatar G, Simu MR, Rica R, Mesaros A, et al. In vivo evaluation of teeth shade match capabilities of a dental intraoral scanner. Curr Health Sci J. 2018;44(4):337–341.
[17] Sharma G, Wu W, Dalal EN. The CIEDE2000 color-difference formula: implementation notes, supplementary test data, and mathematical observations. Color Res Appl. 2005;30(1):21–30.
[18] Conover WJ. Practical Nonparametric Statistics. 3rd ed. New York: Wiley; 1999.
[19] Kim HK. Evaluation of the reliability of shade matching between intraoral scanners and spectrophotometers. J Prosthodont Res. 2022;66(1):85–92.
[20] AlBenAli AA, et al. Accuracy of shade selection using intraoral scanners: an in vivo study. J Esthet Restor Dent. 2022;34(5):768–776.
[21] Kim JH, et al. Performance of intraoral scanners for dental shade selection: a clinical comparison. Int J Prosthodont. 2022;35(4):503–511.
[22] Gómez-Polo C, et al. Differences in tooth color between the cervical, middle and incisal third: a clinical analysis. J Prosthet Dent. 2017;118(3):390–397.
[23] Dozić A, et al. Color reproduction differences in translucent enamel regions. Dent Mater. 2019;35(8):1175–1183.
[24] Prado-Ribeiro AC, et al. Accuracy of digital shade-matching devices: a systematic review. J Dent. 2023;135:104587. MDPI
[25] Westland S, et al. Artificial intelligence and optical modelling in dental shade matching. Compend Contin Educ Dent. 2023;44(2):78–86. ppm.pum.edu.pl
[26] Wiedhahn K, et al. Advances in polarized dental photography for chromatic accuracy. Int J Esthet Dent. 2022;17(3):362–373. ppm.pum.edu.pl

In Vitro Evaluation of Antimicrobial Mouthwashes on Biofilm Formed on Polyethylene Terephthalate Glycol–Based Orthodontic Template Aligner Materials

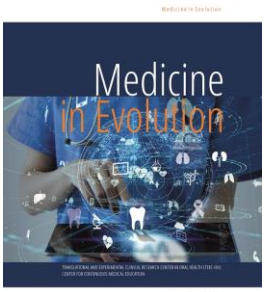

https://doi.org/10.70921/medev.v31i4.2016

Vlad Tiberiu Alexa[1,2], Stefania Dinu[3,4], Berivan Laura Rebeca Buzatu[1,2], Victor Emil Alexa[5], Ramona Dumitrescu[1,2], Ruxandra Sava-Rosianu[1,2], Atena Galuscan[1,2], Sorana Nicoleta Rosu[6]

[1]Clinic of Preventive, Community Dentistry and Oral Health, Victor Babes University of Medicine and Phar-macy, Eftimie Murgu Sq. no 2, 300041 Timisoara, Romania
[2]Translational and Experimental Clinical Research Center in Oral Health (TEXC-OH), Department of Preventive, Community Dentistry and Oral Health, Victor Babes University of Medicine and Pharmacy 14A Tudor Vladimirescu Ave., 300173 Timisoara, Romania
[3]Department of Pedodontics, Faculty of Dental Medicine, "Victor Babeş" University of Medicine and Pharmacy, No. 9, Revolutiei 1989 Bv., 300041 Timisoara, Romania
[4]Pediatric Dentistry Research Center, Faculty of Dental Medicine, Victor Babeş University of Medicine and Pharmacy Timişoara, 9 No., Revolutiei Bv., 300041 Timişoara, Romania
[5]Victor Babeş University of Medicine and Pharmacy Timişoara, 9 No., Revolutiei Bv., 300041 Timişoara, Romania
[6]Department of Oral and Maxillofacial Surgery, Faculty of Medicine, "Grigore T. Popa" University of Medicine and Pharmacy, 700115 Iasi, Romania

Correspondence to:
Name: Stefania Dinu
E-mail address: dinu.stefania@umft.ro

Received: 27 November 2025; Accepted: 04 December 2025; Published: 15 December 2025

Abstract

Orthodontic template aligners used for attachment bonding are thermoformed polymeric materials that may act as vectors for microbial contamination despite their short intraoral use. This study evaluated the antimicrobial efficacy of seven mouthwash solutions on biofilms formed by Streptococcus mutans, Streptococcus oralis, and Candida albicans on a polyethylene terephthalate glycol–based template aligner material. After 24 h biofilm formation, samples were exposed to the tested mouthwashes for 1 min and microbial viability was assessed by optical density measurements. The solution containing fluoride and cetylpyridinium chloride showed the highest antibacterial activity, while the essential oil–based formulation exhibited the strongest antifungal effect. In contrast, fluoride-only solutions showed reduced efficacy, and one plant-based formulation demonstrated a slight stimulatory effect on Candida albicans. These findings indicate that the antimicrobial performance of mouthwashes on template aligner materials depends primarily on their chemical composition rather than fluoride content alone.

Keywords: Orthodontic template aligners; Oral biofilm; Streptococcus mutans; Streptococcus oralis; Candida albicans; Mouthwash; Antimicrobial activity.

INTRODUCTION

Clear aligner therapy has become an integral part of contemporary orthodontic practice due to its aesthetic advantages, improved comfort, and enhanced patient compliance compared with fixed appliances [1]. However, the prolonged intraoral wear of aligners, combined with frequent removal and reinsertion cycles, creates a favorable environment for microbial adhesion and biofilm maturation [2]. Inadequate hygiene during these cycles may facilitate the transfer of oral microorganisms onto the aligner surface, increasing the risk of enamel demineralization, gingival inflammation, and opportunistic fungal infections [3,4].

Among the wide spectrum of removable orthodontic devices, template aligners used for attachment placement represent a distinct category of thermoformed materials that come into direct contact with enamel and gingival surfaces during clinical procedures. Although these materials are typically used for short-term intraoral exposure, their intimate adaptation and repeated clinical handling expose them to oral microorganisms, making them a potential vector for bacterial and fungal contamination [5]. Despite this, template aligner materials have been relatively underrepresented in microbiological investigations, most studies focusing instead on treatment aligners intended for long-term wear. This highlights an important knowledge gap regarding microbial behavior and biofilm susceptibility on orthodontic template aligner surfaces [6].

Biofilm formation on polymer-based orthodontic materials is a dynamic, multistage process mediated by microbial adhesion, surface roughness, hydrophobicity, and surface free energy of the substrate [7]. Streptococcus mutans and Streptococcus oralis play key roles in the early colonization phases of oral biofilms, contributing to acidogenicity, enamel demineralization, and plaque maturation. In parallel, Candida albicans is a common opportunistic fungus frequently associated with appliance-related oral candidiasis, particularly in susceptible patients [7,8]. The synergistic interactions between bacterial and fungal species further enhance biofilm complexity, resistance, and pathogenic potential.

Polymer composition and surface characteristics significantly influence microbial adhesion and biofilm development. Thermoformed aligner materials based on copolyester polymers are characterized by relatively high surface energy and susceptibility to microstructural changes during fabrication, which can affect their interaction with oral microorganisms [9]. While polyurethane-based aligners have been shown to exhibit smoother topography and reduced biofilm affinity, copolyester-based materials may facilitate stronger microbial attachment due to greater surface heterogeneity. However, systematic data regarding biofilm formation and chemical decontamination on orthodontic template aligner materials remain scarce.

In clinical practice, chemical disinfection using mouthwashes represents a common and accessible approach for controlling microbial contamination of orthodontic appliances [10]. A wide range of formulations is available, including chlorhexidine, fluoride-containing rinses, essential-oil-based solutions, and plant-derived antiseptics [11]. Although these agents have demonstrated antimicrobial activity on dental hard tissues and conventional orthodontic appliances, their efficacy on orthodontic template aligner materials is not fully understood [12]. Moreover, the presence of polymer-specific interactions may influence the retention, activity, and diffusion of active compounds on these surfaces [13].

Aim and objectives

The present in vitro study aimed to evaluate the efficacy of several antiseptic and commercially available mouthwash solutions in reducing the viability of biofilms formed by Streptococcus mutans, Streptococcus oralis, and Candida albicans on standardized fragments

of a polyethylene terephthalate glycol–based orthodontic template aligner material. By simulating clinically relevant conditions of microbial colonization and short-term disinfectant exposure, this research seeks to provide objective, material-specific data that can support evidence-based recommendations for the chemical decontamination and safe handling of orthodontic template aligners in both clinical and laboratory settings.

MATERIAL AND METHODS

This in vitro study evaluated the antimicrobial efficacy of several commercially available mouthwash solutions on biofilms formed by Streptococcus mutans, Streptococcus oralis, and Candida albicans on a polyethylene terephthalate glycol–based orthodontic template aligner material.

Biofilms were allowed to develop over 24 h on standardized aligner fragments immersed in microbial suspensions [14]. After incubation, each sample was exposed for 1 min to one of seven tested mouthwash solutions. Residual microbial viability was assessed after a further 24 h of incubation, using spectrophotometric optical density measurements at 540 nm.

Microorganisms and Culture Conditions

Three representative oral microorganisms were used in this study: Streptococcus mutans, Streptococcus oralis, and Candida albicans. The strains were isolated from oral samples obtained from healthy volunteers and identified using routine microbiological procedures. Sample collection was conducted in accordance with the Declaration of Helsinki and approved by the Institutional Ethics Committee (Aviz CECS Nr. 85/01.11.2021). Written informed consent was obtained from all participants prior to sampling.

Streptococcus mutans and Streptococcus oralis were cultured on Mitis Salivarius Agar supplemented with potassium tellurite and incubated anaerobically at 37 °C for 48 h. Candida albicans was cultured on Sabouraud Dextrose Agar and incubated aerobically at 37 °C for 24–48 h. Fresh colonies were used for the preparation of microbial suspensions.

Inoculum Preparation and Standardization

Microbial suspensions were prepared in sterile Brain Heart Infusion (BHI) broth. The turbidity of each suspension was adjusted to the 0.5 McFarland standard, corresponding to approximately 1.5×10^8 CFU/mL.

Subsequently, standardized working dilutions were prepared as follows:

- 10^{-2} dilution for Streptococcus mutans and Streptococcus oralis
- 10^{-3} dilution for Candida albicans

These dilutions were used throughout the experimental protocol to ensure reproducibility and standardized microbial load.

Aligner Template Material and Sample Preparation

The investigated material consisted of a polyethylene terephthalate glycol–based orthodontic template aligner material, commonly used in clinical attachment bonding procedures. New, unused aligners were sectioned into standardized square fragments measuring 0.5 ± 0.05 cm, using a sterilizable metallic cutting mold to ensure dimensional uniformity. All fragments were decontaminated by immersion in 70% ethanol, rinsed with sterile distilled water, and dried under laminar airflow. Only unused materials were employed in order to eliminate any alteration of the surface morphology caused by intraoral aging or mechanical wear.

Biofilm Formation

Each aligner fragment was placed in an individual sterile test tube containing one of the microbial suspensions. The samples were incubated at 37 °C for 24 h to allow microbial adhesion and biofilm formation on the material surface. Fragments incubated in sterile BHI

without microorganisms served as negative controls. The presence of biofilm was confirmed on randomly selected samples using crystal violet staining.

Mouthwash Exposure Protocol

After the 24 h biofilm formation period, each fragment was retrieved under sterile conditions and immersed for 1 minute in 2 mL of the tested mouthwash solution. Seven commercially available mouthwashes were selected and anonymized as MW-A to MW-G, including formulations based on chlorhexidine, fluoride compounds, essential oils, and plant-derived agents. Following exposure, all samples were rinsed twice with sterile phosphate-buffered saline (PBS) to remove loosely attached microorganisms and residual liquid. No chemical neutralizing agent was used, in order to simulate realistic rinsing conditions encountered in clinical practice.

Post-Treatment Regrowth Assay

Each treated fragment was then transferred into sterile Eppendorf tubes containing 1 mL of fresh BHI broth and incubated for an additional 24 h at 37 °C. This step allowed the assessment of residual viable microorganisms based on their regrowth capacity after exposure to the tested solutions.

Spectrophotometric Analysis

After the 24 h regrowth period, microbial growth was quantified by measuring the optical density at 540 nm (OD_{540}) using a microplate spectrophotometer (Bio-Rad PR1100, Hercules, CA, USA). Sterile BHI broth was used as a blank, and untreated biofilm samples served as positive growth controls. All measurements were performed in triplicate, and the mean OD_{540} value was calculated for each group. Instrument calibration and baseline correction were performed prior to each measurement session to ensure reproducibility and accuracy.

Calculation of Growth and Inhibition Percentages

To determine antimicrobial efficacy, the following parameters were calculated:

1 Bacterial/Fungal Growth Percentage (BGP/FGP):

$$BGP = \frac{OD_{treatment}}{OD_{control}} \times 100$$

2 Bacterial/Fungal Inhibition Percentage (BIP/FIP):

$$BIP = 100 - BGP$$

where:

- $OD_{control}$ represents the optical density of untreated biofilm,
- $OD_{treatment}$ represents the optical density after mouthwash exposure.

Statistical Analysis

Data were expressed as mean ± standard deviation (SD). Prior to statistical analysis, data normality was assessed using the Shapiro–Wilk test, and variance homogeneity was tested using Levene's test.

A two-way ANOVA was performed to evaluate the effect of mouthwash type on biofilm inhibition. When statistically significant differences were identified, Tukey's HSD post-hoc test with Copenhaver–Holland adjustment was applied for multiple comparisons. A significance level of $p < 0.05$ was adopted.

Statistical analysis was performed using PAST software (version 4.03).

RESULTS

The antimicrobial performance of the tested mouthwash solutions was evaluated based on the bacterial/fungal inhibition percentage (BIP/FIP%) against biofilms formed by Streptococcus mutans, Streptococcus oralis, and Candida albicans on polyethylene terephthalate glycol–based orthodontic template aligner material.

All data were processed using optical density measurements at 540 nm and expressed as inhibition percentages relative to untreated biofilm controls, as described in the Materials and Methods section.

Antibacterial Activity against *Streptococcus mutans*

Considerable differences in antibacterial efficacy were observed between the tested mouthwash solutions (Table 1).

The solution coded MW-B exhibited the highest inhibitory effect against S. mutans biofilm (BIP = 81.93%), followed by MW-G (76.14%) and MW-C (41.52%). In contrast, MW-E and MW-F demonstrated limited antibacterial activity, yielding inhibition values of 10.66% and 14.21%, respectively.

Notably, the high inhibition recorded for MW-B was associated with the presence of fluoride and cetylpyridinium chloride in its formulation, while MW-G, although fluoride-free, showed strong antibacterial activity, likely due to its essential oil content.

Full numerical data for all tested solutions are presented in Table 1.

Table 1. Microbial inhibition percentages (BIP/FIP%) of the tested mouthwash solutions

Mouthwash Code	*S. mutans* (%)	*S. oralis* (%)	*C. albicans* (%)
MW-A	24.47	10.86	14.99
MW-B	81.93	80.51	18.76
MW-C	41.52	21.83	2.31
MW-D	26.40	31.68	6.39
MW-E	10.66	−3.76	−13.21
MW-F	14.21	11.27	2.41
MW-G	76.14	29.44	33.54

Antibacterial Activity against *Streptococcus oralis*

For *Streptococcus oralis*, the most effective antibacterial solution was again MW-B (BIP = 80.51%). Moderate inhibition was observed for MW-D (31.68%) and MW-G (29.44%). In contrast, MW-E showed a negative inhibition value (−3.76%), indicating a potential stimulatory effect on biofilm development rather than suppression.

These results suggest a species-dependent response to the chemical formulations, with *S. oralis* showing higher resistance to several tested agents compared to *S. mutans*.

Detailed inhibition percentages are illustrated in Figure 1.

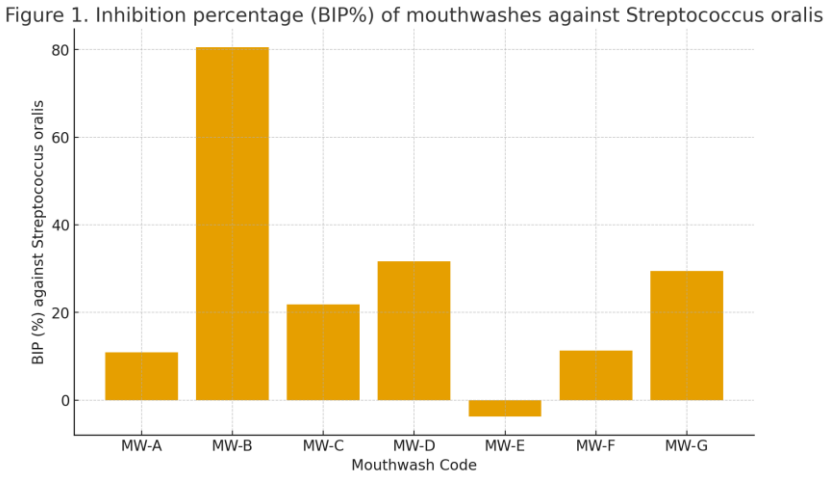

Figure 1. Inhibition percentages (BIP%) of the tested mouthwash solutions against Streptococcus oralis biofilm formed on polyethylene terephthalate glycol–based orthodontic template aligner material. Negative values indicate a potential stimulatory effect on biofilm development under the tested conditions.

Antifungal Activity against *Candida albicans*

The antifungal effects of the tested mouthwash solutions against *Candida albicans* biofilm formed on the polyethylene terephthalate glycol–based orthodontic template aligner material are summarized in Table 1 and illustrated in Figure 2.

Among the tested formulations, the highest fungal inhibition was recorded for MW-G, which achieved a fungal inhibition percentage (FIP) of 33.54%. This enhanced activity may be attributed to its essential oil–based composition, whose active components are known to exhibit antifungal properties and the ability to interfere with fungal membrane integrity and biofilm maturation.

In contrast, most of the other tested solutions demonstrated minimal or negligible antifungal activity, with inhibition values below 3%. Notably, MW-E showed a negative inhibition value (−13.21%), indicating a possible stimulatory effect on *C. albicans* biofilm development under the tested conditions.

Overall, the antifungal results highlight the limited efficacy of fluoride-based formulations when used alone against fungal biofilms on polymeric orthodontic surfaces, while essential oil–based solutions demonstrated superior performance in reducing fungal viability.

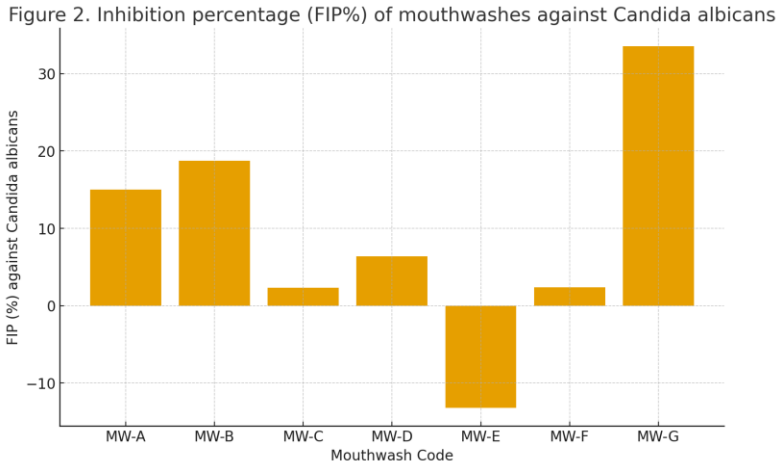

Figure 2. Inhibition percentages (FIP%) of the tested mouthwash solutions against Candida albicans biofilm developed on a polyethylene terephthalate glycol–based orthodontic template aligner material. Negative values indicate a possible stimulatory effect on fungal biofilm growth.

Comparative Antimicrobial Efficacy of Mouthwash Formulations

The overall antimicrobial performance was assessed by calculating the mean inhibition percentage across all three microbial strains.

The solution coded MW-B exhibited the highest overall efficacy, with a mean inhibition value of approximately 60.0%, followed by MW-G (46.4%). The remaining solutions demonstrated significantly lower overall activity, with MW-E presenting the poorest performance (mean BIP = −2.8%).

A moderate positive correlation was identified between the presence of fluoride in the formulation and the mean inhibition percentage (Spearman $\rho \approx 0.40$), indicating that fluoride contributes to antimicrobial efficacy but does not solely determine performance. In this context, essential oil–based formulations demonstrated notable efficiency despite the absence of fluoride.

A summary of the mean antimicrobial performance and fluoride content of the tested solutions is presented in Table 2.

Table 2. Fluoride concentration and mean antimicrobial inhibition of the tested mouthwash solutions.

Mouthwash Code	Fluoride Concentration (ppm F^-)	Mean BIP/FIP (%) across all strains
MW-A	0	16.8
MW-B	~225	60.0
MW-C	~100	21.9
MW-D	~250 (+ 0.05% CHX)	21.5
MW-E	0	−2.8
MW-F	~250	9.3
MW-G	0	46.4

Influence of the Aligner Template Material Surface

The polyethylene terephthalate glycol–based template aligner material showed a relatively smooth and hydrophobic surface, which may partially limit microbial adhesion. However, biofilm formation was still evident for all tested microorganisms.

The interaction between the polymer surface and the active compounds in the mouthwash solutions likely contributed to the observed differences in efficacy. Substances with higher substantivity on polymeric surfaces (such as chlorhexidine and certain essential oil compounds) showed prolonged antimicrobial effects compared to fluoride ions, which exhibit limited affinity for polymer substrates.

These surface–compound interactions may explain why some non-fluoridated solutions outperformed fluoridated ones in specific microbial contexts, particularly for *Candida albicans*.

DISCUSSIONS

This in vitro study evaluated the antimicrobial effects of seven commercially available mouthwash formulations on biofilms formed by Streptococcus mutans, Streptococcus oralis, and Candida albicans on a polyethylene terephthalate glycol–based orthodontic template aligner material. The results demonstrate that biofilm inhibition is strongly influenced by the chemical composition of the tested solutions, rather than solely by the presence or absence of fluoride [15].

Across all three microbial strains, the fluoride-containing antiseptic solution MW-B exhibited the highest overall antimicrobial efficacy, achieving inhibition percentages of 81.93% against S. mutans and 80.51% against S. oralis. This strong performance can be attributed to the combined presence of fluoride and cetylpyridinium chloride (CPC), a quaternary ammonium compound known for its membrane-disrupting antibacterial properties [16]. These findings support previous reports indicating that fluoride enhances

antimicrobial activity more efficiently when combined with additional antiseptic agents, rather than when used as a single active compound.

Interestingly, MW-G, a fluoride-free formulation based on essential oils, demonstrated high inhibitory activity against Candida albicans (33.54%) and good antibacterial performance against both streptococcal species. This confirms the antifungal and antibacterial potential of essential oil components such as eugenol, terpinen-4-ol, and cinnamaldehyde, which are known to alter microbial cell membrane permeability and disrupt enzymatic activity [9]. The superior antifungal performance of this formulation highlights the limited efficacy of fluoride alone against fungal biofilms and suggests that plant-derived bioactive compounds may represent valuable adjuncts in aligner hygiene protocols [17].

In contrast, MW-F, which contained amine fluoride, showed relatively low antimicrobial efficacy, despite its high fluoride concentration. This finding suggests that the chemical form of fluoride significantly influences its bioavailability and antimicrobial behavior on polymeric surfaces. While amine fluorides are effective for enamel remineralization due to their affinity for mineralized tissues, their antimicrobial performance on polymeric substrates such as orthodontic aligner materials may be limited, particularly in the absence of complementary antiseptic compounds [18] .

Of particular interest was the negative inhibition percentage observed for Candida albicans following exposure to MW-E, a plant-based formulation containing herbal extracts and low fluoride concentration. This phenomenon, also reported in the original Romanian study, may be explained by the presence of nutritive phytocompounds or carbohydrates that can transiently support fungal metabolism and biofilm development when present at subinhibitory concentrations [19] . Such effects have also been described in the literature, where certain botanical extracts act as prebiotic substrates for fungal species under specific conditions [20].

The moderate positive correlation identified between fluoride presence and mean inhibition percentage (Spearman's $\rho \approx 0.40$) further supports the hypothesis that fluoride contributes to antimicrobial activity but does not solely determine it. Instead, the overall formulation—including antiseptic agents, essential oils, alcohol, and excipients—plays a central role in modulating antimicrobial performance on polymer-based orthodontic materials [21].

From a clinical perspective, these findings are particularly relevant for orthodontists using template aligners during attachment bonding procedures. Although these materials are usually employed for short-term intraoral contact, their close adaptation to tooth surfaces and frequent handling make them potential vectors for microbial contamination. The results of this study indicate that not all mouthwashes provide equal decontamination efficacy on template aligner surfaces and that essential oil–based or CPC-containing formulations may offer superior antimicrobial benefits compared to fluoride-only rinses.

Nevertheless, this study has several limitations. It was conducted under in vitro conditions, using mono-species biofilms and a single exposure time of one minute, which may not fully replicate the complexity of the oral environment. In clinical reality, aligners and templates are exposed to mixed microbial communities, saliva proteins, and dynamic forces that may influence biofilm adhesion and disinfectant efficacy. Additionally, the absence of a chemical neutralizer after mouthwash exposure may have led to a slight overestimation of antimicrobial effects; however, since all specimens were treated uniformly, the comparative integrity of the results remains valid.

Future studies should explore multispecies biofilm models, repeated disinfection cycles, and longer exposure protocols to better simulate clinical conditions. Furthermore, evaluating the surface morphology and physicochemical changes of template aligner

materials after repeated exposure to different disinfectant agents would provide valuable insight into the long-term implications for clinical usability and aesthetic stability [16].

CONCLUSIONS

This in vitro study demonstrated that the antimicrobial efficacy of mouthwash solutions on biofilms formed on a polyethylene terephthalate glycol–based orthodontic template aligner material depends primarily on their overall formulation rather than on fluoride concentration alone. The mouthwash containing fluoride and cetylpyridinium chloride showed the strongest antibacterial activity, while the essential oil–based solution proved most effective against Candida albicans. In contrast, some fluoride-only formulations exhibited limited antimicrobial effects. These findings suggest that essential oil–based and combination antiseptic mouthwashes may represent more suitable options for reducing microbial contamination of orthodontic template aligner materials in clinical practice. Further research using multispecies biofilm models and repeated exposure protocols is needed to better simulate clinical conditions.

Acknowledgments

We would like to acknowledge Victor Babes University of Medicine and Pharmacy, Timisoara, for their support in covering the costs of publication for this research paper. The authors are truly grateful to the staff of the Faculty of Dental Medicine, Victor Babes University of Medicine and Pharmacy, Timisoara, Romania, and to the Faculty of Food Engineering, University of Life Sciences "King Mihai I", Timisoara, Romania, for their valuable support. The authors used ChatGPT, an AI language model developed by OpenAI, exclusively to improve the manuscript's language and readability. All the scientific content, interpretations, and conclusions are the original work of the authors.

Conflicts of Interest

The authors declare no conflicts of interest.

REFERENCES

[1] Kiatwarawut K, Rokaya D, Sirisoontorn I. Antimicrobial Activity of Various Disinfectants to Clean Thermoplastic Polymeric Appliances in Orthodontics. Polymers. 2022 May 31;14(11):2256.

[2] Charavet C, Gourdain Z, Graveline L, Lupi L. Cleaning and Disinfection Protocols for Clear Orthodontic Aligners: A Systematic Review. Healthcare. 2022 Feb 10;10(2):340.

[3] Lucchese A, Marcolina M, Mancini N, Ferrarese R, Acconciaioco S, Gherlone E, et al. A comparison of the alterations of oral microbiome with fixed orthodontic therapy and clear aligners: a systematic review. Journal of Oral Microbiology. 2025 Dec 31;17(1):2372751.

[4] Belanche Monterde A, Flores-Fraile J, Pérez Pevida E, Zubizarreta-Macho Á. Biofilm Composition Changes During Orthodontic Clear Aligners Compared to Multibracket Appliances: A Systematic Review. Microorganisms. 2025 Apr 30;13(5):1039.

[5] Hamdoon SM, AlSamak S, Ahmed MK, Gasgoos S. Evaluation of biofilm formation on different clear orthodontic retainer materials. J Orthod Sci. 2022;11:34.

[6] Pasaoglu Bozkurt A, Demirci M, Erdogan P, Kayalar E. Comparison of microbial adhesion and biofilm formation on different orthodontic aligners. American Journal of Orthodontics and Dentofacial Orthopedics. 2025 Jan;167(1):47–62.

[7] Baybekov O, Stanishevskiy Y, Sachivkina N, Bobunova A, Zhabo N, Avdonina M. Isolation of Clinical Microbial Isolates during Orthodontic Aligner Therapy and Their Ability to Form Biofilm. Dentistry Journal. 2023 Jan 3;11(1):13.

[8] Kiatwarawut K, Kuvatanasuchati J, Thaweboon B, Sirisoontorn I. Comparison of Various Antimicrobial Agents for Thermoplastic Polymeric Retainers. Polymers. 2022 Sep 8;14(18):3753.
[9] Alqarni H, Ba-Armah I, Almutairi N, Alenizy M, Arola DD, Oates TW, et al. Novel antimicrobial and bioactive resin-based clear aligner attachment orthodontic materials. Front Oral Health. 2025 Aug 7;6:1630019.
[10] Bona C, Camacho-Alonso F, Vaca A, Llorente-Alonso M. Oral Biofilm Control in Patients Using Orthodontic Aligners: Evidence from a Systematic Review. Asian J Periodontics Orthod. 2025;5(1):33–42.
[11] Astasov-Frauenhoffer M, Göldi L, Rohr N, Worreth S, Dard E, Hünerfauth S, et al. Antimicrobial and mechanical assessment of cellulose-based thermoformable material for invisible dental braces with natural essential oils protecting from biofilm formation. Sci Rep. 2023 Aug 18;13(1):13428.
[12] Harzivartyan S, Yilmaz HN, Nalbantoglu ER, Topcuoglu N. Evaluation of Microbial Colonisation on Clear Aligners With Different Cleaning Methods: A Prospective In Vivo Cross-Over Study. Orthod Craniofacial Res. 2025 Sep 25;ocr.70039.
[13] Esmaeili S, Shahbazi S, Ziaei H, Younessian F. Evaluating the Impact of Clear Dental Aligners on Dental and Periodontal Conditions, Oral Microbial Patterns, and the Immune System. In: Rezaei N, Ziaei H, editors. Oral Immunology [Internet]. Cham: Springer Nature Switzerland; 2026 [cited 2025 Nov 25]. p. 605–24. (Advances in Experimental Medicine and Biology; vol. 1492). Available from: https://link.springer.com/10.1007/978-3-032-03176-1_29
[14] Badnjević M, Petković Didović M, Jelovica Badovinac I, Lučić Blagojević S, Perčić M, Špalj S, et al. Disruption of Early Streptococcus mutans Biofilm Development on Orthodontic Aligner Materials. Processes. 2025 Sep 25;13(10):3069.
[15] Latimer J, Munday JL, Buzza KM, Forbes S, Sreenivasan PK, McBain AJ. Antibacterial and anti-biofilm activity of mouthrinses containing cetylpyridinium chloride and sodium fluoride. BMC Microbiol. 2015 Aug 21;15:169.
[16] Arce-Toribio JP, Arbildo Vega HI, López-Flores AI. Antimicrobial Efficacy of the Use of Mouthwash with Cetylpiridinium Chloride for Aerosol Producing Procedures. A Systematic Review. Odovtos - Int J Dent Sc. 2023 May 8;10–23.
[17] Valdivia-Tapia AC, Lippert F, Gregory RL. Evaluation of the antimicrobial potential of fluoride-free mouthwashes against Scardovia wiggsiae. Eur Arch Paediatr Dent [Internet]. 2025 Oct 8 [cited 2025 Nov 25]; Available from: https://link.springer.com/10.1007/s40368-025-01116-4
[18] Brookes ZLS, Bescos R, Belfield LA, Ali K, Roberts A. Current uses of chlorhexidine for management of oral disease: a narrative review. Journal of Dentistry. 2020 Dec;103:103497.
[19] Takenaka S, Sotozono M, Ohkura N, Noiri Y. Evidence on the Use of Mouthwash for the Control of Supragingival Biofilm and Its Potential Adverse Effects. Antibiotics. 2022 May 28;11(6):727.
[20] Gaaloul H, Amor WB, Dhia RB, Haddad O, Tobji S, Mastouri M, et al. Qualitative Modifications of the Aligners' Bacterial Flora under the Effect of Tea Tree Essential Oil. Saudi J Oral Dent Res. 2022 Apr 16;7(4):107–15.
[21] Bichu YM, Alwafi A, Liu X, Andrews J, Ludwig B, Bichu AY, et al. Advances in orthodontic clear aligner materials. Bioactive Materials. 2023 Apr;22:384–403.

3D facial Scanning Technologies - Comparative Analysis of Three Modern Three-Dimensional Acquisition Systems

https://doi.org/10.70921/medev.v31i4.2017

Raluca Todor[1,2†], Tareq Hajaj[1,2†], Cristian Zaharia[1,2*], Doina Chioran[1*], Cristina Modiga[1,2], Emanuela Lidia Petrescu[1,2], Meda-Lavinia Negrutiu[1,2], Cosmin Sinescu[1,2], Andreea Codruta Novac[1,2]

[1]*Faculty of Dental Medicine, "Victor Babes" University of Medicine and Pharmacy of Timisoara, 2 Eftimie Murgu Square, 300041 Timisoara, Romania;*
[2]*Research Center in Dental Medicine Using Conventional and Alternative Technologies, Department of Prostheses Technology and Dental Materials, Faculty of Dental Medicine, "Victor Babes" University of Medicine and Pharmacy of Timisoara, 9 Revolutiei 1989 Ave., 300070 Timisoara, Romania*
[†]*These authors contributed equally to this work.*

Correspondence to:
Name: Cristian Zaharia
E-mail address: cristian.zaharia@umft.ro

Name: Doina Chioran
E-mail address: chioran.doina@umft.ro

Received: 30 November 2025; Accepted: 09 December 2025; Published: 15 Deceember 2025

Abstract

1.Background: Three-dimensional (3D) facial scanning technologies have advanced rapidly, offering new possibilities for clinical, engineering, and educational applications. However, performance varies substantially across mobile, portable, and professional systems, and a direct comparison using standardized acquisition protocols is essential for determining their suitability in medical practice. *2.Methods*: Eight healthy adults (20–25 years old) were scanned using three technologies representing different levels of complexity: the iPhone LiDAR sensor with Qlone, the CR-Scan Ferret structured-light scanner, and the professional ProMax 3D Mid ProFace system. All participants were scanned under controlled conditions, maintaining identical positioning and acquisition procedures. Raw data were processed using each system's dedicated software and analyzed comparatively with respect to geometric visual consistency, texture quality, model completeness, artifacts, processing workflow, and cost–performance ratio. *3.Results*: The iPhone LiDAR system produced the least accurate models, characterized by surface discontinuities, loss of fine anatomical detail, and low-resolution texture. The CR-Scan Ferret achieved higher geometric fidelity and more coherent color mapping but remained sensitive to lighting conditions and operator stability. The ProMax 3D Mid ProFace system generated the most complete, consistent, and photorealistic models, with minimal artifacts and fully automated processing. These differences reflect the technological capabilities of each device category. The comparison was qualitative, as no objective numerical measurements of geometric deviation were performed. *4.Conclusions*: The findings confirm that no single scanning technology is universally optimal. Mobile systems are suitable for rapid, non-clinical, or educational applications; portable structured-light scanners offer a balance between visual consistency and accessibility; and professional systems remain the gold standard for advanced clinical environments requiring high precision.

Keywords: 3D facial scanning; LiDAR; structured light scanning; ProMax 3D Mid ProFace; CR-Scan Ferret; photogrammetry; 3D reconstruction; medical imaging.

INTRODUCTION

The rapid advancements in three-dimensional scanning technologies have transformed the way anatomical data is generated, analyzed, and used in medical engineering, especially in oral and cranio-maxillofacial fields [1]. 3D facial scanning has become an essential tool in numerous clinical specialties, from dentistry and cranio-maxillofacial surgery to dermatology, facial aesthetics, and functional rehabilitation [7,8]. By combining geometric visual consistency with the ability to produce detailed digital reconstructions, these technologies facilitate an in-depth understanding of facial morphology and enable personalized treatment planning [2].

The accelerated evolution of optical sensors, compact laser systems, and structured-light techniques has led to the emergence of an increasingly wide range of 3D scanners designed for different levels of precision and complexity [6]. Recent studies have shown that professional three-dimensional capture systems offer superior visual consistency, yet portable solutions or those integrated into mobile devices are becoming increasingly relevant due to their greater accessibility [3,9]. In particular, the introduction of LiDAR sensors in smartphones has expanded the use of these technologies beyond the traditional clinical environment, although their precision remains variable compared with dedicated systems [10].

In this context, the present study aims to provide a comparative analysis of three representative technologies of the moment: the LiDAR sensor integrated into iPhone devices used with the Qlone app – a mobile, accessible, and intuitive solution; the Creality CR-Scan Ferret – a portable structured-light scanner targeted toward users who require medium-to-high fidelity; the professional ProMax 3D Mid ProFace system, used in advanced medical imaging and known for its sub-millimetric accuracy as reported in the literature [1,5].

In this study, visual consistency is examined qualitatively through surface continuity, anatomical detail reproduction, and texture coherence, rather than through quantitative deviation measurements.

The analysis is methodologically structured around essential criteria for medical applicability, such as geometric accuracy, texture quality, acquisition and processing time, ease of use, and the cost–performance ratio. These criteria align with parameters frequently used in previous validation studies of 3D facial scanning systems [4,12].

Through this comparative approach, the study seeks to provide a rigorous and practical evaluation for professionals who must select the appropriate technology for a specific type of application. The results highlight that there is no “ideal universal scanner”, but rather a range of technological solutions that must be chosen according to the clinical context, available resources, and the required level of detail [11].

MATERIALS AND METHODS

The study was designed to comparatively evaluate three distinct 3D facial scanning technologies, each representing a different level of technical complexity and accessibility. The methodology aimed to structure the process so that the results would be reproducible, comparable, and relevant for applications in medical engineering.

The study was conducted on a group of eight participants, consisting equally of four male and four female subjects, aged between 20 and 25. This selection aimed to maintain a high degree of demographic homogeneity, reducing inherent variations linked to skin changes, soft tissue distribution, or age-related asymmetries. All subjects were evaluated under controlled conditions and were instructed to adopt a neutral head position and a

relaxed facial expression to minimize the influence of involuntary movements during acquisition. Ethical approval and written informed consent were obtained prior to participation.

Each participant was scanned successively with all three technologies under analysis, following the same procedural protocol so that the differences observed between models would reflect solely the performance of the capture systems, not interindividual variability. Using the same set of subjects throughout all stages of the study enabled a direct and rigorous comparison of the visual consistency, texturing, and completeness of the models generated.

For the comparative analysis, three representative 3D facial scanning systems were selected, covering different levels of technological sophistication. The selection was intended to span the full spectrum of currently available technologies—from mobile and accessible solutions to professional equipment used in advanced medical imaging. Each system was analyzed not only in terms of technical performance but also regarding how well it can meet the practical requirements of clinical applications. No external geometric reference or quantitative deviation analysis was used; therefore, visual consistency assessments were qualitative and based on visual comparison of surface continuity and anatomical detail.

The iPhone LiDAR System used with the Qlone Application

The first material investigated was the LiDAR sensor integrated into recent generations of iPhones. This system stands out due to its accessibility and mobility, as it enables 3D scanning without the need for additional dedicated equipment. In the study, the LiDAR sensor was used in combination with the Qlone application, which manages the entire process—from data acquisition to the photogrammetric reconstruction of the digital model. This configuration represents the category of emerging technologies aimed at regular users or professionals who require a fast, intuitive, and easily transportable solution (Figure 1).

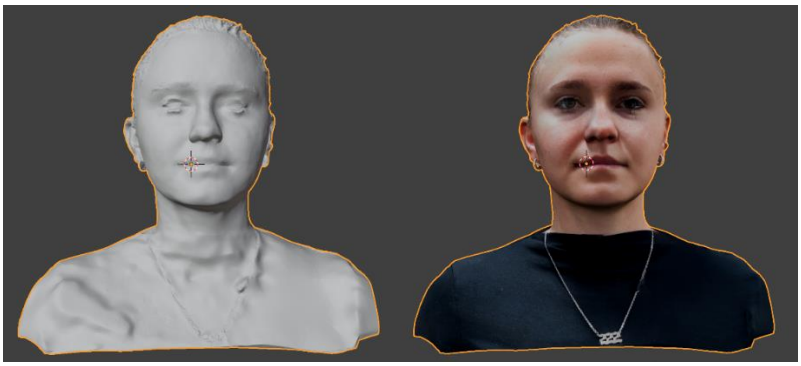

Figure 1. Geometry and color texture of Subject 1 obtained with LiDAR (Qlone Application).

Creality CR-Scan Ferret Scanner

The second system analyzed, the Creality CR-Scan Ferret, was selected as a representative of the intermediate-level class of portable scanners. It operates based on infrared structured light and is equipped with a high-frequency depth sensor, complemented by an RGB camera for capturing color information. Through this combination, the device offers superior geometric fidelity compared to technologies integrated into smartphones, while maintaining good portability. The CR-Scan Ferret was included in the study to evaluate the performance of a solution that combines accessibility with a higher level of detail, being frequently used in educational, engineering, and basic clinical contexts (Figure 2).

Figure 2. Geometry and color texture of Subject 2 obtained with the CR-Scan Ferret.

The Professional ProMax 3D Mid ProFace System

The third system, ProMax 3D Mid ProFace, represents the category of high-precision professional equipment used in specialized medical imaging. Integrated into the Planmeca ProMax 3D Mid unit, the ProFace system enables the acquisition of a 3D facial photograph without the use of radiation, through a combination of lasers that capture geometry and digital cameras that record texture. This technology is also compatible with CBCT data, making it an indispensable tool for maxillofacial surgery, orthodontics, and the planning of complex treatments. In this study, ProFace served as the technological benchmark for evaluating the highest level of precision and detail available in current medical practice (Figure 3).

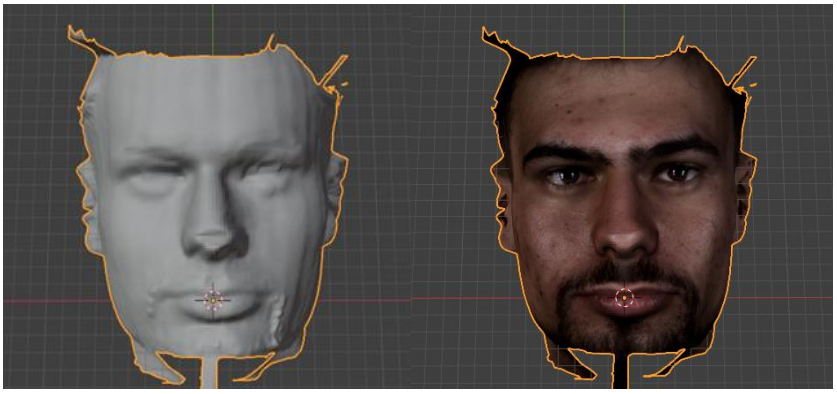

Figure 3. Geometry and color texture of Subject 3 obtained with the Planmeca ProMax 3D ProFace.

The methodology of this study was designed to enable a rigorous and coherent comparison between the three facial scanning systems analyzed. The entire process was organized in logical sequence—from raw data acquisition to the final evaluation of technological performance—aiming to minimize variability and ensure a solid methodological foundation.

To obtain a comparable dataset, all 3D models were acquired under controlled conditions, using the same subject in a neutral position and a static environment. This standardization ensured that the differences observed later reflected only the specific characteristics of each technology and not variations in the procedure.

Each of the three scanning systems required an acquisition protocol adapted to the technology it employs.

For the LiDAR–Qlone combination, scanning was performed by moving the operator in a circular path around the subject, following the visual guidance provided by the application. This procedure enabled simultaneous capture of depth information from the

LiDAR sensor and the images required for photogrammetric reconstruction, resulting in a three-dimensional model generated by combining both data sources.

For the CR-Scan Ferret scanner, the process involved handling the device close to the subject, within the optimal distance specified by the manufacturer (150–700 mm). The operator traced the facial contours from multiple angles, using modes dedicated to capturing geometry and texture, so that the final model would accurately reproduce both the shapes and the chromatic details of the face.

For the ProMax 3D Mid ProFace system, acquisition was carried out differently—in a single, fully automated sequence. The system captured facial geometry and texture simultaneously, without radiation exposure, generating the 3D photograph through the standard workflow integrated into the Planmeca equipment.

To reduce the influence of random errors, each scan was repeated several times. Among the generated models, the version with the best surface continuity and the fewest artifacts was selected, ensuring that the subsequent analysis relied on the most stable and representative results.

Data processing

The raw data obtained from the three technologies were subjected to a processing workflow adapted to the particularities of each system, ensuring that the final models accurately reflected the technical potential of the devices tested.

For the dataset generated using the LiDAR sensor and the Qlone application, reconstruction was performed within the app's software environment. This allowed the alignment of successive frames, stabilization of the photogrammetric reconstruction, and export of the models in standardized formats such as OBJ and STL.

The models produced with the CR-Scan Ferret were processed in the Creality Scan platform, where the point clouds were aligned and merged, and residual noise was removed. The same software also enabled the application of the color texture, contributing to a coherent three-dimensional model in terms of both geometry and visual representation.

For the ProMax 3D Mid ProFace system, data processing was carried out in Planmeca Romexis, the unit's dedicated software. It processed the 3D photograph generated by the system, delivering a complete model with detailed geometry and high-fidelity color mapping—a result of the integrated workflow specific to this type of technology.

After the individual processing steps were completed, all models were imported into a common analysis environment to ensure uniform evaluation conditions. This stage enabled the direct comparison of the models from both geometric and visual perspectives, eliminating the influence of differences between software platforms and strengthening the basis for the comparative analysis.

Evaluation criteria

To rigorously characterize the performance of each scanning system, the evaluation was structured around a coherent set of methodological criteria designed to capture both the technical accuracy of the generated models and their practical applicability. The analysis focused primarily on geometric visual consistency—an essential element in any 3D reconstruction process—by examining surface continuity, fine facial details, and contour fidelity. The quality of visual representation was assessed through the texture criterion, which evaluated color uniformity, realism of facial markings, and the coherence between the geometric model and its color mapping.

Another important aspect of the methodology was the time required for scanning and processing, measured to determine the operational efficiency of each system. This variable is critical in clinical contexts, where procedure duration influences both patient comfort and the integration of technology into existing workflows.

The evaluation also included an analysis of system-specific artifacts and errors, aiming to identify distortions, missing areas, or residual noise in the point clouds. These elements serve as direct indicators of technological limitations and significantly affect the usability of the generated models.

In addition to technical performance, the study examined ergonomics and ease of use—factors reflecting operator experience, procedural stability, and workflow complexity. These criteria were essential for determining the feasibility of adopting each system in a real clinical environment.

Finally, the analysis incorporated economic considerations by assessing the cost–performance ratio, evaluating the extent to which the required investment is justified by the quality and usefulness of the outcomes. This approach enabled not only a technical comparison between devices but also an evaluation of their practical value in diverse clinical and engineering contexts.

To coherently integrate the results, the evaluation criteria were combined into a comprehensive comparative analysis structured to highlight both the advantages and limitations of each scanning system. Synthesizing these criteria into a comparative matrix allowed direct observation of performance differences, revealing how each technology meets the specific requirements of 3D facial reconstruction.

This stage was essential in forming the overall interpretation of the study, as it allowed the correlation of technical performance with practical applicability. The analysis did not limit itself to a mechanical comparison of parameters; it aimed to capture the relevance of each result within the clinical context. Through this approach, the study evaluated how geometric fidelity, texture quality, workflow duration, procedural stability, or cost–benefit balance can influence the decision to integrate a technology into various medical scenarios.

The final interpretation sought to identify the compatibility between the observed performance and the real needs of medical engineering, diagnostic processes, and treatment planning, emphasizing how each system can support, limit, or improve clinical workflows.

RESULTS

The analysis of the results obtained from the three 3D facial scanning technologies revealed notable differences among the devices in terms of geometric fidelity, texture quality, procedural efficiency, and overall acquisition stability. Each system produced a distinct model, reflecting both the limitations and strengths of its underlying technology.

The model generated using the LiDAR system combined with the Qlone application showed satisfactory overall geometry but lower resolution in areas requiring fine detail, such as the nasal edge, cheekbones, and lip contours. The surfaces exhibited minor local fragmentation, and regions less exposed to the camera required photogrammetric completion, leading to some nonuniformities. The applied texture was generally realistic, though less well integrated in areas with abrupt facial relief changes. Total processing time was short, confirming the speed advantage characteristic of mobile technologies.

In contrast, the model produced with the CR-Scan Ferret demonstrated significantly better geometric fidelity. Facial surfaces displayed superior continuity, and anatomical details—particularly those of the nose and cheeks—were captured with noticeably higher clarity. The color texture also stood out for its improved visual consistency and better coherence between relief and coloration. However, the scans were sensitive to lighting variations, and very dark or reflective areas required repeated captures. Processing time was moderate, reflecting the need to integrate and clean a larger volume of data.

For the ProMax 3D Mid ProFace system, the results showed the highest quality among all technologies analyzed. The geometric model exhibited high precision, with no significant

interruptions or artifacts, and the facial texture was reproduced with near-photographic fidelity, featuring smooth chromatic transitions and visibly superior uniformity. Designed for advanced clinical use, the final model provided a complete and highly detailed facial representation, ideal for applications requiring precision, such as surgical planning or orthodontic analysis. Acquisition and processing times were consistent and predictable due to the fully automated workflow.

Comparing the three technologies, a clear differentiation in performance levels was observed (Table 1). The LiDAR–Qlone solution stands out for accessibility and speed but offers limited precision. The CR-Scan Ferret provides a balanced compromise between cost and performance, generating models of considerably higher quality than mobile solutions. The ProMax 3D Mid ProFace system distinguishes itself through exceptional visual consistency and realism but requires complex equipment designed exclusively for professional environments.

Table 1. Comparative results of the three 3D facial scanning technologies

Criteria	*LiDAR + Qlone*	*CR-Scan Ferret*	*ProMax 3D Mid ProFace*
Geometric Visual consistency	Low visual consistency; loss of fine detail (nose, eyelids, jawline); smoothed surfaces and visible interruptions.	Significantly better visual consistency; well-defined details; some sensitivity to lighting and distance.	Highest visual consistency; continuous surfaces with no major artifacts; highly faithful anatomical reproduction.
Texture Quality	Low-resolution texture; uneven color; flat appearance.	Realistic RGB texture thanks to dedicated camera; natural and coherent color mapping.	Photorealistic texture; uniform and smooth chromatic transitions.
Model Completeness	Incomplete model; missing areas on sides and submental region.	Mostly complete model; minor gaps in difficult-to-reach zones.	Fully complete model with no missing regions.
Artifacts	Frequent artifacts due to movement, reflections, and LiDAR limitations.	Moderate artifacts related to lighting, distance, or software errors.	Minimal artifacts; automated workflow reduces operator-dependent variability.
Scan Time	Fast (mobile), but motion consistency affects quality.	Moderate to fast depending on mode (wide / high precision).	Most consistent: single standardized scan sequence.
Processing Time	Very short; processed within the app.	Moderate; requires alignment, fusion, and cleanup.	Automated in Romexis; predictable processing time.
Ergonomics	Very easy to use; requires only an iPhone.	Portable and lightweight; requires stable hand positioning.	Stationary clinical system; high-end ergonomic workflow.
Cost	Lowest cost (existing device).	Medium cost; accessible for labs or engineering work.	Highest cost; professional clinical equipment.
Best Use Case	Telemedicine, education, non-clinical applications.	Prosthetics labs, engineering projects, mid-level clinical tasks.	Surgery, orthodontics, cranio-maxillofacial reconstruction.

These results confirm that selecting the optimal technology depends directly on the clinical or technical context and on the level of detail required for the intended application.

DISCUSSIONS

The results obtained in this study align with trends described in the scientific literature, which consistently emphasize that the visual consistency of a 3D facial scanning system is directly influenced by the technology used, the density of captured points, and the integrated reconstruction algorithms [1]. Recent studies on the use of mobile technologies in cranio-maxillofacial imaging—such as those using iPhone LiDAR—confirm the variable performance of these systems, especially in anatomical areas with complex relief or subtle curvature variations [3,10]. Our findings regarding the limitations of smartphone LiDAR are therefore fully consistent with international reports, which highlight lower precision compared with professional systems [9,10].

Regarding the CR-Scan Ferret, the results confirm observations from other studies focused on portable structured-light technologies, which underline their ability to generate 3D models with higher geometric fidelity than mobile solutions [5]. Clinical and engineering studies evaluating similar devices indicate that structured light offers robust performance but remains sensitive to lighting conditions and operator movement—an aspect also observed in this study [4,6]. This category of scanners occupies an important intermediate space between the accessibility of mobile technologies and the precision of professional systems, confirming the conclusions of recent meta-analyses in the field [9].

The ProMax 3D Mid ProFace system demonstrated, as expected, the best results in terms of both geometric fidelity and texture quality. Previous studies on high-fidelity stereophotogrammetric and structured-light professional systems have consistently shown sub-millimetric precision, making them suitable for applications such as orthodontics, cranio-maxillofacial surgery, or virtual reconstruction [2,7,8]. Our results are consistent with these findings and confirm the major advantage provided by automated workflows and advanced calibration algorithms in these platforms.

The differences observed between technologies can be explained through the fundamental principles of the optical methods used. Commercial LiDAR-based systems have limited point density and simplified reconstruction algorithms, which restrict their ability to capture fine details [10]. In contrast, structured-light technology projects a patterned sequence onto the surface and uses advanced triangulation, giving it higher fidelity according to technical descriptions in the literature [6]. Professional systems combine multiple sensor types and include internal routines for compensating motion or lighting variations, as noted in numerous clinical validation studies [1,5,12].

Considering clinical relevance, the literature clearly distinguishes that mobile solutions can be useful for educational applications, telemedicine, or quick monitoring, while portable scanners are suited for applied research and prototyping, and professional systems are indispensable for interventions requiring high precision [3,7,8]. The findings of our study fully align with these technological classifications and highlight that choosing a solution must be based on the intended purpose, required detail level, and available resources [11].

This indicates that 3D facial scanning technologies should be evaluated not only in terms of precision but also according to the context of use. The results obtained, corroborated with scientific literature, justify the need for a differentiated selection between mobile, portable, and professional systems, in accordance with specific clinical or engineering requirements.

The model obtained using the LiDAR–Qlone system confirms what the literature has emphasized for several years: LiDAR sensors integrated into smartphones represent an

accessible and practical solution for general applications, but they do not reach the level of precision required for advanced clinical analysis. Studies published between 2020 and 2023 highlight that commercial LiDAR models exhibit systematic errors in reproducing fine facial details, especially in regions with pronounced curvature or complex textures, which is consistent with the findings of the present study.

In the case of the CR-Scan Ferret, the results align with research confirming the potential of portable structured-light technologies. The scientific literature shows that such devices can provide high geometric fidelity, approaching that of mid-range professional systems, although their performance remains dependent on ambient lighting and operator experience. This was also reflected in our data: the overall quality of the model was superior to that obtained using the smartphone solution, but required increased operator attention during acquisition.

The ProMax 3D Mid ProFace system generated the best results, in full agreement with established literature on professional systems used in craniofacial imaging. Both manufacturer documentation and independent research published in dentistry, cranio-maxillofacial surgery, and orthodontics consistently report that these systems can reproduce facial morphology with sub-millimetric precision, making them suitable for clinical use and advanced research. The results of this study fully confirm these observations.

The significant differences observed among the three systems can be explained through fundamental technological principles. Smartphone LiDAR operates with a relatively low point density and limited spatial projection, whereas dedicated scanners use higher-resolution optical sensors, more advanced triangulation algorithms, and artifact-compensation mechanisms. Professional systems such as ProFace integrate complex optical assemblies and standardized calibration procedures, contributing to the extremely accurate reproduction of facial geometry.

The literature emphasizes the importance of lighting, subject movement, and operator expertise in obtaining valid results. Our observations confirm this: mobile and portable technologies are more vulnerable to environmental variations and require strict control of the acquisition procedure, whereas the ProFace system offers superior consistency due to its automated workflow [2–7].

Clinical relevance of the results

Comparing the three technologies within the context of clinical applications shows that only systems dedicated to medical imaging can provide the level of detail required for surgical interventions, orthodontic analysis, or virtual reconstructions. Mobile solutions can be useful for telemedicine, rapid monitoring, or educational applications, while portable structured-light scanners occupy an intermediate position, suitable for prosthetic laboratories, engineering projects, and applied research.

The literature confirms this technological hierarchy, emphasizing that the choice of a scanning device must be adapted to clinical objectives, the required level of visual consistency, and the available resources. The results of our study align closely with these conclusions [3–6,8–9].

Study limitations

This study presents several limitations that should be considered when interpreting the results. First, the sample size was small, consisting of only eight healthy young adults aged 20–25, which restricts the generalizability of the findings to other age groups or individuals with complex craniofacial conditions. Second, the portable scanning technologies used—particularly the iPhone LiDAR system and the CR-Scan Ferret—are sensitive to environmental factors such as lighting, operator movement, and distance from the subject. Despite standardized procedures, complete control over these variables is difficult to achieve.

Another limitation lies in the reliance on proprietary software for data processing, as differences in alignment, fusion, and smoothing algorithms may influence the final models independently of the hardware. Moreover, the study did not employ an external geometric reference (such as a calibrated phantom), meaning that the results are based on relative comparisons rather than absolute error measurements. Finally, the study did not assess longitudinal reproducibility, leaving open the question of how consistently each system performs over multiple sessions.

It is important to note that, because the study did not employ a quantitative reference standard, all accuracy-related observations are qualitative and based solely on visual assessment of geometric detail and surface continuity.

Because the study involved only healthy young adults, the findings may not directly translate to clinical populations with facial asymmetries, deformities, or variable soft-tissue characteristics. Such cases may introduce additional challenges for surface acquisition and reconstruction, particularly for lower-resolution systems.

The small and demographically narrow sample restricts generalization to broader clinical populations. The professional systems demonstrated superior qualitative surface fidelity in this study; however, their suitability for precise clinical measurement requires quantitative validation beyond the scope of this work.

Although multiple scans were acquired, no numerical reproducibility metrics were calculated; the model with the fewest visible artifacts and highest surface continuity was selected subjectively for analysis.

CONCLUSIONS

This study provided a qualitative comparison of three contemporary 3D facial scanning technologies, each representing a distinct level of complexity and accessibility. Based on visual assessment of geometric fidelity, texture coherence, model completeness, artifact frequency, and workflow characteristics, clear differences were observed among the systems.

The LiDAR–Qlone configuration offered the most accessible and rapid solution but produced models with limited surface detail and greater variability in reconstruction quality, making it more suitable for general, educational, or non-clinical applications. The CR-Scan Ferret delivered models with higher visual geometric fidelity and more consistent texture mapping, representing a practical intermediate option for engineering tasks, prototyping, and basic clinical documentation. The ProMax 3D Mid ProFace system generated the most complete and visually consistent reconstructions, with smooth surfaces and coherent texture integration, reflecting the capabilities of a fully automated professional platform.

These findings highlight that each system presents strengths aligned with its technological design and intended use-case. Selection should therefore be guided by the required level of visual detail, workflow constraints, and available resources. Because the comparison was qualitative and no quantitative deviation analysis was performed, the conclusions reflect observed visual and procedural differences rather than validated metric accuracy. Further research incorporating standardized geometric references and expanded clinical populations is needed to determine the quantitative precision and broader clinical applicability of these technologies.

Conflicts of Interest

The authors declare no conflict of interest.

REFERENCES

[1] Hartmann R, Weiherer M, Nieberle F, Palm C, Brébant V, Prantl L, Lamby P, Reichert TE, Taxis J, Ettl T. Evaluating smartphone-based 3D imaging techniques for clinical application in oral and maxillofacial surgery: A comparative study with the vectra M5. Oral Maxillofac Surg. 2025 Jan 10;29(1):29. doi: 10.1007/s10006-024-01322-2. PMID: 39792225; PMCID: PMC11723895.

[2] Aldridge K, Boyadjiev SA, Capone GT, DeLeon VB, Richtsmeier JT. Precision and error of three-dimensional phenotypic measures acquired from 3dMD photogrammetric images. Am J Med Genet A. 2005 Oct 15;138A(3):247-53. doi: 10.1002/ajmg.a.30959. PMID: 16158436; PMCID: PMC4443686.

[3] Quinzi, V.; Polizzi, A.; Ronsivalle, V.; Santonocito, S.; Conforte, C.; Manenti, R.J.; Isola, G.; Lo Giudice, A. Facial Scanning Visual consistency with Stereophotogrammetry and Smartphone Technology in Children: A Systematic Review. Children 2022, 9, 1390. https://doi.org/10.3390/children9091390

[4] Ma L, Xu T, Lin J. Validation of a three-dimensional facial scanning system based on structured light techniques. Comput Methods Programs Biomed. 2009 Jun;94(3):290-8. doi: 10.1016/j.cmpb.2009.01.010. Epub 2009 Mar 20. PMID: 19303659.

[5] Pellitteri, F., Scisciola, F., Cremonini, F. et al. Visual consistency of 3D facial scans: a comparison of three different scanning system in an in vivo study. Prog Orthod. 24, 44 (2023). https://doi.org/10.1186/s40510-023-00496-x.

[6] Jason Geng, "Structured-light 3D surface imaging: a tutorial," Adv. Opt. Photon. 3, 128-160 (2011).

[7] Hajeer MY, Millett DT, Ayoub AF, Siebert JP. Applications of 3D imaging in orthodontics: part I. J Orthod. 2004 Mar;31(1):62-70. doi: 10.1179/146531204225011346. PMID: 15071154.

[8] Kau CH, Richmond S, Incrapera A, English J, Xia JJ. Three-dimensional surface acquisition systems for the study of facial morphology and their application to maxillofacial surgery. Int J Med Robot. 2007 Jun;3(2):97-110. doi: 10.1002/rcs.141. PMID: 17619242.

[9] Mai HN, Kim J, Choi YH, Lee DH. Visual consistency of Portable Face-Scanning Devices for Obtaining Three-Dimensional Face Models: A Systematic Review and Meta-Analysis. Int J Environ Res Public Health. 2020 Dec 25;18(1):94. doi: 10.3390/ijerph18010094. PMID: 33375533; PMCID: PMC7795319.

[10] Abbas, Sahar & Abed, Fanar M. (2024). Evaluating the Visual consistency of iPhone Lidar Sensor for Building Façades Conservation. 10.1007/978-3-031-48715-6_31.

[11] Javaid, Mohd & Haleem, Abid & Khan, Shahbaz & Luthra, Sunil. (2020). Different Flexibilities of 3D Scanners and Their Impact on Distinctive Applications: International Journal of Business Analytics. 7. 37-53. 10.4018/IJBAN.2020010103.

[12] Weinberg SM, Naidoo S, Govier DP, Martin RA, Kane AA, Marazita ML. Anthropometric precision and visual consistency of digital three-dimensional photogrammetry: comparing the Genex and 3dMD imaging systems with one another and with direct anthropometry. J Craniofac Surg. 2006 May;17(3):477-83. doi: 10.1097/00001665-200605000-00015. PMID: 16770184.

Redefining Digital Precision: How Scanning Technique Shapes the Quality of Intraoral Impressions

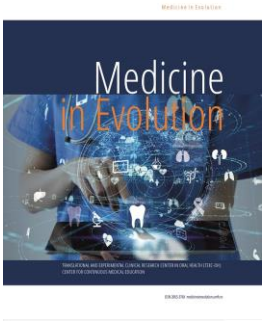

https://doi.org/10.70921/medev.v31i4.2018

Camelia-Alexandrina Szuhanek[1], Iana Grigoreac[2], Andra-Alexandra Stăncioiu[1*], Vlad Tiberiu Alexa[3], Sorana Rosu[4]

[1]*Orthodontic Research Center ORTHO-CENTER, Discipline of Orthodontics I, Faculty of Dental Medicine, "Victor Babes" University of Medicine and Pharmacy Timisoara, 9 No., Revolutiei Bv., 300041 Timisoara, Romania; cameliaszuhanek@umft.ro; andra.stancioiu@umft.ro*
[2]*Faculty of Dental Medicine, "Victor Babes" University of Medicine and Pharmacy, Eftimie Murgu Sq. No. 2, 300041 Timisoara, Romania; grigoreaciana@gmail.com*
[3]*Translational and Experimental Clinical Research Centre in Oral Health, Department of Preventive, Community Dentistry and Oral Health, University of Medicine and Pharmacy "Victor Babes", 300040 Timisoara, Romania; vlad.alexa@umft.ro*
[4]*Department of Surgicals, Faculty of Dental Medicine, University of Medicine and Pharmacy "Grigore T. Popa" Iasi, Romania; rosu.sorana@umfiasi.ro*

Correspondence to:
Name: Andra-Alexandra Stăncioiu
E-mail address: andra.stancioiu@umft.ro

Received: 02 December 2025; Accepted: 05 December 2025; Published: 15 December 2025

Abstract

Background/Objectives: Digital dentistry increasingly relies on intraoral scanners to capture full-arch impressions, yet the influence of scanning technique on the accuracy and efficiency of digital models remains insufficiently clarified. This study compared several scanning strategies—varying in segmentation and scanner motion patterns—to determine which protocols yield the highest precision and operational efficiency. *Methods:* Ten participants underwent full-arch intraoral scanning using seven techniques that combined different segment divisions (one, two, or three segments) with motion types (linear, zig-zag, or combined). Accuracy was assessed by superimposing STL files of each scan onto a reference model using CloudCompare and calculating point-to-point 3D deviations. Efficiency was evaluated based on the number of digital images generated and the total scanning time measured by software and a stopwatch. *Results:* For the maxillary arch, the most accurate technique was a single-segment zig-zag scan; for mandibular arch accuracy, it was a two-segment linear approach. The motion that produced the shortest scanning time was zig-zag, while that which required the least number of digital records was the two-segment linear scan. Combined-motion and three-segment strategies had the lowest accuracy as well as efficiency. *Conclusions:* Scanning techniques employing single uniform motion with minimum segmentation provide the best balance between accuracy and efficiency. Over-segmentation along with combined motions reduces the quality of the scan and increases the duration for scanning, thereby emphasizing a simple yet consistent path in clinical practice.

Keywords: accuracy; CloudCompare; digital dentistry; efficiency; full-arch scan; intraoral scanner; scanning strategy; 3D analysis

INTRODUCTION

The integration of digital technology into dental practices started with the introduction of the CAD/CAM (Computer-Aided Design/Computer-Aided Manufacturing) system in 1973 [1].

The intraoral scanner consists of three components: the intraoral camera, the computer, and the software [2]. The intraoral camera facilitates the generation of a digital imprint, eliminating the need for direct contact with oral tissues, such as alginate. All imaging technologies, whether triangulation or confocal optics, need the projection of light onto the scanned object, enabling the subsequent recording of the reflected image or video by a charge-coupled device (CCD) receiver [2].

The computer is a crucial element for three-dimensional computations. Certain versions are directly integrated with a touch screen, enabling the physician to see the sequences of the 3D imaging process together with pertinent patient data [3]. The program is tailored to the system used. It is tasked with aggregating the acquired pictures to generate a 3D dataset of the scanned item. This dataset is derived by the program identifying the point of interest (POI), with each POI possessing three coordinates (x and y, which delineate the location in a certain plane, and z, which is contingent upon the distance from the object) [3].

The software produced may include various tools for 3D creation and manipulation of digital models. The software's breadth of indicators and functionalities is contingent upon the supplementary modules included. For instance, some software facilitates the use of virtual wax-ups, grin design, virtual articulators, and the creation of entire dentures or implants, among others [4].

The data may be documented in the STL (Standard Tessellation Language or Stereolithography) format as a series of triangulated surfaces, which is the predominant format used in dentistry. A significant issue with these files is the inability to keep patient data with the 3D model, as is possible with DICOM (Digital Imaging and Communications in Medicine) files. Some scanners, however, include color, transparency, and texture using alternative formats, such as PLY (Polygon File Format or Stanford Triangle Format) [4].

The operational concept of an intraoral scanner relies on the projection of a light beam (either laser or structured light) onto the surface of the target item. The sensors at the scanner's apex detect the light pattern altered by the object's geometric surface. Subsequently, with processing software, the shape identified by the laser beam is computed in three-dimensional coordinates (x, y, z), representing several points that ultimately create a network forming the real picture. To provide a comprehensive representation of the item, all photos captured from various angles throughout the scanning process are merged to produce a 3D image [5].

ISO (International Organization for Standardization), particularly ISO 5725-1, characterizes accuracy as a "measurement method" pertaining to trueness and precision. Trueness denotes the proximity of test values to established reference values, while precision pertains to the consistency of findings from repeated testing. This concept is utilized to evaluate the accuracy of scanned data, whereby the accuracy of an intraoral scanner is assessed by superimposing the data acquired from the intraoral scanner onto reference scan data of a specific object, typically obtained via an industrial scanner, while precision is determined by superimposing data from multiple scans of the same object [6].

The efficacy of intraoral scanning may be assessed by many methodologies, contingent upon: Electronic documentation—this option specifies the quantity of pictures acquired during each scan. Upon initiation of the scan, the used program documents the quantity of photographs captured until the digital model is fully realized. Consequently, a

higher quantity of pictures indicates an elevated complexity of the scan or worse clinical circumstances. The scanning duration is ascertained by timing instruments that provide accurate values in seconds, to two decimal places. The duration from the beginning of the scanning phase to its full conclusion is measured. Scanning fails. When the scanner fails to identify a region for scanning, the imaging procedure is halted, despite the scan duration continuing, necessitating the operator to revisit a previously scanned area to complete the process. Scan failures are documented by recording the number of interruptions that occur throughout the scanning process [7].

The first notion of an intraoral scanner was presented by Francois Duret in his thesis, titled "Empreinte Optique," in 1973 at Claude Bernard University in Lyon, France [8].

In contrast to traditional plaster models, digital imprints may be more efficiently stored inside a database, eliminating the need for physical storage and reducing the risk of damage during handling. They may be conveniently kept as digital files for extended periods, allowing the doctor to view the data at any time and from any location with computer access [9]. Digital models enable users to examine three-dimensional historical alterations in a patient's oral cavity, including tooth position displacement, occlusal wear, abrasion, and gingival retraction. Documenting and preserving data on the initial condition of the patient's oral cavity is particularly advantageous in cases of substantial defects or loss of dental structures in the future [9].

Aim and objectives

The aim of this study was to evaluate how different intraoral scanning techniques—defined by segmentation patterns and scanner motion—affect the accuracy and efficiency of full-arch digital impressions.

MATERIAL AND METHODS

The study concentrated on patients enrolled in the Orthodontics I Discipline at the Faculty of Dental Medicine, "Victor Babeş" University of Medicine and Pharmacy, Timişoara. All participants provided written informed permission, and the research received approval from the Institutional Ethics Committee of "Victor Babeş" University of Medicine and Pharmacy in Timişoara, Romania (CECS Nr. 04/26.01.2024).

The research sample included 10 participants, in whom the scanning of the complete upper and lower dental arches, as well as the static occlusion, was observed. The patients originate from the Orthodontics I university clinic and are represented by students participating in the orthodontics internship and by the patients attending the internships.

The study's inclusion criteria are as follows:

• Patients aged 18 to 40 years, possessing a minimum of 28 teeth across both dental arches, without edentulous conditions or extensive carious lesions complicated by coronal destruction;

• Patients devoid of significant systemic diseases that could impact the oral mucosa, particularly the gingival mucosa;

• Patients exhibiting satisfactory overall oral health, free from extensive carious lesions, advanced periodontal disease, or other dental conditions that may compromise scan accuracy;

• Patients who have undergone prior dental cleaning;

• Cooperative patients willing to engage in all phases of the study.

Exclusion criteria:

• patients receiving orthodontic treatment with fixed appliances;

• pregnant individuals to mitigate possible risks and the unpredictability of the oral mucosa due to hormonal fluctuations;

• patients exhibiting restricted oral cavity openings (trismus).

The Aoralscan 3 intraoral scanner from SHINING 3D was used to perform all the scanning procedures (Figure 1a,b).The manufacturer's [10] data indicates that it features an ergonomic design for optimal functionality, weighing 240 ± 10 g and measuring 281 x 33 x 46 mm (L x W x H), while being light and compact. It works on the premise of eschewing structured light, generating outputs in the formats of STL, OBJ, and PLY data. The scanner has an automatic antifog function and a dynamic LED indication and is controlled by a single button located on its handle. The manufacturer claims to have enhanced the scanning field of view by 58% relative to its predecessor, Aoralscan 2, and can now scan to a depth of 22 mm. The scanner tips are detachable and autoclavable, enduring up to 100 autoclave cycles, and are offered in two sizes: one for adults and one for children. The shape of the tips, characterized by their slender and elongated form, ensures a pleasant therapeutic experience for patients [10].

(a) (b)

Figure 1. The Aoralscan 3 intraoral scanner (SHINING 3D). (a) Handpiece of the Aoralscan 3 intraoral scanner. (b) Mobile scanning unit with the attached Aoralscan 3 scanner

The scanned images were recorded using the SHINING 3D Dental Cloud software (IntraoralScan v 3.3.2.9) (Figure 2), after which the datasets were saved and exported in STL format for analysis and comparison. The software logs both the scanning duration and the number of digital images captured to generate a complete scan.

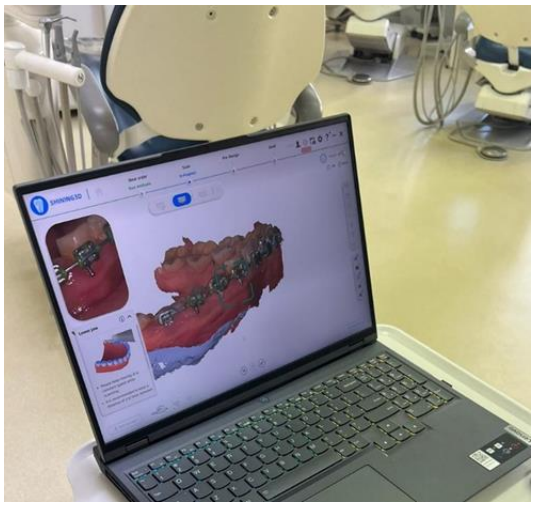

Figure 2. Interface of the SHINING 3D Dental Cloud, IntraoralScan v 3.3.2.9 used for digital image acquisition and file registration

SCANNING METHODOLOGIES— Each scanning method is defined by the quantity of segments scanned and the motion used during the scanning process. The segments to be scanned include the complete arch for one segment, half an arch or a hemiarch (including molars, premolars, canines, and incisors) for two segments, and one-third of the dental arch when scanning in three segments. In a 3-segment scan, the first segment encompasses the molars, premolars, and canine of one hemiarch; the second segment comprises the central group, specifically the canines, lateral incisors, and central incisors; and the third segment includes the molars, premolars, and canine of the opposing hemiarch. Consequently, in segment scanning, some dental components will overlap and be scanned many times, as shown with canines.

Three kinds of scanning movements will be employed: linear/continuous, zig-zag, and a combination of linear and zig-zag movements. During the linear/continuous movement, the scanner sequentially traverses each tooth surface, first with the occlusal and incisal surfaces of all teeth in the designated segment, followed by the vestibular and oral surfaces. The zig-zag motion sequentially scans the surfaces of a tooth. For instance, if the scanning of a tooth begins from the oral aspect and then transitions to the occlusal and vestibular surfaces, the scanning of the next tooth will begin from the vestibular side, followed by the occlusal and oral surfaces. The integrated method entails the preliminary scanning of the occlusal/incisal surfaces via a continuous motion, upon which a zig-zag movement is then overlaid to capture the vestibular and oral surfaces.

By combining these experimental factors, including the number of segments and the type of movement, we have identified 7 scanning techniques that can be used (Table 1 and Figure 3). Among these techniques, two protocols combine linear and zig-zag motions but differ in the extent of the zig-zag area: S1L+Za uses zig-zag only in the anterior region, whereas S1L+Zf applies the zig-zag pattern across the entire arch.

Table 1. Evaluated Intraoral Scanning Techniques

Scanning Technique	Scanned Segment & Arch Portion	Scanning Motion	Overlapping Surfaces
S1L	Entire arch (1 segment)	Linear	–
S1L+Za	Entire arch (1 segment)	Linear + zig-zag in the anterior region; linear in the posterior region	–
S1L+Zf	Entire arch (1 segment)	Linear + zig-zag across the full arch	–
S1Z	Entire arch (1 segment)	Zig-zag	–
S2L	Right and left hemi-arches (2 segments)	Linear	Incisal region
S3L	Right posterior, left posterior, anterior region (3 segments)	Linear	Canine, first premolar
S3L+Z	Right posterior, left posterior, anterior region (3 segments)	Linear + zig-zag	Canine, first premolar

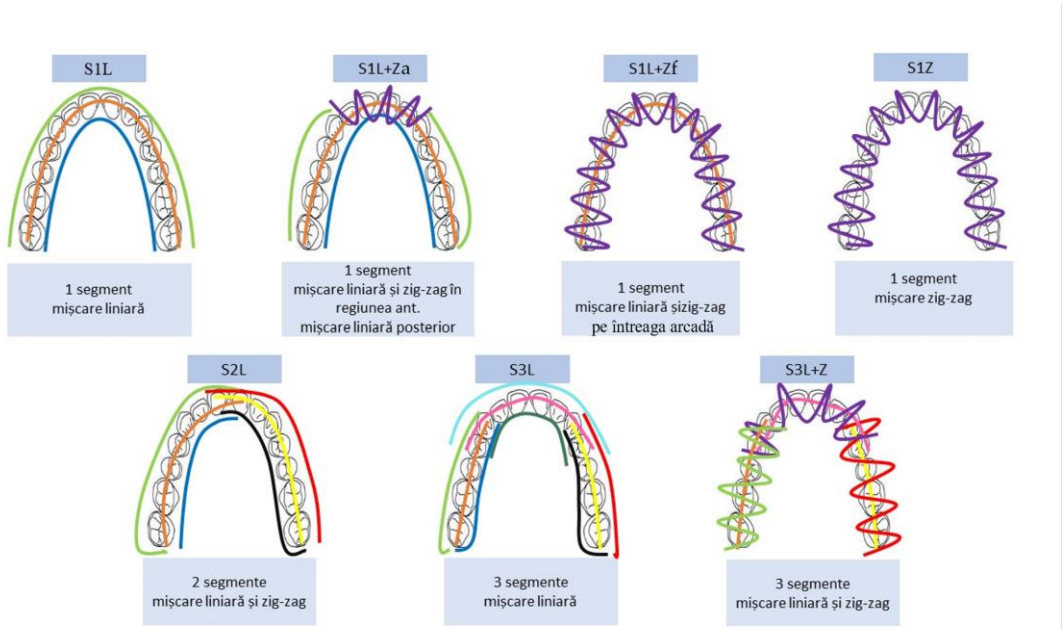

Figure 3. Schematic illustration of the scanning techniques used in the study

DATA GATHERING AND ANALYSIS – Each scanning approach was used once for all patients and is applicable to both the upper and lower arches. To prevent any possible order impact, the order of the scanning modalities was randomized for each participant using a computer-generated random sequence. If a scan was not finished or the program didn't catch a certain area, the scan was done again right away. The final dataset only comprised full and technically valid scans. All scans were included after repetition. To eliminate differences between operators, all intraoral scans were done by one trained operator who knew how to use the Aoralscan 3 intraoral scanner. This yielded a total of 70 comprehensive scans, with 10 images allocated to each approach. The data acquired by the software application was stored in STL format.

ASSESSMENT OF ACCURACY—To assess accuracy, the digital model for each scanning approach will be sequentially overlaid with a digital reference model, which is derived from the scanning technique endorsed by the manufacturer of the intraoral scanner. The manufacturer advises scanning the arch, one segment, using a linear motion (S1L), first with the occlusal surfaces, subsequently followed by the oral and vestibular surfaces, respectively. The STL format files of each digital model acquired from the SHINING 3D Dental Cloud software, IntraoralScan v 3.3.2.9, will be used. These will be imported into the CloudCompare v2.13.1 application, software for processing 3D data. A reference plane is used to alter the points that cause the model to be overlaid. The program identifies the reference plane as a mesh, using a technique to compare the distance between the point cloud of the overlaid model and the reference plane, which denotes the mesh. Consequently, C2M (cloud to mesh) serves as the metric used by the software to quantify the distance between the 3D coordinates of the overlaid digital models.

The reference model will be loaded first, followed by the model whose accuracy requires evaluation. To achieve optimal superimposition of the 3D images, the program option that ensures the most precise alignment of the digital models will be selected. It is essential to designate the reference model, and the model is to be aligned (Figure 4). After superimposition, the option to compute the distance between the point network of the digital model under analysis and that of the reference model will be chosen. Consequently, the lowest distance, typically equal to 0, the maximum distance, the average distance, and the

greatest error will be shown (Figure 5). A distance approaching zero indicates a higher fidelity of the analyzed model to the reference model, thereby reflecting greater precision in the scanning technique. The results are presented as a color code accompanied by a color scale, enabling direct visualization of the areas with varying scanning precision (Figure 6).

Figure 4. Alignment Procedure of Digital Models Using CloudCompare

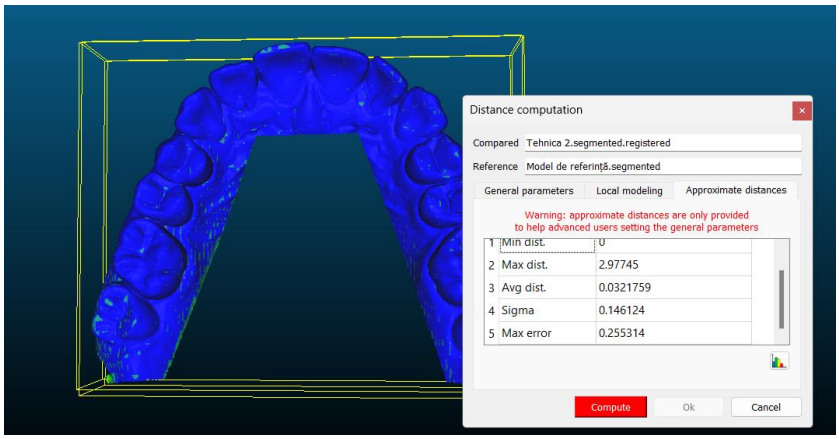

Figure 5. Numerical Visualization of Results in CloudCompare

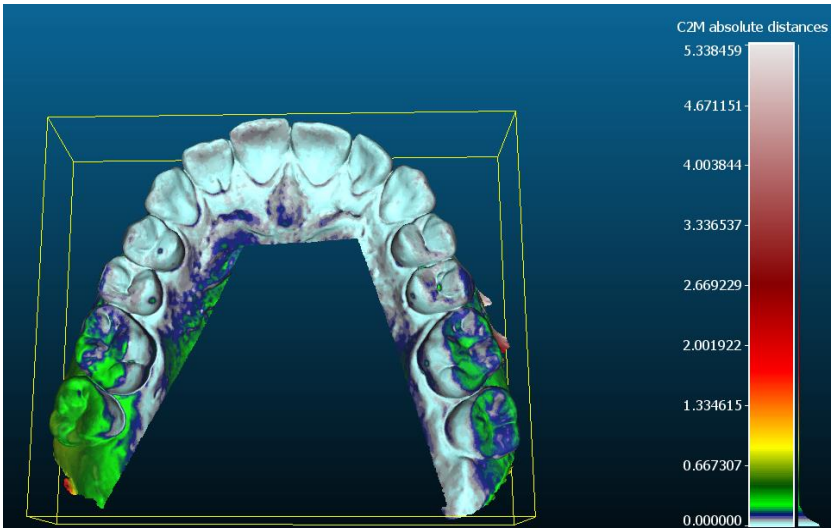

Figure 6. Visualization of Results Using Color Maps in CloudCompare

We will use the data in the graph made by the Ilustart software in Figure 7 to get a more accurate picture of the results. It displays on the abscissa the values of the distance

between points, ranging from 0 to the maximum distance, and on the ordinate the quantity of 3D points in the examined model. The Gaussian curve is overlaid over the graph to illustrate the distribution of distances among the dots. The average value of the curve signifies the mean distance among the 3D points of the overlapped models. This denotes, on average, the distance between the points on the model, which we will examine using a scanning approach, and the points associated with the reference model. A minimal value, approaching 0, indicates that the models are well-aligned, with the majority of points situated at a minimal distance, hence enhancing the accuracy of the scanning process used for the digital model.

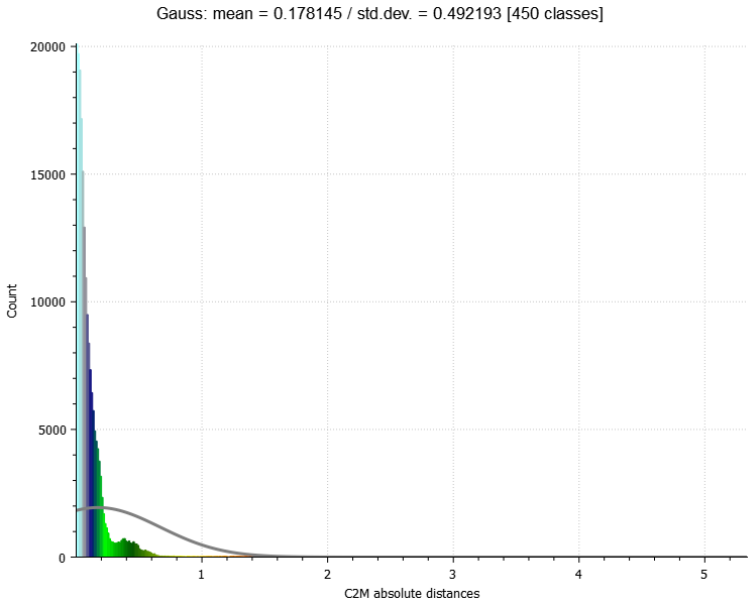

Figure 7. Graphical Visualization of Results with Gaussian Distribution Overlay in CloudCompare

ASSESSMENT OF EFFICIENCY—Digital records and scanning duration were used as measures to assess the efficacy of the scanning methodologies.

Digital records indicate the quantity of photos acquired during the scanning process until the digital model is finalized. A substantial quantity of digital records indicates increased scanning difficulties and reduced approach efficiency, whereas a minimal number of records implies excellent efficiency. The quantity of digital data was acquired from the program used to create the digital model (SHINING 3D Dental Cloud, IntraoralScan v 3.3.2.9) of the upper and lower arches, as well as the static occlusion for each patient and scanning approach.

The scanning duration was measured using a stopwatch, exhibiting accuracy to two decimal places in seconds. Consequently, the scanning approach becomes more efficient as the duration of the scan decreases. The duration from the commencement of the scan to its conclusion was considered. During the software's data processing phase, the time was paused between arch scans to accurately ascertain the duration assigned to each scanning method.

RESULTS

Table 2 summarizes the mean point-to-point 3D deviations obtained from the superimposed digital models.

Table 2. Average 3D Deviations Between the Compared Digital Models

Patient	S1L+Za Max	S1L+Za Mnd	S1L+Zf Max	S1L+Zf Mnd	S1Z Max	S1Z Mnd	S2L Max	S2L Mnd	S3L Max	S3L Mnd	S3L+Z Max	S3L+Z Mnd
1	0.022583	0.152093	0.032778	0.040701	0.008467	0.078166	0.013445	0.110322	0.042463	0.100978	0.060587	0.051273
2	0.178145	0.027712	0.142570	0.036524	0.079770	0.038810	0.105270	0.057564	0.163930	0.300532	0.063763	0.258782
3	0.014573	0.149652	0.013681	0.081077	0.034136	0.031977	0.041444	0.026761	0.021987	0.018992	0.100356	0.035365
4	0.022493	0.040580	0.016188	0.053069	0.024656	0.024010	0.019317	0.072086	0.017379	0.087690	0.022404	0.063726
5	0.086998	0.018420	0.020286	0.063753	0.024254	0.078023	0.039627	0.064897	0.021069	0.041440	0.027393	0.053836
6	0.017843	0.042702	0.029464	0.120362	0.025409	0.102304	0.013520	0.085245	0.015758	0.089594	0.134875	0.173458
7	0.020397	0.157772	0.079570	0.192049	0.010859	0.184315	0.024630	0.054123	0.035264	0.068945	0.052431	0.071213
8	0.045264	0.039856	0.035689	0.074536	0.023265	0.041298	0.034512	0.048532	0.023215	0.085612	0.053214	0.082354
9	0.039865	0.041516	0.028934	0.059483	0.015324	0.026143	0.031728	0.041132	0.025132	0.102030	0.042139	0.042561
10	0.013120	0.052134	0.036214	0.064123	0.036891	0.052196	0.041090	0.036710	0.029360	0.083791	0.034120	0.034821
Mean	0.046128	0.072244	0.043537	0.078568	0.028303	0.065724	0.036458	0.059737	0.039556	0.097960	0.059128	0.086739

The columns denote the scanning methods used in the research, while the rows signify the patients. The mean distance between the 3D points of the stacked models was recorded for each patient and each procedure. The values for both the maxilla and mandible were recorded in the table. The mean value for each scanning method will be computed in the last row, which will facilitate the identification of the technique with the greatest and lowest accuracy. Each arch will be reviewed independently.

Upon analysing the results, we determined that for the maxillary arch, the technique demonstrating the highest accuracy is the arch, 1 segment, utilizing zig-zag scanning movements (S1Z). The approach exhibiting the lowest accuracy for the maxillary arch was identified as the one executed in three segments using combined linear and zig-zag motions (S3L+Z). Furthermore, the analysis shows that the greatest distance is linked to strategies involving combined motions, with average values ranging between 0.04 and 0.06.

For the mandibular arch, it was shown that the 2-segment approach with linear motions (S2L) yields the most precise scan. The least accurate method is the one executed in three segments with a linear or continuous motion (S3L). The analysis shows that the greatest distances were obtained with the 3-segment scanning approaches, whereas the smallest distances were associated with strategies using a single type of movement, specifically the 2- and 1-segment methods.

The findings indicate that the accuracy of the scanning procedures varies depending on the dental arch. It is evident that for both arches, the 3-segment scan is the least accurate.

Tables 3 and 4 summarize the digital recording outcomes and the average scanning time associated with each scanning technique.

Table 3. Digital recordings obtained for each scanning technique

Patient	S1L	S1L+Za	S1L+Zf	S1Z	S2L	S3L	S3L+Z
1	2310	1436	2201	1952	1856	1837	2089
2	2322	2467	2161	1819	1661	1745	2013
3	1556	2026	2154	1949	1917	1975	1138
4	1904	1512	1456	1511	1691	1515	1773
5	1243	1161	1094	1002	1237	1037	1167
6	1152	1138	1154	1093	901	1148	1331
7	1061	1206	1203	1103	1032	1132	1320
8	1125	1203	1210	1115	1047	1122	1232
9	1097	1185	1175	1106	1033	1165	1178
10	1146	1095	1203	1186	1027	1152	1126
Mean	**1491.6**	**1442.9**	**1501.1**	**1383.6**	**1340.2**	**1382.8**	**1436.7**

The columns denote the scanning methods used in the research, while the rows signify the patients. The table included the number of records for each patient and each procedure.

The last row will provide the average value for each scanning method, which will be used to identify the technique with the greatest and lowest efficiency based on this criterion. Among all the assessed techniques, the 2-segment method employing linear scanning movements (S2L) exhibited the lowest average number of recordings. Consequently, this technique was the most effective regarding the criterion of digital recordings. The full-arch scanning approach using combined linear and zig-zag movements (S1L+Zf) yields the maximum number of recordings and is therefore the least efficient technique based on this criterion. A reduction in the quantity of digital recordings is seen with the segmentation of the dental arch, indicating that as the number of segments increases, the scanning procedures become more efficient.

Table 4. Scanning time allocated to each technique (minutes and seconds)

Patient	S1L	S1L+Za	S1L+Zf	S1Z	S2L	S3L	S3L+Z
1	0:04:20	0:04:15	0:03:52	0:02:56	0:02:53	0:03:25	0:03:33
2	0:04:00	0:04:07	0:03:40	0:02:57	0:02:48	0:03:17	0:03:24
3	0:03:08	0:03:23	0:03:37	0:02:12	0:03:20	0:03:10	0:03:24
4	0:02:30	0:02:40	0:02:28	0:02:42	0:02:42	0:02:36	0:02:53
5	0:04:50	0:03:53	0:02:59	0:03:07	0:04:26	0:03:05	0:03:06
6	0:03:14	0:03:26	0:02:40	0:03:05	0:02:40	0:03:12	0:03:17
7	0:02:38	0:03:04	0:03:00	0:02:45	0:02:50	0:03:09	0:03:23
8	0:02:53	0:03:16	0:03:15	0:02:53	0:03:13	0:03:20	0:03:14
9	0:03:25	0:03:32	0:03:19	0:02:43	0:03:28	0:03:11	0:03:32
10	0:03:37	0:03:55	0:03:12	0:02:54	0:03:04	0:03:22	0:03:42
Mean	**0:03:28**	**0:03:33**	**0:03:12**	**0:02:49**	**0:03:08**	**0:03:11**	**0:03:21**

The columns denote the scanning methods used in the research, while the rows signify the patients. The scanning duration for each patient and procedure was recorded in the table. The last row computes the average value for each scanning method, which was used to identify the technique with the greatest and lowest efficiency based on this time-related criterion. Among all the assessed techniques, the single-segment scanning approach using a zig-zag motion (S1Z) showed the shortest mean scanning time and was therefore the most time-efficient technique. The longest average scanning duration was recorded for the full-arch scan using linear motion supplemented by an anterior zig-zag segment (S1L+Za).

The analysis of efficiency based on scanning time reveals that the single-segment scanning approach using a zig-zag motion (S1Z) had the lowest duration. This makes it the most efficient scanning technology based on the time criteria. The maximum scanning duration was recorded for the technique involving a full-arch scan using linear motion supplemented by an anterior zig-zag segment (S1L+Za).

The findings indicate that the scanning approach deemed most efficient based on digital recording criteria does not align with the technique identified as most efficient according to time criteria. Consequently, it is evident that there is no connection between these two criteria.

DISCUSSIONS

This study made it possible to investigate the accuracy and efficiency of different scanning strategies performed through distinct methods, including various arch segmentations (one, two, or three segments) and motion patterns (linear, zig-zag, or combined). Results were inconsistent across criteria and varied with respect to the scanned arch. Better results were obtained with strategies that employed only one movement type rather than a combination; therefore, digital records indicated that the linear method had the best efficiency, while zig-zag scanning provided optimal results for scanning time. There was

no clear disadvantage to one- versus two-segment scans of the arch, although they did have different profiles in terms of efficiency.

Concerning accuracy, we noted that the findings vary based on the scanned arch, yielding distinct outcomes for the maxilla and mandible. For the maxilla, superior precision is achieved by the arch scan, using one segment in a zig-zag pattern, but for the mandible, the linear approach employing two segments is preferred. These findings align with those deemed most efficient based on the examined criteria. It was noted that when the number of segments increased to three and combined motions were used, the precision of the scans diminished.

In summary, the research indicates that intraoral scans attain the optimal equilibrium of accuracy and efficiency when executed in a singular, uniform motion—either linear or zig-zag. Scanning the arch in one or two segments did not significantly affect the findings; however, segmenting the arch into three parts and using various scanning movements consistently decreased both accuracy and scanning efficiency. From an efficiency perspective, the zig-zag method exhibited the briefest scanning duration, while the two-segment linear methodology yielded the most consistent digital records. Conversely, the S1L+Zf procedures had the lowest efficiency. In terms of precision, the maxilla had the greatest accuracy with the single-segment zig-zag approach, but the mandible demonstrated optimal performance with the two-segment linear scan. The lowest accuracy results were linked to the three-segment combined-motion methodologies.

Numerous research studies in the literature have examined the influence of various scanning processes on the precision and efficacy of the final digital models. These studies may vary based on the scanner used, the methodologies utilized, the proficiency of the operator, the quantity of scans conducted, the software used for analysis, and several other factors.

A study aimed at identifying the most precise scanning technique through segmental methods and combined movements concluded that the results of arch scans are not highly comparable to those of two-segment scans, with accuracy diminishing as the number of segments increases to three and when employing zig-zag movements [5]. A plastic arch was used for scanning and affixed to a mannequin for this investigation. In our investigation, we used several scanning segments (1, 2, 3) and utilized linear, zig-zag, or mixed motions for analysis, culminating in 10 distinct scanning strategies. The scans were conducted by a seasoned physician using a distinct scanner (i700; Medit, Seoul, Korea). To evaluate accuracy, the geometric disagreement of the scans was computed using software by measuring the interpremolar, intermolar, and anteroposterior distances, along with the overall surface deviation, using the same methodology used in the current investigation. Consequently, our findings align on the beneficial effects of methods using a singular scanner movement and minimizing the segmentation of arch scans. Although the study indicates that zig-zag movement diminishes accuracy, our research suggests that this movement yields the maximum accuracy for the maxillary arch.

Further research also investigated the influence of the scanning method on both accuracy and efficiency, including an assessment of scanning duration [11].

Fifteen undamaged models of the post-orthodontic treatment mandibular arch were scanned using a laboratory scanner as a reference model and an office scanner (i500 Medit) using three scanning approaches, all arch-based, differing only in the movement of the scanner head. The manual scans were conducted twice by one examiner and then duplicated by a second examiner, yielding 180 digital models. The reference models were overlaid using the Viewbox 4 program. The accuracy was assessed by measuring the distance between the 3D points constituting the digital models. Consequently, the most advantageous values were noted with the mixed movement approach, while the least beneficial were associated with the linear technique [11]. The findings contradict our observations, which indicate that the most

precise procedures include linear or zig-zag motion, rather than combination methods. The zig-zag motion scanning recorded the smallest duration, whereas the combined motion scanning recorded the greatest duration [11]. The findings align with our studies on scan efficiency, indicating that the least scanning duration occurs during arch scanning using zig-zag movements, whereas strategies employing combined motions need more time for execution.

Further research sought to ascertain the impact of scanning technology on the accuracy, precision, and speed of full-arch scanning, using four distinct kinds of intraoral scanners [12]. A custom model was employed as a reference, possessing the identical refractive index of dentin and enamel found in natural teeth, to replicate natural dentition. The digital reference model was initially created using an ATOS III Triple Scan 3D optical scanner. Four scans were conducted with each scanner, matching to each procedure, executed by seasoned physicians with a minimum of three years of expertise with the relevant scanner. A total of 16 scans were conducted for each scanner type. The scanning methodologies adhered to the manufacturers' specifications. Consequently, arch scanning methodologies employing combined movements, two-segment scans utilizing a singular movement type, either linear or zig-zag, and integrated movements were implemented. The duration of each scan was also documented. All experimental scans were transformed into the standard STL format, and with the software Geomagic Control X, the experimental images were juxtaposed with the reference scans [12]. The findings indicated that the 2-segment scanning methodology with linear motions achieved the best accuracy, aligning with our study's identification of the most precise method for the mandibular arch. The analysis determined that the most rapid method is executed in two segments using coupled movements, whilst the approach employing zig-zag motions in two segments exhibited the longest average duration [12]. Consequently, these findings are inconsistent with those from our investigation; rather, they are contradictory, since we recorded a shorter duration for the zig-zag arch scan and a less favorable scanning time for the arch scan using combined motions.

A separate research [3] examined the most precise scanning approach by using a novel procedure for assessing scan data correctness. Five sets of plastic dental arches—maxillary and mandibular—were used, yielding a total of 10 models, which were scanned using two distinct intraoral scanners. A reference digital model was acquired for each arch using an industrial high-precision scanner. The scanning methodologies were categorized into two comprehensive arch linear approaches—one executed horizontally and the other including a 180° vertical rotation of the scanner tip in the front area—and a third segmental technique, whereby the arch was partitioned into three parts. In the horizontal linear method, the scanner head was mostly aligned parallel to the occlusal plane, but in the rotated-linear method, the scanner was vertically inverted at the front tooth level to enhance data acquisition in that area. The acquired digital models were individually overlaid onto their respective reference scans, and accuracy was determined based on absolute distance measurements. The findings indicated that, irrespective of the scanner used, the three-segment scanning method consistently yielded the lowest accuracy, suggesting that single-segment full-arch scans are superior. The findings correspond closely with the results of the current investigation, where the least favorable values were also seen for the three-segment combined-motion scans. The cited research emphasized the significance of scanner orientation in the front area, demonstrating that optimal accuracy is attained when the scanner tip is positioned vertically at the level of the incisors.

The present findings correspond to earlier work that supported the conceptual framework of this study [13].

Upon comparing the current results with those documented in worldwide research, several commonalities emerge, especially about the methods that improve scanning

efficiency. As previous studies have shown, the zig-zag motion was the fastest, but the combined-motion methods were the least effective. Both concordances and discrepancies were noted regarding accuracy. Consistent with two of the cited studies, our findings indicate that optimal accuracy is achieved with a single scanning motion and by scanning the arch in minimal segments. Divergences across research may be attributed to discrepancies in materials, experimental configurations, and scanning methodologies. A crucial divergence is in the sort of sample used. This investigation used direct scanning of human individuals, in contrast to several worldwide studies that utilize prosthetic dental arches affixed to mannequins. Clinical factors—such as humidity, soft-tissue movement, restricted mouth opening, and illumination—can profoundly affect scan precision and efficacy. The limited sample size and anatomical diversity across individuals further exacerbate these discrepancies. The proficiency of the operator is an additional significant consideration. This research included scans conducted by a physician with less competence in intraoral scanning, while other trials used proficient operators or scanning specialists. Differences in scanning technique—velocity, orientation, force, and hand steadiness—can lead to discrepancies even among skilled practitioners. Moreover, variations in scanner technology, software algorithms, and file-processing platforms (Aoralscan 3, SHINING 3D Dental Cloud, and CloudCompare) may influence the results. Variations in sensor resolution, data-processing algorithms, and lighting sensitivity across scanner types need a thorough comprehension and accurate implementation of manufacturer standards. These criteria underscore significant issues for further study. Research using bigger and more heterogeneous samples, consistent imaging techniques, and controlled assessment of factors such as operator expertise, moisture, illumination, and anatomical morphology might greatly enhance the comprehension and optimization of intraoral scanning precision.

Additional data from the literature confirm the effects of the scanning approach, arch length, and operator variables on intraoral scan performance. Ender and Mehl have demonstrated that full-arch scans progressively accumulate stitching errors, in particular when long spans are scanned with irregular or multidirectional motions; thus, it is pointed out that a scanning path with a stable and predictable scanning trajectory is necessary to keep accuracy and precision [14]. Mangano et al. reached the same conclusions and revealed that even high-tech scanners present large accuracy deviations when they are frequently rescanned or moved unpredictably; hence, the importance of proper, uninterrupted scanning to achieve the best results is emphasized [15]. Joda and Brägger argued that the digitally optimized processes not only improve the clinical efficiency as more operating time is saved but also reduce the clinician's fatigue, which is of great advantage when limited scanning repetitions or overlapping runs are performed [16]. Their findings are consistent with the current research, as the single-motion approach was found to be more time-efficient and predictable than the combined-motion one. Moreover, extensive research on full-arch impressions is a strong source of evidence for pointing out the problems that arise with lengthy digital impressions. Keul and Güth reported that full-arch scans are more prone to distortions than short-span impressions under both laboratory and real-life conditions, and it is particularly true when the scanning paths involve abrupt changes in the direction of the segments [17]. Their findings strongly support the present results, as the inaccuracies that accumulate along the arch due to the three-segment and combined-motion methods are indicated. Rutkunas et al. made similar conclusions that the accuracy of full-arch digital imprints is greatly lowered, especially in vivo, where factors like saliva, soft-tissue motion, and patient movement make stitching inconsistencies more severe [18]. Their study emphasizes the effects of clinical considerations on the exacerbation of the negative impacts of complex scanning patterns. Thus, it is consistent with the decline of accuracy associated with three-segment or mixed-motion procedures in this research. Taking all together, our findings

back up the claim that simplified, continuous scanning strategies that are done in one or two segments and without unnecessary changes in the direction of the scan provide higher accuracy and speed most of the time. The combined evidence from carefully controlled in vitro experiments and clinical trials conducted in real life shows the significance of the scanning route in the enhancement of full-arch digital impressions regardless of the type of the scanner or the skills of the operator.

Clinical Implications

Finding from this research have several practical applications that can directly affect everyday clinical practice. To begin with, clinicians ought to employ simple and uniform scanning movements, a linear or zig-zag motion being the most preferable, to attain higher accuracy in full-arch scans and thus, eliminate the occurrence of complex combined-motion patterns. Next, performing the scan of the arch in one or two segments is generally enough, and thus, the number of the stitching errors caused by three-part scans is lowered. Also, newcomers to digital dentistry can yield more dependable results if they go for continuous full-arch scan paths, as these require less proficiency and the possibility of a rescan is kept at a minimum. Lastly, by merely changing the direction of their scanning, clinicians could free up more time in their schedules, make their patients more comfortable, and enhance their productivity, thereby achieving accurate digital impressions and better clinical outcomes.

Study Limitations and Future Directions

This study is limited by its sample size that is small and taken from only one educational institution. The demographic characteristics of the sample include people with complete arches and limited age ranges. The authors also mention that the results are probably not generalizable to people with extensive restorations, edentulous areas, and severe periodontal disease. Moreover, this study compared the use of an intraoral scanner and software workflow (Aoralscan 3, SHINING 3D; SHINING 3D Dental Cloud, IntraoralScan) for all scans. This means that the results of the paper are part of the local ecosystem of this particular device and platform and cannot be easily transferred to other equipment or platforms. Additionally, a single operator performed all the scans, and this person was somewhat inexperienced. So the representative clinical setting of early adopters is achieved; however, the issue of inter-operator variability and the effect of the learning curve cannot be investigated. Lastly, the experimental assessment solely focused on static occlusion and full-arch scans, neglecting dynamic occlusal connections or partial-arch situations. Further studies should correct the above-mentioned shortcomings of this study, including bigger and more diverse samples from other institutions, different clinical illnesses, and prosthetic scenarios. The comparative analyses of various intraoral scanners, software versions, and hardware configurations will help discern whether the scanning approach effects depend on the device or are generally applicable. It would be advantageous to design studies that classify operators according to their skill level and systematically evaluate the learning curve for different scanning patterns. In addition, future studies could examine the impact of environmental and clinical factors such as moisture regulation, soft-tissue handling, lighting, and oral aperture under controlled conditions. Finally, the use of advanced analytical tools such as automated error mapping and AI-assisted route optimization may ultimately provide standardized, evidence-based scanning methods that are not only accurate but also efficient in everyday clinical practice.

CONCLUSIONS

This study effectively determined scanning protocols that optimize accuracy and efficiency for full-arch intraoral digital impressions. The most accurate protocols were a single-segment zig-zag scan for the maxilla (S1Z) and a two-segment linear scan for the

mandible (S2L). Zig-zag motion yielded the shortest time to complete a scan, while two-segment linear motion required the least amount of digital data. Combined-motion approaches were always less accurate and efficient than single-motion protocols. Direct in vivo scanning with a novice operator added clinically relevant information on how the choice of scanning method affects results in day-to-day practice. Consistent motion patterns with minimal segmentation provide the best reliability in terms of accuracy versus operational efficiency trade-offs. Future studies should use larger and more varied samples, different types of scanners, and operator-related variables to further refine support for scanning techniques. This study supports an immediate clinical move toward streamlined scanning procedures and suggests standardization of full-arch scanning protocols within digital dentistry.

Conflicts of Interest

The authors declare no conflict of interest.

REFERENCES

[1] Christopoulou I, Kaklamanos EG, Makrygiannakis MA, Bitsanis I, Perlea P, Tsolakis AI. Intraoral Scanners in Orthodontics: A Critical Review. Int J Environ Res Public Heal. 2022;19(3):1407.

[2] Nulty AB. 3D Printing Part 1: A History and Literature Review of 3D Printing Technologies Used in Dentistry. Preprints. 2021; 202105.0221.v1.

[3] Richert R, Goujat A, Venet L, Viguie G, Viennot S, Robinson P, et al. Intraoral Scanner Technologies: A Review to Make a Successful Impression. J Healthc Eng. 2017; 2017:8427595.

[4] Ramiro GP, Coronel CA, Navarro AF, Hassan B, Tamimi F. Digital Restorative Dentistry, A Guide to Materials, Equipment, and Clinical Procedures. 2019;41–54.

[5] Mai HY, Mai HN, Lee CH, Lee KB, Kim S yeun, Lee JM, et al. Impact of scanning strategy on the accuracy of complete-arch intraoral scans: a preliminary study on segmental scans and merge methods. J Adv Prosthodont. 2022;14(2):88–95.

[6] Oh KC, Park J, Moon HS. Effects of Scanning Strategy and Scanner Type on the Accuracy of Intraoral Scans: A New Approach for Assessing the Accuracy of Scanned Data. J Prosthodont. 2020;29(6):518–23.

[7] Martínez-Rodríguez C, Patricia JP, Ricardo OA, Alejandro IL. Personalized Dental Medicine: Impact of Intraoral and Extraoral Clinical Variables on the Precision and Efficiency of Intraoral Scanning. J Pers Med. 2020;10(3):92.

[8] Hong-Seok P, Chintal S. Development of High Speed and High Accuracy 3D Dental Intra Oral Scanner. Procedia Eng. 2015;100:1174–81.

[9] SUESE K. Progress in digital dentistry: The practical use of intraoral scanners. Dent Mater J. 2020;39(1):52–6.

[10] SHINING 3D. Aoralscan 3: User Manual [manual]. Hangzhou, China: SHINING 3D; 2021.

[11] Gavounelis NA, Gogola CMC, Halazonetis DJ. The Effect of Scanning Strategy on Intraoral Scanner's Accuracy. Dent J. 2022;10(7):123.

[12] Latham J, Ludlow M, Mennito A, Kelly A, Evans Z, Renne W. Effect of scan pattern on complete-arch scans with 4 digital scanners. J Prosthet Dent. 2020 Jan;123(1):85-95. doi: 10.1016

[13] Grigoreac I. Impactul tehnicii de scanare asupra preciziei şi eficienţei scanării intraorale [dissertation]. Timişoara: Universitatea de Medicină şi Farmacie „Victor Babeş"; 2024.

[14] Ender A, Mehl A. Accuracy of complete-arch dental impressions: a new method of measuring trueness and precision. J Prosthet Dent. 2013;109(2):121–8.

[15] Mangano FG, Veronesi G, Hauschild U, Mijiritsky E, Mangano C. Trueness and precision of four intraoral scanners in oral implantology: a comparative in vitro study. PLoS One. 2016;11(9):e0163107.

[16] Joda T, Brägger U. Digital vs. conventional implant prosthetic workflows: a cost/time analysis. Clin Oral Implants Res. 2015;26(12):1430–5.

[17] Keul C, Güth JF. Accuracy of full-arch digital impressions: an in vitro and in vivo comparison. Clin Oral Investig. 2019;23(5):2061–6.
[18] Rutkunas V, Gedrimiene A, Akulauskas M, Fehmer V, Sailer I, Jegelevicius D. In vitro and in vivo accuracy of full-arch digital implant impressions. Clin Oral Implants Res. 2022;33(1):89–100.

Internal Fit of Cobalt–Chromium Metal–Ceramic Crowns Fabricated by Conventional Casting and Selective Laser Sintering: An In Vitro Comparison of Three Measurement Techniques

https://doi.org/10.70921/medev.v31i4.2019

Daniela-Maria Pop[1,2†], Lucian Floare[3,4†], Delia Abrudan Luca[3,4], Vlad Tiberiu Alexa[3,4*], Tareq Hajaj[1,2], Boris Dusan Caplar[1,2], Lavinia Simona Florea[2], Cristian Zaharia[1,2], Doina Chioran[5]

[1]*Victor Babes University of Medicine and Pharmacy, Faculty of Dentistry, Department of Prostheses Technology Propaedeutics and Dental Materials, Bd. Revolutiei 1989 nr. 9, et IV, Timisoara 300041, Romania*
[2]*Research Center in Dental Medicine Using Conventional and Alternative Technologies, Department of Prostheses Technology and Dental Materials, Faculty of Dental Medicine, "Victor Babes" University of Medicine and Pharmacy of Timisoara, 9 Revolutiei 1989 Ave., 300070 Timisoara, Romania*
[3]*Clinic of Preventive, Community Dentistry and Oral Health," Victor Babes" University of Medicine and Pharmacy, Eftimie Murgu Sq. no. 2, 300041, Timisoara, Romania*
[4]*Translation and Experimental Clincal Research Center in Oral Health (TEXC-OH), Department of Preventive, Community Dentistry and Oral Health," Victor Babes" University of Medicine and Pharmacy, 14 A Tudor Vladimirescu Ave., 300173, Timisoara, Romania*
[5]*Department of Anesthesiology and Oral Surgery, "Victor Babeş" University of Medicine and Pharmacy, Eftimie Murgu Sq. No. 2, 300041 Timisoara, Romania*
[†]*These authors contributed equally to this work.*

Correspondence to:
Name: Vlad Tiberiu Alexa
E-mail address: vlad.alexa@umft.ro

Received: 02 December 2025; Accepted: 05 December 2025; Published: 15 Deceember 2025

Abstract

1.Background/Objectives: *The purpose of this study was to compare the internal fit of cobalt-chromium metal-ceramic single crowns fabricated through conventional casting versus selective laser sintering (SLS), and to determinate the relative accuracy of three internal space measurement techniques.* ***2.Methods:*** *A standardized CAD design of a maxillary first molar was used to create two metal frameworks, one produced by was-pattern milling followed by casting and the other by SLS. Internal fit was assessed before and after ceramic firing using methods: differential micrometer measurements on frameworks with and without impression material, direct micrometer readings of detached silicons replicas, and digital microscopy of sectioned silicone specimens.* ***3.Results:*** *For the cast metal framework, mean internal gaps ranged from 0.08 to 0.09 mm with micrometer-based techniques and reached 0.1056 mm under digital microscopy. In contrast, the SLS framework showed larger discrepancies, with microscopic mean values up to 0.1806 mm and maximum occlusal gaps of 0.354 mm. After ceramic veneering, the cast crown maintained uniform internal fit (mean values of 0.08 mm with micrometers and 0.0784 mm with microscopy), whereas the SLS crown preserved higher variability and occlusal gaps up to 0.352 mm. Across all specimens, micrometer techniques yielded mean gaps of approximately 0.08–0.10 mm, while digital microscopy provided*

higher means of 0.1056–0.1806 mm, reflecting greater sensitivity to local irregularities. ***4. Conclusions:*** *Within the limitation of the study, conventionally cast frameworks demonstrated a more favourable internal fit than SLS frameworks, and digital microscopy proved to be the most reliable method for evaluating internal adaptation in metal-ceramic crowns.*

Keywords: metal-ceramic crowns; internal fit; CAD/CAM, prosthodontics; selective laser sintering

INTRODUCTION

Metal–ceramic restorations remain a cornerstone of fixed prosthodontics due to their favourable combination of mechanical strength, versatility and long-term clinical performance [1-3]. Despite the increasing popularity of all-ceramic systems, metal–ceramic single crowns and fixed partial dentures continue to be widely prescribed, particularly in posterior regions where high masticatory loads require reliable frameworks [1-3]. In such clinical scenarios, the longevity of treatment is not determined solely by the intrinsic properties of the materials used, but also by how accurately the restoration reproduces the prepared tooth geometry. Among the multiple factors that influence success, the quality of the fit between the crown and the prepared abutment has been consistently identified as a key determinant of biological and mechanical outcomes.

Internal and marginal discrepancies may compromise the integrity of the luting cement, promote microleakage and plaque accumulation, and ultimately increase the risk of secondary caries, periodontal inflammation, loss of retention and biological or technical complications over time [5-7]. Even when restorations are fabricated from materials with excellent mechanical properties, an inadequate internal fit may produce unfavourable stress distributions within the cement layer and at the tooth–restoration interface, potentially predisposing to debonding, fracture or failure under functional loading [5-8]. Consequently, the assessment of internal fit has become an essential component in the evaluation of new restorative materials, manufacturing technologies and clinical protocols.

From a clinical perspective, internal fit is generally defined as the perpendicular distance between the internal surface of the restoration and the prepared tooth surface, measured at specific reference points. Optimal values should allow sufficient space for the luting agent to achieve complete seating and adequate flow, while avoiding excessive thicknesses that may weaken the cement layer or impair seating [5-8]. Previous investigations have suggested that internal gaps in the range of approximately 50–150 μm can be considered clinically acceptable, depending on the restorative material, cement type and loading conditions [5-8]. However, these thresholds are not absolute and may be influenced by the location of the discrepancy (axial versus occlusal), the type of finish line and the geometry of the preparation. Notably, many experimental studies report a wide variation of gap values for apparently similar restorative systems, reflecting not only differences in fabrication workflows but also substantial variation in measurement methodologies and evaluation criteria.

The evolution of computer-aided design and computer-aided manufacturing (CAD/CAM) has profoundly changed the traditional fabrication of fixed restorations. Subtractive milling of wax patterns or pre-sintered blocks and, more recently, additive manufacturing technologies such as selective laser sintering (SLS) and direct metal laser sintering (DMLS) have been introduced with the aim of reducing the technique sensitivity associated with manual wax-up and conventional casting [4,9-13]. These digitally driven workflows were developed to standardize production, minimize human error and improve the reproducibility of prosthetic frameworks. In particular, SLS technology allows the fabrication of cobalt–chromium (Co–Cr) frameworks directly from STL files, theoretically enabling a closer correspondence between the virtual design and the final metal infrastructure [4,9-13].

However, the translation of digital design into a physical restoration is influenced by a complex chain of events. In subtractive workflows, milling strategies, bur diameter, tool wear and material properties can all affect the dimensional accuracy of the wax pattern or pre-

sintered framework [4,9-13]. In additive manufacturing, the layer-by-layer consolidation of metal powder, the characteristics of the alloy, build orientation, laser parameters and post-processing procedures (heat treatment, support removal, surface finishing) may introduce distortions and residual stresses, which can negatively influence marginal and internal adaptation [9-13,14-18]. As a result, the theoretical advantages of digital workflows do not automatically translate into superior internal fit in all clinical or laboratory situations.

The literature currently offers conflicting evidence regarding the comparative performance of additive and conventional fabrication techniques in terms of internal and marginal fit. Some in vitro and clinical studies suggest that SLS or DMLS frameworks may offer improved consistency and can achieve internal and marginal gaps within clinically acceptable ranges, comparable to or even better than those obtained with traditionally cast restorations [9-13]. Conversely, other investigations indicate that conventionally cast Co–Cr infrastructures still provide superior or more homogeneous internal adaptation, particularly in occlusal areas or in regions with complex preparation geometry [9-13,14-18]. These discrepancies may be explained, at least in part, by differences in study design (tooth type, preparation geometry, finish line configuration), scanner and software systems, alloy composition, cement space settings and the specific parameters used for additive manufacturing and post-processing [9-13,14-18]. As a consequence, direct comparison between studies is challenging, and clinicians receive mixed messages regarding which fabrication workflow offers more predictable internal fit in daily practice.

Methodological variability in the assessment of fit further complicates the interpretation of published data. A wide range of techniques has been used to evaluate marginal and internal adaptation, including direct sectioning of restorations and microscopic analysis, various adaptations of the replica technique, computed tomography and 3D digital evaluation [5-8,14-16]. Micrometer-based methods are relatively accessible, do not require sophisticated equipment and can be implemented in many laboratory settings; however, they are sensitive to operator handling, specimen positioning and potential elastic deformation of the silicone material used to reproduce the internal space [5-8]. Digital optical microscopy of sectioned replicas improves visualization and allows repeated measurements at standardized reference points, but it is more time-consuming and may yield higher gap values because of its greater sensitivity to local irregularities and minor surface defects [5-8,14-16]. The absence of a universally accepted gold standard, together with variations in replica thickness, sectioning protocols and calibration of measurement devices, can significantly influence the reported outcomes and contribute to apparent inconsistencies across studies.

In addition, internal fit may be affected not only by the framework fabrication process but also by the subsequent ceramic veneering procedures. Repeated firing cycles, differences in the coefficient of thermal expansion (CTE) between metal and ceramic, and residual stresses induced during cooling can all influence the final adaptation of the crown [14-18]. Some authors have reported minimal changes in internal and marginal gaps after veneering, while others have observed increased discrepancies in certain areas, especially at the occlusal surface [14-18]. Therefore, studies that assess internal fit both before and after ceramic firing provide more clinically relevant information than those restricted to framework analysis alone.

Given this complex background, there is a clear need for investigations that control the design and manufacturing variables as strictly as possible and, at the same time, systematically compare different measurement techniques within the same experimental setup. In particular, studies that derive both conventional and SLS frameworks from an identical CAD design, apply standardized cement space parameters, evaluate internal fit at predefined reference points and analyse changes induced by ceramic veneering can help clarify whether discrepancies arise primarily from the fabrication workflow, the veneering

process or the evaluation method itself [9-18]. Such data are especially relevant for clinicians and dental technicians who must decide whether the transition to additive manufacturing technologies offers tangible benefits in terms of internal adaptation and long-term prosthetic performance.

Aim and objectives

The primary aim of this in vitro study was to evaluate and compare the internal fit of cobalt–chromium metal–ceramic crowns fabricated using two distinct production workflows, namely conventional casting based on a wax pattern and additive manufacturing through selective laser sintering (SLS). A further objective was to investigate the extent to which different internal space assessment protocols influence the recorded gap values and, consequently, the perceived accuracy and reliability of internal fit evaluation. By jointly analysing fabrication method and measurement technique, the study sought to generate more robust evidence regarding the internal adaptation of metal–ceramic crowns produced by conventional and additive technologies.

MATERIAL AND METHODS

This in vitro study evaluated the internal fit of two cobalt–chromium metal–ceramic single crowns fabricated using different production workflows: conventional casting and selective laser sintering (SLS). A maxillary first molar abutment (tooth 2.6) mounted on a mobilizable study model served as the substrate for all analyses.

This research was designed as an exploratory in vitro pilot study. Consequently, the experimental sample was intentionally limited to two cobalt–chromium frameworks per fabrication workflow (conventional casting and SLS), all derived from the same standardized CAD design. This restriction reflects both the laboratory constraints associated with the complex multi-step fabrication and measurement protocol and the primary objective of the study, which was to document qualitative trends and descriptive differences rather than to perform formal statistical inference. In line with this design, the results are presented as individual values, ranges and arithmetic means, and no inferential statistical tests were undertaken; therefore, the findings should be interpreted as preliminary data that may inform and support future studies with larger sample sizes.

The working model and the antagonist arch were scanned using the Medit T310 extraoral scanner (Medit Corp., version 2.5.1). A standardized crown design was created in Exocad DentalCAD (Exocad GmbH, version Galway 3.1), ensuring identical morphology and cement space parameters for both metal frameworks

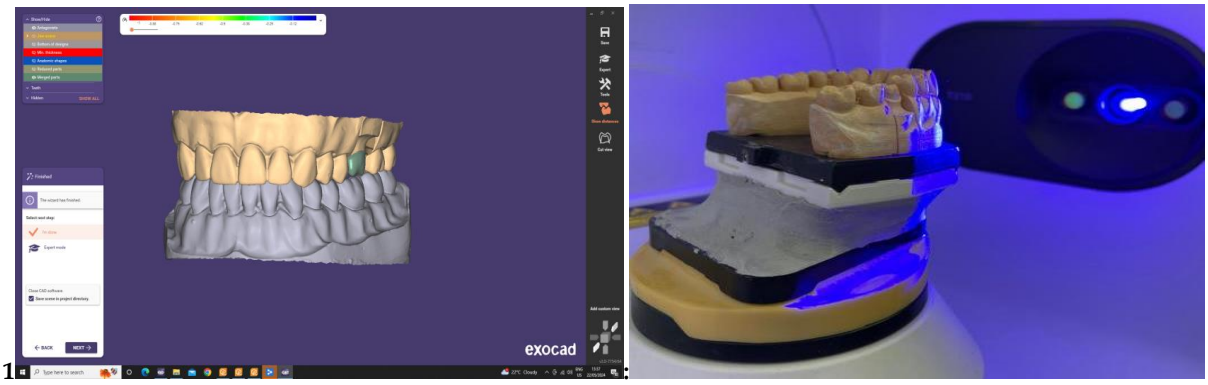

Figure 1. Scan & CAD design

Fabrication of the Cast Framework

The STL design file was exported to the UpMill P53 UP3D milling unit to generate a wax pattern from a prefabricated CAD/CAM wax disc. The pattern was sprued, invested, and cast using a Co–Cr alloy (Realloy-C) in a vacuum-assisted induction casting machine (Galloni Fusus 72). Post-processing included divesting, sprue removal, finishing, and airborne-particle abrasion with 110 µm aluminum oxide.

Fabrication of the SLS Framework

Using the same STL file, a second framework was produced by selective laser sintering in the GE Additive M2 Cusing Lab 200R system, employing CoCrW alloy powder. Post-processing included controlled cooling, powder removal, heat treatment, support removal, finishing, and identical airborne-particle abrasion to standardize surface preparation.

Both metal frameworks were veneered using the IPS InLine ceramic system (Ivoclar Vivadent). The protocol included bonding application, opaque firing, dentin and incisal layering, correction firing, finishing, and final glazing performed in the Programat EP 3010 furnace, following manufacturer specifications.

Internal fit was evaluated before and after ceramic veneering using three distinct techniques at five predetermined reference points: vestibular, oral, mesial, distal, and occlusal.

At each of the five reference sites (vestibular, oral/palatal, mesial, distal and occlusal), three consecutive measurements were performed per specimen and per technique, and their arithmetic mean was calculated to obtain a single value for each point. The Ritter Dent micrometer and the wax micrometer used in this study had a nominal resolution of 0.01 mm and an accuracy of ±0.01 mm, according to the manufacturers' specifications, and both instruments were checked for zero error and proper function before each measurement session. All micrometer readings were carried out by the same operator, who was trained in the use of the devices and followed a standardized measurement sequence in order to minimize operator-dependent variability. The digital optical microscope was calibrated before data collection using a certified calibration slide, and linear distances were recorded with the dedicated software at fixed magnification under controlled room temperature conditions.

Using a Ritter Dent micrometer, the thickness of each metal framework was measured before and after injecting low-viscosity condensation silicone (Zhermack Oranwash L with Indurent Gel) into the crown and seating it on the abutment. The internal gap was calculated as the difference between the two measurements.

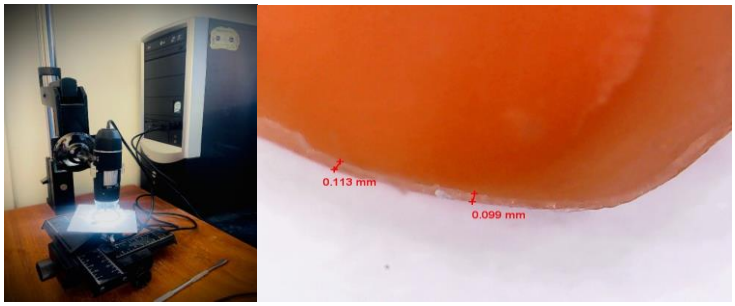

Figure 2. Measurement Procedure

After polymerization, silicone was carefully removed intact, sectioned vestibulo-orally, and measured directly with a wax micrometer to prevent perforation. Care was taken to preserve the integrity of the replica to avoid measurement errors.

For the replica-based assessments, low-viscosity condensation silicone (Zhermack Oranwash L with Indurent Gel) was injected into the crowns and allowed to polymerize fully before removal. After setting, the silicone films reproducing the internal space were carefully detached from the crowns, sectioned and inspected to exclude specimens with visible defects or tearing. The thickness of the silicone layer at the measured sites, corresponding to the local internal gap, ranged approximately between 0.05 and 0.35 mm, depending on the reference point and fabrication method. To reduce elastic deformation during measurement, replicas were handled with minimal manual stress, positioned in a reproducible manner between the micrometer anvils and on the microscope stage, and measured under constant, low contact pressure.

Sectioned silicone replicas were stabilized on the microscope support and analyzed using a digital optical microscope with dedicated software. Measurements were obtained directly from the digital interface to ensure precision.

Figure 3. Digital Microscopy Measurement

After ceramic veneering, the same three measurement techniques were repeated on the finished metal–ceramic crowns to determine whether firing induced changes in internal adaptation.

RESULTS

Internal fit measurements were performed on four cobalt–chromium specimens: two metal frameworks (P1—cast, P2—SLS) and their corresponding metal–ceramic crowns after veneering (P3—cast, P4—SLS). Three measurement techniques were applied: differential micrometer readings, direct silicone replica measurement, and digital optical microscopy. The numerical outcomes obtained through these methods are presented in Tables 1–4. Given that internal gaps between 0.05 and 0.15 mm (50–150 µm) are generally regarded as clinically acceptable for cemented crowns [5–8], the following results are described in relation to this threshold.

Given the extremely small sample size inherent to this pilot design, inferential statistical analysis was not performed. All results are therefore reported descriptively, as individual measurements, ranges and arithmetic means, without claims of statistical significance.

Overall, the internal gap values recorded with the two micrometer-based techniques were closely aligned, whereas digital microscopy consistently produced higher measurements and showed greater sensitivity to subtle variations in silicone thickness.

For the cast metal framework (P1), internal gap values ranged between 0.05 and 0.10 mm at the five reference points, with a mean value of 0.09 mm for both micrometer techniques. Digital microscopy revealed a slightly higher mean of 0.1056 mm, indicating that this method may detect finer discrepancies that are not captured manually. These findings are

summarized in Table 1. All internal gap values recorded for the cast metal framework (P1), irrespective of the measurement technique, remained within the 0.05–0.15 mm clinically acceptable interval.

Table 1. Internal Fit Measurements for Cast Metal Framework (P1)

Measurement (mm)	Vestibular	Oral	Mesial	Distal	Occlusal	Mean
Differential micrometer	0.10	0.05	0.10	0.10	0.10	0.09
Direct silicone measurement	0.10	0.05	0.10	0.10	0.10	0.09
Digital microscopy	0.079	0.087	0.105	0.113	0.144	0.1056

In the SLS framework (P2), a similar distribution pattern was observed; however, the occlusal area exhibited notably larger discrepancies, reaching up to 0.354 mm under microscopic evaluation. This resulted in the highest mean internal gap among all frameworks (0.1806 mm). Such values suggest a lower precision of internal adaptation compared with the cast specimen, particularly in the occlusal region, where additive manufacturing processes are more susceptible to cumulative layering deviations, as shown in Table 2.

Table 2. Internal Fit Measurements for SLS Metal Framework (P2)

Measurement (mm)	Vestibular	Oral	Mesial	Distal	Occlusal	Mean
Differential micrometer	0.10	0.05	0.10	0.10	0.10	0.09
Direct silicone measurement	0.10	0.05	0.10	0.05	0.10	0.08
Digital microscopy	0.134	0.106	0.148	0.161	0.354	0.1806

Following ceramic veneering, both cast and SLS crowns (P3 and P4) demonstrated internal fit values consistent with those recorded at the metal stage. The cast crown (P3) exhibited the most uniform measurements, with mean values of 0.08 mm using micrometer techniques and 0.0784 mm under microscopy. This indicates that ceramic firing did not induce clinically relevant distortion of the cast infrastructure. The complete dataset for P3 is presented in Table 3**.**

All measurements obtained for the cast metal–ceramic crown (P3) were contained within the 0.05–0.15 mm clinically acceptable interval, confirming a favorable and homogeneous internal adaptation after ceramic veneering.

Table 3. Internal Fit Measurements for Cast Metal–Ceramic Crown (P3)

Measurement (mm)	Vestibular	Oral	Mesial	Distal	Occlusal	Mean
Differential micrometer	0.10	0.05	0.10	0.05	0.10	0.08
Direct silicone measurement	0.10	0.05	0.10	0.05	0.10	0.08
Digital microscopy	0.073	0.096	0.116	0.028	0.079	0.0784

In contrast, the SLS crown (P4) showed greater variation across measurement points, particularly at the occlusal surface, where microscopy again revealed values as high as 0.352 mm. These findings parallel those seen in the metal-only stage, indicating that the differences intrinsic to the two fabrication workflows persist even after ceramic application, as reflected in Table 4.

In the SLS metal–ceramic crown (P4), axial and proximal values generally remained within the 0.05–0.15 mm range, while the occlusal microscopic gap of 0.352 mm again exceeded this limit, suggesting that the main area of clinical concern is confined to the occlusal surface.

Table 4. Internal Fit Measurements for SLS Metal–Ceramic Crown (P4)

Measurement (mm)	Vestibular	Oral	Mesial	Distal	Occlusal	Mean
Differential micrometer	0.15	0.10	0.10	0.05	0.10	0.10
Direct silicone measurement	0.15	0.10	0.10	0.05	0.10	0.10
Digital microscopy	0.165	0.169	0.106	0.096	0.352	0.1776

When comparing manufacturing methods, cast specimens consistently demonstrated smaller internal gaps across all three measurement techniques. On average, cast restorations exhibited mean values between 0.08 and 0.09 mm, whereas SLS specimens showed higher means ranging from 0.10 to 0.18 mm, primarily influenced by the more pronounced occlusal discrepancies.

A comparison of the three measurement techniques showed that digital microscopy yielded the highest mean internal gap values (approximately 0.135 mm), whereas both micrometer-based methods produced lower and nearly identical means (approximately 0.09 mm). This confirms the superior sensitivity of microscopic evaluation, while also highlighting its tendency to detect micro-irregularities that may not be clinically significant.

DISCUSSIONS

The present study evaluated the internal fit of cobalt–chromium metal–ceramic restorations fabricated through two distinct manufacturing workflows: conventional casting based on wax patterning and selective laser sintering (SLS), a digital additive technique. Across all measurement methods, cast frameworks and their corresponding ceramic restorations demonstrated smaller and more uniform internal gaps compared with SLS specimens, indicating superior adaptation to the abutment surface. These findings align with the working hypothesis that conventional patterning techniques may still provide enhanced accuracy in marginal and internal fit relative to certain additive workflows [14;15].

The differences observed between fabrication methods are consistent with previously published data. Arora et al. reported that SLS crowns generally exhibited improved marginal fit but inferior internal adaptation compared with conventionally fabricated Co–Cr restorations, highlighting the influence of manufacturing technology on spatial accuracy. Likewise, Ullattuthodi et al. [15] demonstrated that conventional metal frameworks produced better internal fit values than DMLS restorations, with no significant differences observed in marginal adaptation. The results of the present study reinforce these findings by showing that SLS specimens displayed greater variability and more pronounced occlusal discrepancies, likely attributable to the layer-by-layer material consolidation characteristic of additive manufacturing.

In the current analysis, digital microscopy consistently produced higher internal gap values compared with micrometer-based techniques. This is unsurprising, as microscopy allows visualization and quantification of micro-irregularities not detectable manually. Although this confirms the superior sensitivity of microscopic evaluation, it also indicates that some discrepancies identified through microscopy may fall within clinically acceptable thresholds. Literature suggests that internal gap values between 0.05 and 0.15 mm are generally acceptable for cementation, depending on the restorative material used. Approximately half of the measurements obtained in this study fall within this interval, suggesting that both fabrication methods can produce clinically functional restorations, although the cast technique provides more predictable results [5-8].

From a clinical perspective, the pattern of internal adaptation observed in this study suggests that the main area of concern for SLS restorations is confined to the occlusal surface, where microscopic gaps exceeded the 0.15 mm upper limit of the commonly accepted interval. Localized occlusal discrepancies of approximately 0.35 mm may result in excessively thick cement layers, which could compromise complete seating in the presence of viscous luting agents or generate occlusal “pools” of cement that are more susceptible to void formation, dissolution and fatigue. Under functional loading, such non-uniform internal support may alter occlusal load distribution, increasing tensile and shear stresses within the cement layer and at the ceramic–metal interface, thereby predisposing to microcracking, loss

of occlusal contact or chipping over time. By contrast, the more homogeneous internal fit of cast restorations, with all values remaining within the 0.05–0.15 mm interval, is expected to favour more predictable cementation, more uniform stress transfer and, potentially, more stable long-term prosthesis performance.

Ceramic firing did not introduce significant dimensional changes in either workflow, as indicated by the strong correspondence between values recorded for metal frameworks and those obtained for the final veneered restorations. This observation suggests that both Co–Cr alloys used—regardless of fabrication method—exhibit satisfactory thermal stability under the firing cycles applied. However, although global deformation was not observed, microstructural differences at the alloy level may still contribute to subtle changes in internal fit not easily detected without advanced metallurgical evaluation [11;16].

This study has several important limitations that should be acknowledged when interpreting the results. Only one anatomical region (a maxillary first molar) and a single crown design were investigated, which restricts the generalizability of the findings to other tooth morphologies, preparation geometries or multi-unit restorations. Moreover, the experimental sample was extremely small, with only two specimens per manufacturing technique, so the study was not powered for inferential statistics and all data must be regarded as exploratory. In addition, micrometer-based assessments are inherently operator dependent; although all measurements were performed by a single trained operator following a standardized protocol and with regularly calibrated instruments, subtle variations in specimen positioning and contact pressure cannot be entirely excluded. The replica technique also introduces potential sources of error related to silicone handling and elastic recovery, despite efforts to minimize deformation. Finally, the results reflect the performance of one specific combination of scanner, CAD software, Co–Cr alloys, SLS machine and ceramic system, and may not be directly transferable to other digital workflows or material configurations. Despite these limitations, the findings provide relevant insights into the performance of conventional and additive manufacturing workflows. The superior consistency of cast specimens suggests that traditional techniques remain highly reliable for achieving precise internal adaptation. However, continued advancement in laser-based powder fusion technologies may narrow the gap in accuracy, offering opportunities for workflow optimization in fully digital restorative dentistry [17;18].

CONCLUSIONS

This in vitro pilot study showed that cobalt–chromium metal–ceramic restorations fabricated through conventional casting exhibited smaller and more uniform internal gaps than those produced by selective laser sintering (SLS), with cast frameworks and their veneered crowns demonstrating superior internal adaptation, particularly in the occlusal region. Digital microscopy proved more sensitive than micrometer-based methods, revealing additional micro-discrepancies and underscoring the value of high-resolution assessment for evaluating restorative accuracy. Within the limitations of the small sample size and single tooth morphology, these findings reinforce the predictable precision of conventional casting and clarify current constraints of additive manufacturing in achieving uniformly optimal internal fit, providing clinically relevant guidance for selecting and refining manufacturing workflows.

Conflicts of Interest

The authors declare no conflict of interest.

REFERENCES

[1] Bratu D, Nussbaum R. Bazele clinice şi tehnice ale protezării fixe. Bucureşti: Signata; 1992.
[2] Ardelean L, Rusu LC. Materiale, instrumente şi aparate în laboratorul de tehnică dentară. Timişoara: Eurostampa; 2013.
[3] Negruţiu ML, Sinescu C, Leretter M, Lakatos S, Romînu M, Sandu L, et al. Tehnologia protezelor dentare. Vol. I – Proteze unidentare. Timişoara: LITO UMF "Victor Babeş"; 2005.
[4] Porojan L, Savencu C, Vasiliu R, Porojan S, Topală F. Tehnologii computerizate în protetica dentară. Timişoara: Eurobit; 2020.
[5] Stappert CFJ, Dai M, Chitmongkolsuk S, Gerds T, Strub JR. Marginal adaptation of three-unit fixed partial dentures constructed from pressed ceramic systems. J Prosthet Dent. 2004;92(3):235–240.
[6] Cunali RS, Saab RC, Correr GM, et al. Marginal and internal adaptation of zirconia crowns: A comparative study. J Prosthodont. 2017;26(3):235–243.
[7] Ural C, Burgaz Y, Saraç D. In vitro evaluation of marginal adaptation in five ceramic restoration fabricating techniques. J Prosthodont. 2010;19(8):652–660.
[8] Bhowmik H, Parkhedkar R, et al. Marginal fit of glass-infiltrated alumina copings fabricated using two techniques. J Prosthodont. 2011;20(3):214–223.
[9] K, Farjood E, Khaledi A. Comparison of marginal and internal fit of metal copings cast from CAD/CAM and conventional wax-ups. J Dent (Shiraz). 2013;14(3):118–129.
[10] Svanborg P, Skjerven H, Carlsson P, et al. Marginal and internal fit of Co–Cr FDPs from digital vs. conventional impressions. Int J Dent. 2014;2014:534382.
[11] Gurel K, Toksavul S, Toman M, Tamac E. Adaptation of metal-ceramic Co-Cr frameworks fabricated with CAD/CAM and casting. J Prosthet Dent. 2019;122(4):445–450.
[12] Huang Z, Zhang L, Zhu J, Zhao Y. Clinical marginal and internal fit of SLM vs. cast metal-ceramic crowns. J Prosthet Dent. 2015;113(6):623–627.
[13] Chou WT, Chuang CC, Wang YB, Chiu HC. Comparison of the internal fit of metal crowns fabricated by traditional casting, computer numerical control milling, and three-dimensional printing. PLoS One. 2021;16(9):e0257158.
[14] A, Upadhyaya V, et al. Internal adaptation of copings: three fabrication techniques compared. J Indian Prosthodont Soc. 2018;18(1):42–47.
[15] Ullattuthodi S, Cherian KP, Anandkumar R, et al. Marginal and internal fit of Co–Cr copings fabricated by conventional vs. DMLS. J Prosthet Dent. 2017;117(1):102–108.
[16] Savencu CE, Porojan L, Porojan SD, et al. Adaptability evaluation of metal–ceramic crowns made by additive/subtractive technologies. Appl Sci. 2020;10(16):5563.
[17] Örtorp A, Jönsson D, Mouhsen A, von Steyern VP. Fit of Co–Cr FDPs fabricated with four different techniques. Dent Mater J. 2011;30(1):53–59.
[18] Kocaağaoğlu H, Kılınç HI, Albayrak H, Aslan Y, Kılıçarslan MA. Internal and marginal adaptation of different crown manufacturing methods. Niger J Clin Pract. 2020;23(5):670–676.

Comparative Evaluation of Icon Resin Infiltration and Clinpro XT Varnish on the Remineralization of Enamel White Spot Lesions: An in Vitro Study

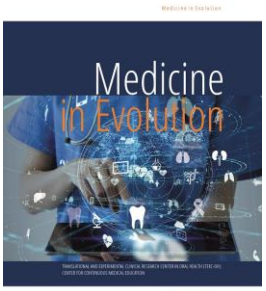

https://doi.org/10.70921/medev.v31i4.2020

Sorana Nicoleta Rosu[1†], Ioan Alexandru Simerea[2†], Malina Popa[3,4*], Anamaria Matichescu[2,5*], Vlad Tiberiu Alexa[2,5]

[1]*Department of Oral and Maxillofacial Surgery, Faculty of Medicine," Grigore T. Popa" University of Medicine and Pharmacy, 700115 Iasi, Romania*
[2]*Translation and Experimental Clincal Research Center in Oral Health (TEXC-OH), Department of Preventive, Community Dentistry and Oral Health," Victor Babes" University of Medicine and Pharmacy, 14 A Tudor Vladimirescu Ave., 300173, Timisoara, Romania*
[3]*Department of Pedodontics, Faculty of Dental Medicine," Victor Babes" University of Medicine and Pharmacy, No. 9, Revolutiei 1989 Bv., 300041 Timisoara, Romania*
[4]*Pediatric Dentistry Research Center, Faculty of Dental Medicine, "Victor Babes" University of Medicine and Pharmacy, No. 9, Revolutiei 1989 Bv., 300041 Timisoara, Romania*
[5]*Clinic of Preventive, Community Dentistry and Oral Health, "Victor Babes" University of Medicine and Pharmacy, Eftimie Murgu Sq. no. 2, 300041, Timisoara, Romania*
[†]*These authors contributed equally to this work.*

Correspondence to:
Name: Malina Popa
E-mail address: popa.malina@umft.ro

Name: Anamaria Matichescu
E-mail address: matichescu.anamaria@umft.ro

Received: 04 December 2025; Accepted: 06 December 2025; Published: 15 December 2025

Abstract

1.Background: The aim of this research is to investigate microscopically the behavior of two materials, Clinpro XT Varnish and Icon Vestibular, on the surfaces of teeth with chalky white lesions induced by 37% phosphoric acid. Microscopic evaluation is performed based on different degrees of penetration and infiltration. *2.Methods*: The materials tested in this study were Icon – Vestibular DMG (LOT 281473) and 3M ESPE Clinpro XT – Varnish (LOT 9703392).*3.Results*: Phosphoric acid demineralizes the superficial enamel layer, exposing prisms and hydroxyapatite crystals, and generating a rough surface with uniform etching patterns visible at different magnifications, which favor the adhesion of restorative materials. The use of the infiltrant resin Icon fills microcracks and interprismatic spaces, integrating the enamel prisms into a compact, smooth mass that stabilizes the enamel structure and prevents the progression of demineralization. SEM images show that the varnish forms a thin, relatively uniform film on the enamel, but with small discontinuities and uncovered areas, indicating a less effective seal and protection compared with Icon. 4.Conclusion: The integration of materials such as Icon and fluoride varnishes makes it possible to postpone invasive restorative treatments and is particularly useful in the management of white spots, while maintaining the structural integrity of the teeth.

Keywords: Clinpro XT varnish, icon resin infiltration, scanning electron microscopy

INTRODUCTION

Incipient carious lesions manifest clinically as chalky white spots corresponding to a subsurface zone of enamel demineralization located beneath an apparently intact surface, which is initially reversible through remineralization. They represent a dynamic caries process driven by an imbalance between pathological factors (fermentable carbohydrates, hyposalivation, acidogenic bacteria) and protective factors (salivary flow, fluoride, antibacterial agents, diet), progressing from initial enamel demineralization to dentin involvement and cavity formation. Histopathologically, the initial enamel lesion shows two main demineralization zones (the translucent zone and the body of the lesion, located 15–30 µm below the surface) and two remineralization zones (the dark zone and the surface zone) [1].

Over the past decades, a change in the caries pattern has been noted, with a decrease in lesions on smooth surfaces and an increase on occlusal surfaces, which makes early detection and implementation of preventive measures essential. Traditional diagnostic methods – visual inspection and radiography – are limited: inspection depends on changes in color and texture, and radiography detects carious enamel only after a mineral loss of more than about 40%, and it also involves exposure to ionizing radiation. Lesions occur frequently on the maxillary anterior teeth, especially on plaque-retentive surfaces, and the risk is influenced by poor oral hygiene, age (adolescents), initial caries experience, and the extent of the etched surface. Chalky white spots may represent developmental defects (fluorosis, hypoplasia), areas of demineralization in patients without appliances, or consequences of fixed orthodontic treatment [2].

In orthodontics, chalky white spots are among the most frequent complications and have a long lasting negative esthetic impact, with carious lesions being rough and porous, in contrast to non carious spots, which are smooth and glossy. Reported prevalence is highly variable (about 2–96%), depending on the detection method, with studies using quantitative fluorescence showing higher rates than those based only on visual inspection; before orthodontic treatment, prevalence is roughly 15–40%, and during treatment the incidence of new clinical lesions often ranges between 30–70% of patients. Fixed orthodontic appliances increase plaque retention and reduce self cleansing by saliva, tongue, and cheeks, especially on vestibular surfaces; in contrast, lingual appliances appear to be associated with a lower incidence of white spot lesions, probably due to better cleaning by the tongue and salivary flow [3].

Individual caries risk during treatment is multifactorial: in addition to oral hygiene, salivary flow and composition, enamel solubility, immune response, genetic predisposition, diet, and the general medical context all play a role. Early lesions are easily missed in the presence of appliances, plaque, and gingival inflammation and often become evident only after appliance removal, which is why systematic assessment of at-risk teeth is recommended at every check-up, with inspection performed on clean and dry arches. Preventive responsibility is often perceived as resting with the patient, but the orthodontist and dentist have a central role in identifying high-risk patients, counselling them, and implementing a structured preventive protocol [4].

After completion of orthodontic treatment, management depends on the severity and esthetic impact of the spots: in mild cases one may opt for monitoring and natural remineralization, possibly combined with tooth whitening; for more pronounced lesions, resin infiltration, micro /macro abrasion techniques, and, in severe situations, direct composite restorations or indirect veneers are described. Ideally, the risk of white spot lesion development should be discussed in detail as part of the informed consent process, and

preventive measures, hygiene monitoring, and lesion status should be thoroughly documented in the patient's record [5].

Current minimally invasive concepts in dentistry focus on controlling etiological factors using non invasive and micro invasive methods and strategies. Whereas non invasive strategies aim to arrest or reverse non cavitated carious lesions, micro invasive strategies include barriers that prevent the enamel from being further exposed to the acidic attack of cariogenic bacteria. Among the micro invasive approaches, two procedures are currently used: pit and fissure sealants applied to enamel etched with phosphoric acid, and low viscosity resins that either penetrate or infiltrate, by capillary action, non cavitated lesions etched with hydrochloric acid [5].

It has been shown that resin infiltration with ICON provides immediate restoration of the esthetics of mild white spot lesions that appear after orthodontic treatment, matching the healthy enamel of the area adjacent to the spot [6]. This effect has been demonstrated to remain stable for 6 months, with no significant changes at 12 and 24 months. In the case of moderate lesions, an improvement has been observed over time following sequential treatment. Loss of fluorescence in the lesions recovered significantly immediately after resin infiltration and remained unchanged at the end of 6 weeks in artificially created lesions. These findings demonstrate that ICON resin infiltration is a benchmark intervention method for the esthetic restoration of white spot lesions [7].

The concept of resin infiltration with Icon is relatively new, being a product developed in Germany and used in the treatment of incipient lesions. It improves retention and prevents caries on smooth surfaces, but not on cavitated surfaces. The resin fills the pores of the lesion and blocks the further diffusion of bacteria by creating barriers and halting lesion progression, restoring the tooth without anesthesia and drilling in order to preserve its natural morphology [6].

Icon infiltrates the lesion, renders the bacteria inactive, and prevents caries progression, in contrast to sealant material, which only acts as a mechanical barrier between the dental structure and the oral environment [6]. It works on the principle of light scattering. Sound enamel has a refractive index of 1.62. The porosities of a carious white spot lesion are usually filled either with an aqueous medium or with air, which have refractive indices of 1.33 and 1, respectively. The whitish appearance of the lesion is due to the difference in refractive index between the enamel crystals and the surrounding medium, which causes light scattering. The microporosities in the body of the lesion are infiltrated with a resin material that has a refractive index of 1.46, thereby making the differences between enamel and porosities negligible so that the lesion appears similar to the surrounding enamel [7].

Fluoride, in its many forms, is used in dentistry as an effective measure for the prevention of carious lesions. In lower concentrations it is usually used by patients, whereas higher concentrations are applied by professionals. A wide range of fluoride products is available, but fluoride varnish has been the preferred option for the past 20 years because of its effectiveness, patient acceptance, and ease of application. It is also one of the most frequently reimbursed procedures by dental insurance companies and is widely recommended for use in children, even in infants. An increasing number of healthcare providers, such as pediatricians, family physicians, and nurses, now apply fluoride varnishes to children's teeth, advocating good oral health as an integral part of overall health [8].

Clinpro XT varnish is a resin modified glass ionomer cement product from 3M ESPE that has been widely used in the past for the treatment of dentin hypersensitivity. In orthodontics, it has been shown to be effective in preventing the occurrence of white spot lesions during orthodontic treatment and in managing artificially induced demineralized areas [9].

Aim and objectives

The objectives of the research are to investigate the microscopic behavior of two materials, Clinpro XT Varnish and Icon Vestibular, on the surfaces of teeth with chalky white lesions induced by 37% orthophosphoric acid. Microscopic evaluation is carried out based on the different degrees of penetration and infiltration.

MATERIAL AND METHODS

The materials tested in this study were Icon – Vestibular DMG (LOT 281473) and 3M ESPE Clinpro XT – Varnish (LOT 9703392). The composition and instructions for use of these materials are presented in Table 1.

Table 1. Composition and manufacturing instructions of the tested materials

Material	**Icon – Vestibular DMG**	**Clinpro XT - Varnish**
Manufacturer	DMG – Hamburg, Germany	3M Germany GmbH
Composition	1. Icon-Etch (HCl 15%) 2. Icon-Dry (99% etanol) 3. Icon-Infiltrant (Methacrylate-based resin matrix, initiators, additives)	2-Hydroxyethyl methacrylate Water 2-Propenoic acid, 2-methyl-, 3-(trimethoxysilyl) propyl ester, hydrolysis products with silica.
Instructions for use	1. Clean the tooth. 2. Apply Icon-Etch. Allow it to act for 2 min. 3. Rinse with water for 30 s. Dry with air. 4. Apply Icon-Dry. Allow it to act for 30 s. Dry with air. 5. Apply Icon-Infiltrant. Allow it to act for 3 min. 6. Light-cure for 40 s. 7. Apply Icon-Infiltrant again. Allow it to act for 1 min. 8. Light-cure for 40 s	1. Clean the tooth. 2. Ultra etch: 35% phosphoric acid for 30 s. 3. Rinse with water for 30 s. Dry with air. 4. A thin layer of Clinpro XT varnish was applied and light-cured for 20 s.
Batch number	281473	9703392

Sample preparation:

A total of 11 extracted molar teeth without carious lesions were cleaned using pumice powder in suspension and a rotary toothbrush mounted on a contra-angle handpiece. The teeth used in this study were collected and stored in saline until the day of measurement, with inclusion criteria being molars without cracks, restorations, or developing lesions. The roots were removed and the crowns were sectioned longitudinally in a mesio-distal direction using a disc mounted on a straight handpiece, yielding 22 samples that were embedded in ZetaPlus impression material so that the crowns were exposed and the convex tooth surfaces could be examined; after measurements, all samples were stored in distilled water.

Chalky white lesions were created on all 22 samples using 37% orthophosphoric acid for 30 minutes, after which the samples were rinsed with water and dried. According to the protocols, Icon – Vestibular DMG was applied to 10 samples and Clinpro XT – Varnish to the other 10 samples, and both materials were light-cured with a Woodpecker cordless LED curing lamp. The remaining 2 samples, on which only 37% orthophosphoric acid had been applied, were used as control specimens for comparison of the subsequent results.

Figure 1. Samples treated with 37% orthophosphoric acid solution

Following treatment of the teeth, the samples were sent to the laboratory for analysis of the results using scanning electron microscopy (SEM).

RESULTS

Effect of orthophosphoric acid on the dental enamel prism
It acts by removing the superficial enamel layer and exposing the enamel prisms, thereby compromising their crystalline structure. This process is analyzed starting at high magnification and then gradually moving to lower magnifications to observe the changes in their overall context.

At high magnification (×25), the structure of dental enamel becomes clear and detailed. At this stage, grooves between cusps and other fine details of the enamel surface are evident, and orthophosphoric acid begins to exert its effects, especially in the fissure areas where enamel is more exposed to erosion. Enamel prisms, hexagonal or prismatic structures arranged perpendicular to the tooth surface, are the basic components of enamel. At this magnification, 37% orthophosphoric acid causes prism demineralization, removing the organic matrix and exposing hydroxyapatite crystals, a process that is essential for creating a rough surface that will facilitate adhesion of dental restorative materials.

By reducing the magnification (×250), a more integrated image of the dental enamel appears. At this level, enamel prisms are still visible, but their fine details merge into a broader view, and it becomes clear how orthophosphoric acid has affected the superficial layer as the initially smooth surfaces become rough and porous, highlighting the effectiveness of the acid treatment. Acid etching creates characteristic patterns in the enamel, which at this magnification are seen to be uniformly distributed, preparing the surface for application of dental composites; typical etching patterns include honeycomb- and cobweb-like forms resulting from selective dissolution of the enamel prisms.

At lower magnifications (×5000), the image becomes even more integrated, revealing large-scale changes in enamel structure. The increased roughness and uniform distribution of the etching pattern indicate effective surface preparation for subsequent procedures, and the interaction between etched enamel and underlying dentin becomes evident. It is crucial to understand that excessive demineralization can weaken the tooth structure and compromise the integrity of the tooth.

In the study of enamel prism behavior after acid exposure, two enamel specimens were used, both being uniformly and equally affected by orthophosphoric acid, as shown in Figure 2.

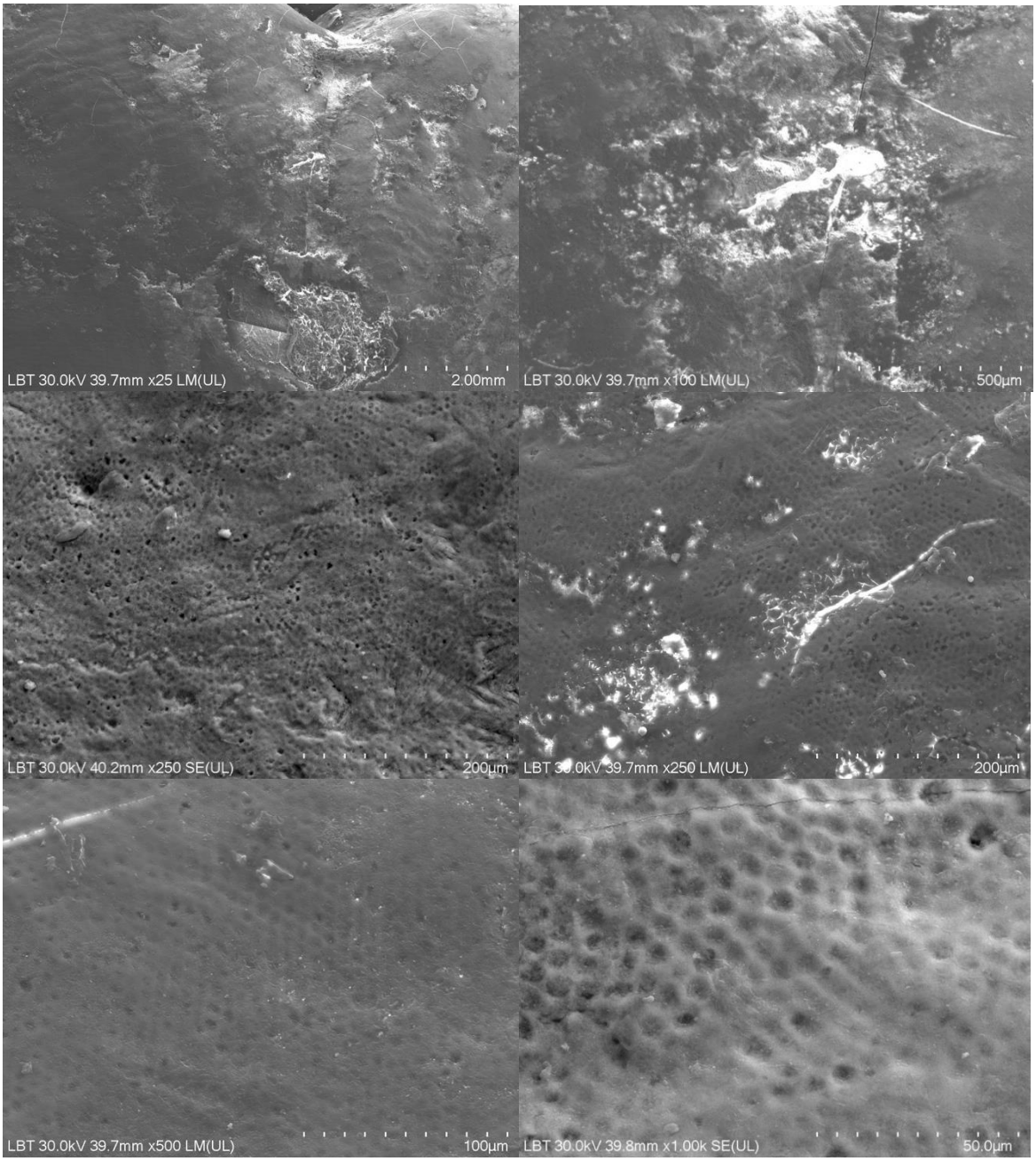

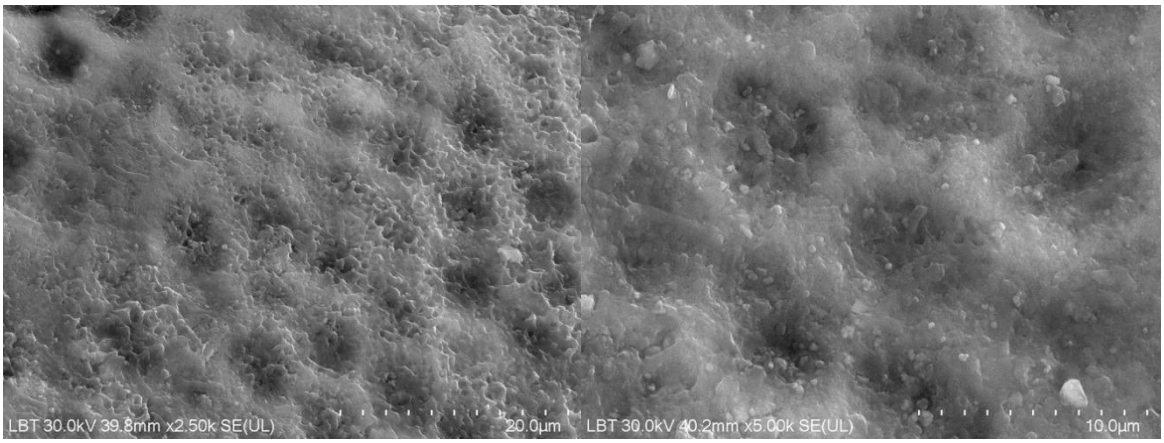

Figure 2. SEM specimen with acid

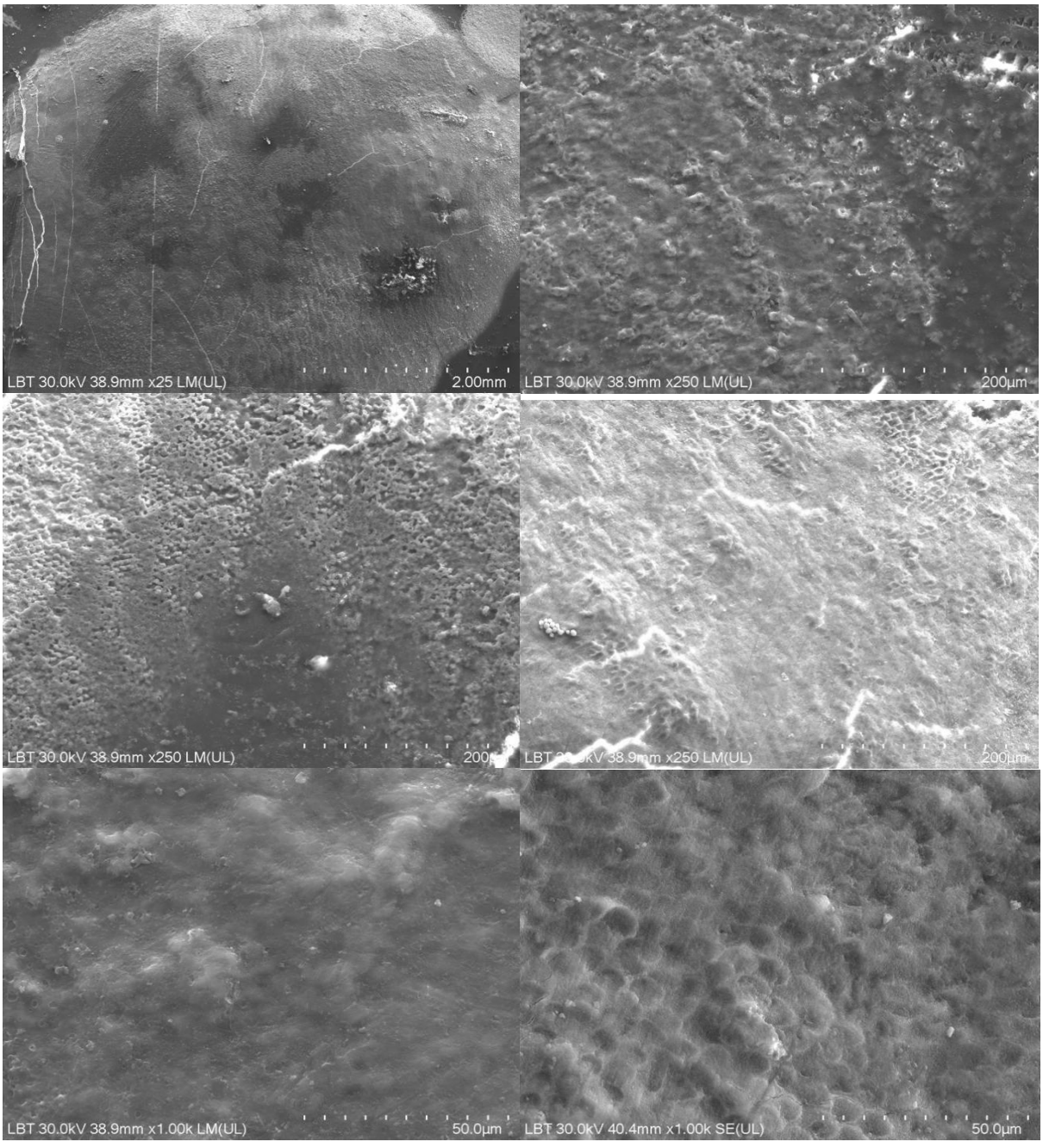

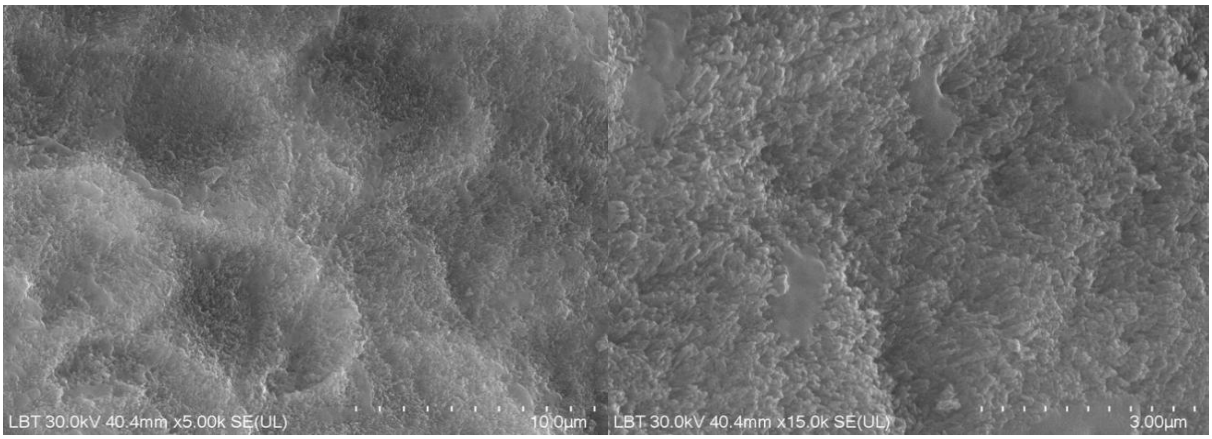

Figure 3. SEM specimens with ICON at different incidences

At ×25 magnification, the overall surface of enamel treated with Icon can be observed, showing visible uniformity and smoothness without clearly distinguishable prismatic structures, as Icon has filled the microcracks and visible pores to create a compact, homogeneous surface.

At ×250 magnification, Icon is seen to have penetrated deeply into the enamel, infiltrating interprismatic spaces and enamel prisms so that these structures appear less distinct and the interprismatic spaces almost completely sealed.

At ×5000 magnification, enamel prisms, which are usually well-defined hexagonal structures, now appear fused and homogenized due to Icon infiltration, with interprismatic spaces completely filled with resin, leading to consolidation of the enamel structure and prevention of caries progression. The treated enamel surface exhibits a markedly smoother and more compact texture, reflecting the efficiency of Icon in infiltrating and stabilizing the enamel.

At ×15000 magnification, the fine details of the enamel structure are extremely clear. The enamel prisms, which at lower magnifications may appear separate and distinct, now seem fully integrated into the homogeneous mass of Icon resin, with the previously porous interprismatic spaces almost completely sealed and no longer susceptible to acid attack. At this scale, Icon appears as a protective barrier that fills and stabilizes the microcrystalline structures of the enamel, preventing further demineralization.

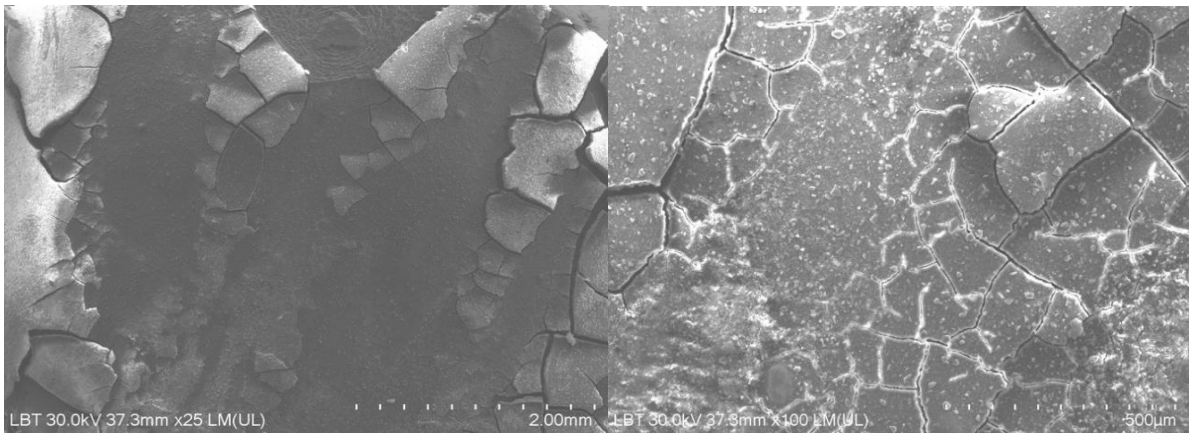

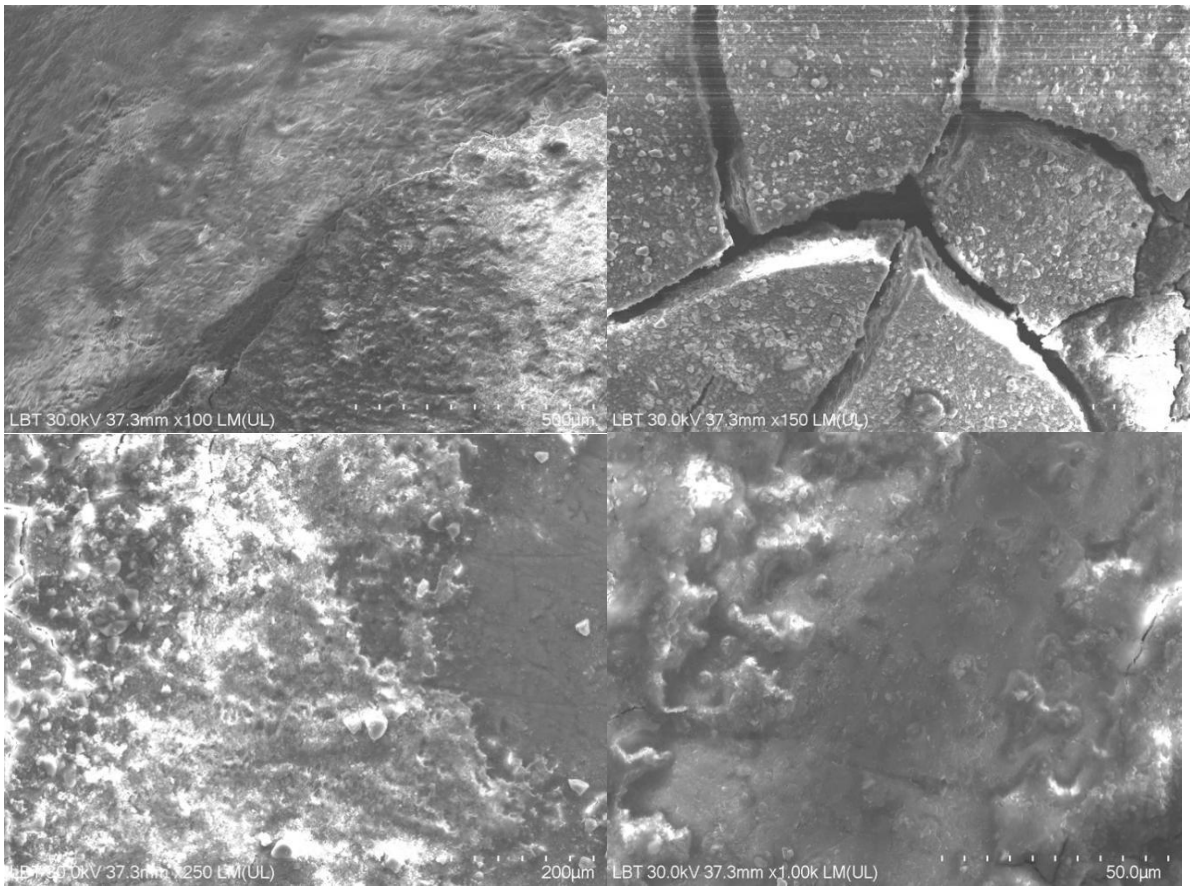

Figure 4. SEM specimens with VARNISH at different incidences

Seal provided by varnish in dental enamel

SEM images show the varnish layer forming a thin, relatively uniform film that covers the entire treated surface. However, it exhibits slight discontinuities or uncovered areas, indicating an application and protection that are not as effective as in the case of Icon application.

DISCUSSIONS

In our days, the amount and frequency of consumption of acidic foods and drinks have increased [10]. As a result, examining the etiology, prevalence, prevention, and treatment of dental erosion has become very important. Many factors can cause enamel erosion: diet, oral hygiene routine, medications, and the professional environment [11]. Maintaining poor oral hygiene also leads to the appearance of chalky white spot lesions. Studies show that low pH beverages cause dental erosion of varying degrees [12]. Case reports as well as other studies suggest that dietary acid erosion plays a significant role in tooth wear. The degree of demineralization of a solution depends on the type of acid it contains, its pH value, the acid concentration, and its temperature [13]. The results of other studies show that acids in liquid form are more harmful to dental tissues than gels; therefore, beverages and acid reflux are a greater concern.

The management of chalky white spot lesions can be divided into prevention (before lesion formation), intervention (during orthodontic treatment), and treatment (after completion of orthodontic treatment). In the prevention and intervention categories, fluorides in the form of varnish, toothpaste, mouthwash, sealants, laser therapy, silver nanoparticles, and ozone have been widely used [14]. The effectiveness of preventive methods is inadequate,

because their efficacy is limited to remineralization of the superficial part of the lesion and not of the lesion body [15].

Dental photography is of utmost importance in several respects. It is simple, quick, and extremely useful for documenting the techniques, stages, and outcomes of this study [16]. The 37% orthophosphoric acid solution was the most effective in dissolving enamel [17]. The appearance of the teeth after 30 minutes of demineralization, as shown in Figures 14–16, is that of pure white spots, as if the teeth were covered with a thin layer of chalk.

The use of an unfilled resin to seal lesions (chalky white spots) proves effective in preventing further demineralization. Various materials containing unfilled resins have shown promising results regarding lesion infiltration and arresting acid attack [18]. The infiltration technique has several advantages over other techniques. First, deeper lesions can be improved by infiltration techniques, which can induce both remineralization and aesthetic enhancement. Second, when compared with other techniques, infiltration is far less invasive [19].

The purpose of using ICON is to block the porosities within the body of white spot lesions with a light curing resin specially optimized to penetrate porous enamel. The infiltrants are light curable and have low viscosity, low contact angles with enamel, and high surface tension, which together enable complete penetration into the lesion's porosities [20]. Before application of the material, the enamel is conditioned with 15% hydrochloric acid gel. The resin then penetrates the lesion driven by capillary forces, and ICON infiltrant is a blend with a very high penetration coefficient [21], so that a diffusion barrier is created within the lesion rather than on its surface. After the material has infiltrated, the excess is removed from the lesion surface with a cotton pellet and then polymerized using ultraviolet light.

Alternatively, ClinproTM XT varnish is a specialty material available on the market that releases fluoride, calcium, and phosphate in a controlled manner [22]. It is a chemical agent with an occlusive action, sealing dentinal tubules through chemical adhesion to dentin mediated by polyalkenoic acid, which forms ionic bonds with calcium hydroxyapatite, the primary mineral of dentin. This is followed by a chelation mechanism in which the carboxylic groups of the polyacrylic acid in Clinpro XT react with calcium in the enamel and with apatite in the dentin [23]. It also contains calcium glycerophosphate, which increases the bioavailability of calcium and phosphate in saliva. The calcium released from covering or restorative materials can contribute to strengthening enamel surfaces, and studies report that Clinpro XT releases fluoride into saliva for up to six months [24]. Enamel has increased resistance to acid when fluoride is incorporated into the apatite, which reduces enamel degradation [25]. At present there are relatively few studies in the orthodontic field. For this reason, the present study aimed to evaluate the effectiveness of ClinproTM XT varnish, which could potentially be used during orthodontic treatment to prevent the occurrence of white spot lesions in orthodontic practice.

The purpose of using Clinpro XT is to occlude dentinal tubules, efficiently reduce permeability by increasing resistance to abrasive or acidic stimuli, and inhibit tubule reopening after erosive or abrasive challenges. In addition, a statistically significant reduction in surface roughness is achieved after a single application. Furthermore, the product has increased the bioavailability of calcium and phosphate in saliva, demonstrated its ability to release fluoride into saliva over six months, promoted enamel remineralization, and partially inhibited enamel demineralization under acidic challenge, resulting in greater immediate and long term protection of enamel against dentin hypersensitivity [26].

CONCLUSIONS

Due to a refractive index close to that of sound enamel and their low viscosity, these resins mask chalky white spots and provide a superior aesthetic outcome while blocking acid diffusion and slowing or arresting caries progression.

Infiltration provides the treated enamel with a degree of mechanical stabilization, improving surface resistance and durability without additional removal of dental tissue, which allows for a conservative approach.

The use of materials such as Icon, together with fluoride varnishes, enables postponement of invasive restorative treatments and is particularly useful in the management of white spot lesions, while preserving the structural integrity of the teeth.

However, infiltrative resins are indicated only for non cavitated lesions that are superficial or limited to the outer third of the dentin; advanced or cavitated lesions require other types of restorative treatment.

Conflicts of Interest

The authors declare no conflict of interest.

REFERENCES

[1] Korishettar BR, Pathak S, Poornima P, et al. White spot lesions: a literature review. Department of Pedodontics and Preventive Dentistry, College of Dental Sciences, Davangere, Karnataka, India; 2015 Jan.
[2] Toumba DC. Diagnosis and prevention of dental caries. In: Welbury R, Duggal MS, Hosey MT, et al., editors. Paediatric dentistry. 3rd ed. Oxford: Oxford University Press; 2015. p.109.
[3] Heymann GC, Grauer D. A contemporary review of white spot lesions in orthodontics. J Esthet Restor Dent. 2013.
[4] Boersma JG, van der Veen MH, Lagerweij MD, et al. Caries prevalence measured with QLF after treatment with fixed orthodontic appliances: influencing factors.
[5] Perdigao J. Resin infiltration of enamel white spot lesions: an ultramorphological analysis. Department of Restorative Sciences, University of Minnesota; 2019 Nov.
[6] Kannan A, Padmanabhan S. Comparative evaluation of Icon resin infiltration and Clinpro XT varnish on colour and fluorescence changes of white spot lesions: a randomized controlled trial. 2019 Jun.
[7] Icon [Internet]. Ridgefield Park (NJ): DMG America; c2025. Available from: https://www.dmg-america.com/en/products/product/icon/.
[8] Ahovuo-Saloranta A, Forss H, Walsh T, et al. Sealants for preventing dental decay in the permanent teeth. Cochrane Database Syst Rev. 2013.
[9] Mascarenhas AK. Is fluoride varnish safe? Nova Southeastern University College of Dental Medicine and College of Osteopathic Medicine; 2021 May.
[10] Bonetti D, Clarkson JE. Fluoride varnish for caries prevention: efficacy and implementation. Dental Health Services Research Unit, Dundee Dental Education Centre, University of Dundee; 2016 Apr.
[11] Bishara SE, Ostby AW. White spot lesions: formation, prevention and treatment. 2013 Sep.
[12] Vicente A, Ortiz Ruiz AJ, Gonzalez Paz BM, et al. Efficacy of fluoride varnishes for preventing enamel demineralization after interproximal enamel reduction. 2017 Apr.
[13] Carey CM. Focus on fluorides: update on the use of fluoride for the prevention of dental caries. J Evid Based Dent Pract. 2014 Feb.
[14] Sezici YL, Yetkiner E, Yetkiner AA, et al. Comparative evaluation of fluoride varnishes, self assembling peptide based remineralization agent, and enamel matrix protein derivative on artificial enamel remineralization in vitro. Prog Orthod. 2021.

[15] Donovan T, Nguyen Ngoc C, Abd Alraheam I, Irusa K. Contemporary diagnosis and management of dental erosion. J Esthet Restor Dent. 2021;33:78 87.
[16] Lussi A, von Salis Marincek M, Ganss C, et al. Clinical study monitoring the pH on tooth surfaces in patients with and without erosion. Caries Res. 2012;46:507 12.
[17] Kolumban A, Moldovan M, Tig IA, et al. An evaluation of the demineralizing effects of various acidic solutions. Appl Sci. 2021;11:8270.
[18] Nascimento PL, Fernandes MT, Figueiredo FE, Faria e Silva AL. Fluoride releasing materials to prevent white spot lesions around orthodontic brackets: a systematic review. Braz Dent J. 2016;27(1):101 7.
[19] Garcia Godoy F, Summitt JB, Donly KJ. Caries progression of white spot lesions sealed with an unfilled resin. J Clin Pediatr Dent. 1997;21:141 3.
[20] Ardu S, Castioni NV, Benbachir N, Krejci I. Minimally invasive treatment of white spot enamel lesions. Quintessence Int. 2007;38:633 6.
[21] Paris S, Meyer Lueckel H. Masking of labial enamel white spot lesions by resin infiltration: a clinical report. Quintessence Int. 2009;40:713 8.
[22] Martignon S, Ekstrand KR, Ellwood R. Efficacy of sealing proximal early active lesions: an 18 month clinical study evaluated by conventional and subtraction radiography. Caries Res. 2006;40:382 8.
[23] Gonçalves FMC, Delbem ACB, Gomes LF, et al. Effect of fluoride, casein phosphopeptide amorphous calcium phosphate and sodium trimetaphosphate combination treatment on the remineralization of caries lesions: an in vitro study. Arch Oral Biol. 2021;122:105001.
[24] Franco AM, Saldarriaga A, Gonzalez MC, Martignon S, Arbelaez MI, Ocampo A. Concentración de fluor en la sal de cocina en cuatro ciudades colombianas. Rev CES Odontol. 2003;16:21 6.
[25] Walsh KI, Cury JA. Fluoride concentrations in salt marketed in Managua, Nicaragua. Braz Oral Res. 2018;32.
[26] Ilufi MSM, Redel PBU, Vallespir CA. Clinpro XT resin modified polymerizable glass ionomer varnish: an alternative treatment for tooth sensitivity. A systematic literature review. Odontoestomatología. 2022;24:39.

Impact of Skeletal Class II Malocclusions with Different Vertical Growth Patterns on the Upper Airway

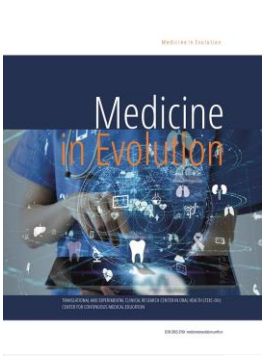

https://doi.org/10.70921/medev.v31i4.2021

Mălina Popa[1,2†], Ştefania Dinu[1,2†], Cristina-Fulga Lazăr[1,2], Andreea Igna[1,2], Robert-Paul Avrămuţ[3], Roxana-Maria Talpoş-Niculescu[4]

[1]*Department of Pediatric Dentistry, Faculty of Dental Medicine, "Victor Babes" University of Medicine and Pharmacy, 9 No., Revolutiei 1989 Bv., 300041 Timisoara, Romania;*
[2]*Pediatric Dentistry Research Center, Faculty of Dental Medicine, "VictorBabes" University of Medicine and Pharmacy, 9 No., Revolutiei 1989 Bv., 300041 Timisoara, Romania;*
[3]*Orthodontic Research Center ORTHO-CENTER, Discipline of Orthodontics I, Faculty of Dental Medicine, "Victor Babes" University of Medicine and Pharmacy Timisoara, 9 No., Revolutiei Bv., 300041 Timisoara, Romania;*
[4]*Discipline of Restorative Dentistry and Endodontics, Research Center TADERP, Faculty of Dental Medicine, "Victor Babes" University of Medicine and Pharmacy, 300041 Timisoara, Romania*

[†]*These authors contributed equally to this work*

Correspondence to:
Name: Andreea Igna
E-mail address: igna.andreea@umft.ro

Name: Robert-Paul Avrămuţ
E-mail address: robert.avramut@umft.ro

Received: 05 December 2025; Accepted: 09 December 2025; Published: 15 December 2025

Abstract

1.Background/Objectives: Considering the clinical relevance of malocclusion in dentistry, the main objective of this study is to assess the changes in the upper airway dimensions in patients with skeletal Class II and a normodivergent growth pattern compared with those with skeletal Class II and a hyperdivergent growth pattern.2.Methods: This observational comparative study was conducted on lateral cephalograms and cephalometric analyses of 52 subjects obtained at the Dentavis imaging center in Timişoara. The sample was divided into two groups of n=25 and n=27 subjects, respectively: Group 1 included subjects with skeletal Class II malocclusion and a normodivergent growth pattern, whereas Group 2 comprised subjects with skeletal Class II malocclusion and a hyperdivergent growth pattern. 3.Results: In Group 2, the mean length of the upper pharyngeal airway was 3.68 mm smaller than the corresponding mean value in Group 1 ($p<0.001$), indicating that subjects with skeletal Class II and a hyperdivergent vertical growth pattern present a significantly more constricted upper pharyngeal airway compared with those with skeletal Class II and a normodivergent pattern. 4.Conclusion: Initiating orthodontic treatment would modify the cephalometric measurements and mandibular rotation, leading to an increase in upper airway dimensions and an improvement in respiratory function.

Keywords: Upper pharyngeal airways, class II malocclusions, vertical growth pattern

INTRODUCTION

The World Health Organization (WHO) regards malocclusion as one of the most important oral health problems, after dental caries and periodontal disease. Its prevalence is highly variable and has been estimated to range between 39% and 93% in children and adolescents, with a wide and heterogeneous distribution that may be explained by ethnic and age-related differences among the populations included in epidemiological studies on malocclusion [1].

In Class II malocclusion, there is an anteroposterior discrepancy between the position of the teeth in the maxillary arch and those in the mandibular arch, which may or may not be associated with an underlying skeletal discrepancy. For orthodontists, this represents one of the most frequently encountered malocclusions in daily clinical practice. Skeletal Class II may result from excessive maxillary growth, deficient mandibular growth, or a combination of both. In such malocclusions, both the upper and lower airways can be affected. Typical features include a narrow maxillary arch, proclination of the upper anterior teeth and the development of oral breathing as a habitual pattern. Moreover, condylar position in skeletal Class II plays a key role in the onset of temporomandibular joint disorders [2].

This malocclusion has a multifactorial etiology and may be caused by hereditary factors, environmental influences, or a combination of the two. Genetically determined factors act during growth and may lead to the development of malocclusion, often in association with etiological factors such as detrimental oral habits: thumb, lip or cheek sucking, tongue interposition between the dental arches, and mouth breathing. If left untreated, persistent malocclusion can seriously affect patients' quality of life, leading to aesthetic, masticatory and phonatory problems that may be more or less evident depending on the severity of the condition. [3].

The assessment of the upper airway has always been of interest in orthodontics, with the main purpose of clarifying the relationship between pharyngeal structures and craniofacial growth and development [4]. The growth and function of the nasal cavities are closely related to normal cranial growth, while morphologic, physiologic or pathologic obstructive processes are recognized risk factors for upper airway obstruction; when present, they may induce a mouth-breathing pattern that alters facial morphology and dental arch form, ultimately leading to malocclusion. Consequently, such obstructive processes can simultaneously result in Class II malocclusion associated with oral breathing and narrowing of the upper airway if left untreated.

Specialist literature has reported a relationship between Class II malocclusions and mouth breathing, as well as an association between vertical growth pattern and airway obstruction. Thus, patients with Class II occlusions and a hyperdivergent growth pattern may present narrower airways than those with a normodivergent pattern or with Class I occlusion. In Class II malocclusions without evident pharyngeal pathology, the nasopharyngeal space has been shown to be vertically narrower than in subjects with a normal growth pattern, and in Class II patients with vertical growth patterns, the nasopharynx is substantially narrower than in Class II patients with normal growth. De Freitas et al. reported that upper pharyngeal width was significantly smaller in individuals with Class I and Class II malocclusions and vertical growth patterns than in those with normal growth [6]. Wang et al. found a reduced airway space in adults with high-angle skeletal Class II, confirming the association between pharyngeal airway space and a vertical skeletal pattern, and suggesting that a vertical growth pattern may predispose individuals to pharyngeal narrowing and potential upper airway obstruction. [7,8]. Ponnada et al. also demonstrated that linear and angular nasopharyngeal

measurements were smaller in Class II subjects with a hyperdivergent growth pattern compared with Class I subjects with an average growth pattern. [9].

Aim and objectives

Given the clinical importance of malocclusion in dentistry, the main objective of the present study is to evaluate changes in the upper airway dimensions in patients with skeletal Class II and a normodivergent growth pattern compared with those with skeletal Class II and a hyperdivergent growth pattern.

MATERIAL AND METHODS

The observational comparative study was conducted on 52 lateral cephalograms and corresponding cephalometric analyses obtained at the Dentavis imaging center in Timișoara, in order to ensure the highest possible accuracy of the results. All subjects in both groups had their cephalograms taken under standardized conditions, and participation was authorized by informed consent, which was signed by the patients and their legal guardians.

The sample consisted of 52 untreated subjects (27 females and 25 males) diagnosed with skeletal Class II malocclusion, aged between 13 and 17 years, with a mean age of 14.75 ± 1.16 years.

For the inclusion criteria in the study, subjects had to present no pharyngeal pathology and no clinical signs, symptoms or suspicion of nasal obstruction. Exclusion criteria were horizontal (hypodivergent) growth pattern and the presence of Class I or Class III malocclusions.

The sample was divided into two groups of n=25 and n=27 subjects, respectively. Group 1 consisted of subjects with skeletal Class II malocclusion and a normodivergent growth pattern, whereas Group 2 included subjects with skeletal Class II malocclusion and a hyperdivergent growth pattern; all subjects in both groups presented Class II molar relationship.

For each lateral cephalogram, a comprehensive cephalometric report was generated, including several established analyses designed to define normative standards for facial proportions. At the Dentavis radiology center in Timișoara, a complete cephalometric analysis was produced individually for every patient, and all measurements were performed digitally using the CephX software.

The growth pattern was classified on the basis of the cephalograms. The following angular measurements were used to distinguish normodivergent from hyperdivergent skeletal patterns: FMA, the angle between the Frankfurt horizontal plane and the mandibular plane; SN-GoGn, the angle between the cranial base plane (Sella–Nasion) and the mandibular plane (Gonion–Gnathion); and NS-Gn, the angle formed by the lines connecting Nasion, Sella and Gnathion, which reflects the vertical and anteroposterior growth of the mandible. The upper pharyngeal airway space was measured on the lateral cephalograms as the linear distance from the posterior contour of the soft palate to the nearest point on the posterior pharyngeal wall.

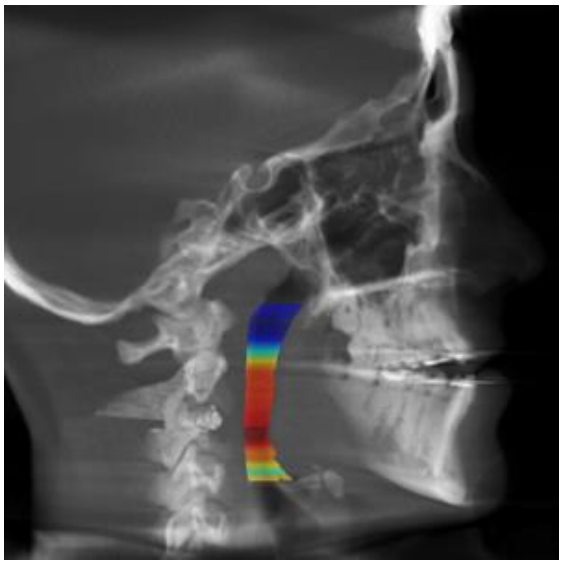

Figure 1. Airway width on lateral cephalograms

Microsoft Excel 2019 was used to calculate and graphically display the parameters of interest in this study. The results are presented as charts, tables and diagrams, and are expressed as absolute numbers or percentages, with the level of statistical significance set at $p<0.05$.

Two previously calibrated investigators performed the measurements to ensure accuracy. The subjects' lateral cephalograms were calibrated to the same scale and printed, and on each image a line was drawn from the posterior contour of the soft palate to the closest point on the posterior pharyngeal wall to represent the upper pharyngeal airway; this tracing was performed by the first investigator using a ruler and a 0.30 mm lead pencil and then checked by the second investigator to verify the accuracy of the anatomic contour identification and landmark placement.

RESULTS

All subjects were diagnosed with skeletal Class II malocclusion, with ANB angle values greater than 2°. The study sample included 52 subjects, of whom 25 (41.66%) were male and 27 (58.34%) were female ($p=0.414$, $\chi^2=0.66$) (Figure 2). The sample was divided into two groups: Group 1, comprising 41.66% of the subjects, with skeletal Class II malocclusion and a normodivergent growth pattern, and Group 2, comprising 58.34% of the subjects, with skeletal Class II malocclusion and a hyperdivergent growth pattern (Figure 3).

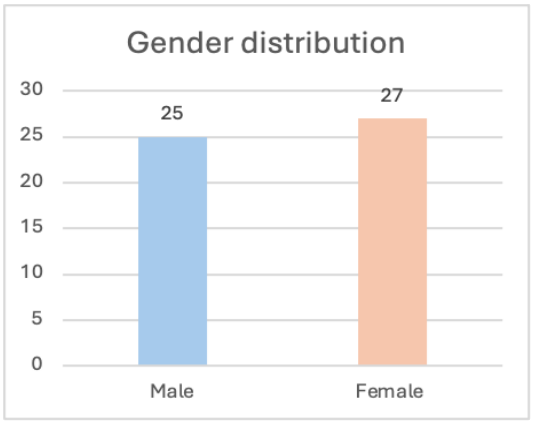

Figure 2. Distribution of the study sample by gender

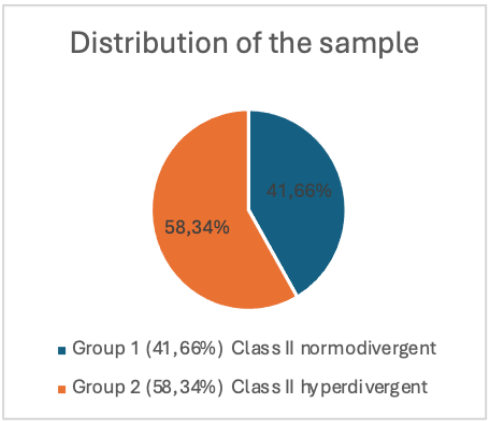

Figure 3. Distribution of the study sample by group

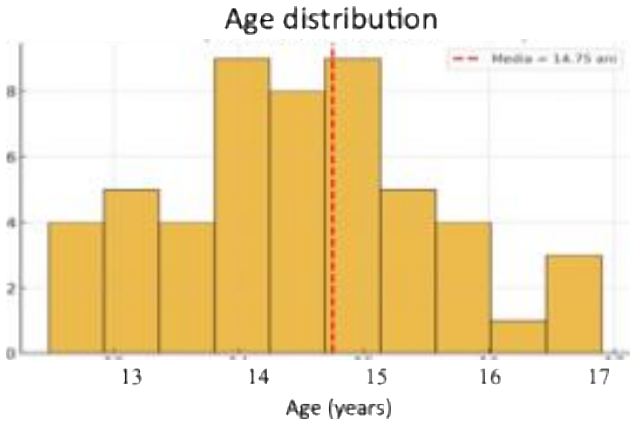

Figure 4. Age distribution of the study groups

The mean age of the total sample was 14.75 ± 1.16 years (Figure 4), with a minimum age of 13 years and a maximum age of 17 years. In Group 1, the mean age was 13.8 years, ranging from 13 to 15 years, with a median of 14 years, whereas in Group 2 the mean age was 15 years, ranging from 14 to 17 years, with a median of 15 years (Table I).

Table I. Statistical analysis of the study groups according to age

	Total group n=52	**Group 1 n=25**	**Group 2 n=27**
Minimum	13	13	14
Maximum	17	15	17
Mean	14,5	13,8	15
Standard deviation	1,16	0,83	1,15
Median	14	14	15

The subjects in Group 1 presented a mean ANB angle of 6.02°, whereas those in Group 2 had a mean ANB angle of 5. 81°.The three cephalometric variables measured on lateral cephalograms—FMA, SN-GoGn, and NS-Gn—were used to differentiate between normodivergent and hyperdivergent vertical growth patterns. FMA represents the angle between the Frankfurt horizontal plane (Po–Or) and the mandibular plane, reflecting the vertical skeletal pattern, with a normal value of 25° ± 3°. In the normodivergent group, all FMA values fall within the normal range, whereas among hyperdivergent subjects, only a small proportion show normal values, with most exceeding the upper limit of 28°.

The SN-GoGn angle represents the relationship between the mandibular plane and the cranial base, with a normal value of approximately 33°. In the normodivergent group, the values are close to this reference, with increases of up to about 4°. In contrast, the hyperdivergent group shows markedly elevated values, in some cases exceeding the normal limit by more than 9°.

NS-Gn is the angle formed by the lines connecting Nasion, Sella, and Gnathion, reflecting both the vertical and anteroposterior growth of the mandible; its normal value is around 67°. Subjects in the normodivergent group present values near this norm, whereas those in the hyperdivergent group display increases reaching 72–74°, exceeding the upper limit by more than 7°.

The values of the ANB angle—defined by points S, N, and A and used to reflect the sagittal position of the maxilla—are also presented. The normal ANB value is approximately 2°; increased values indicate a skeletal Class II pattern, whereas reduced or negative values

suggest skeletal Class III. All patients in both groups show ANB values above 2°, confirming a skeletal Class II relationship, with mean values of 6.02° in Group 1 and 5.81° in Group 2.

In the lateral cephalograms of both groups, the upper pharyngeal airway was assessed as the linear distance between the posterior border of the soft palate and the nearest point on the posterior pharyngeal wall.

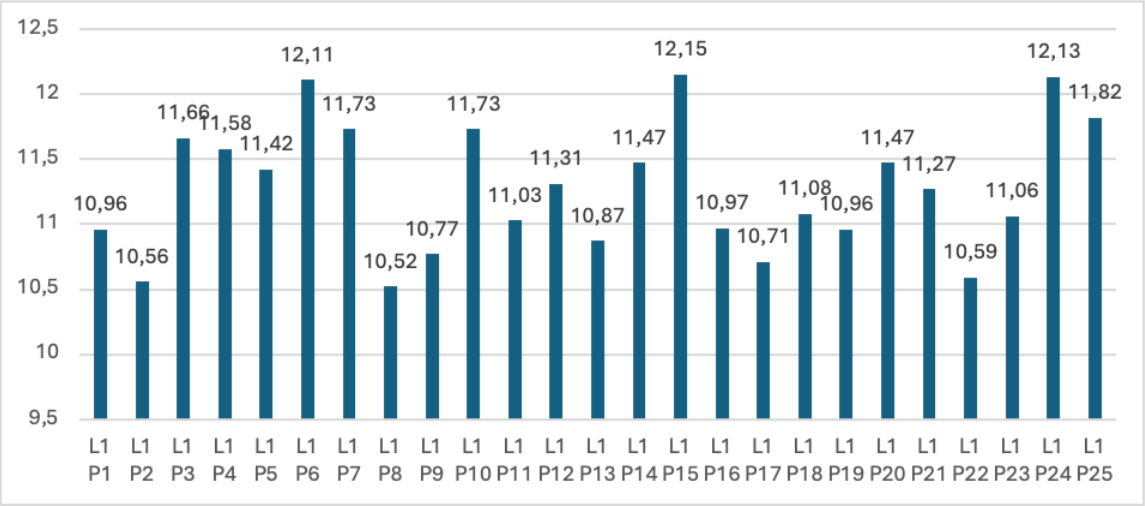

Figure 5. Upper pharyngeal airway measurement values for Group 1

The measurements showed that, in Group 1, the upper pharyngeal airway width ranged from a minimum of 10.50 mm to a maximum of 12.30 mm. The mean upper airway width in subjects with skeletal Class II and a normodivergent growth pattern was 11.28 ± 0.49 mm.

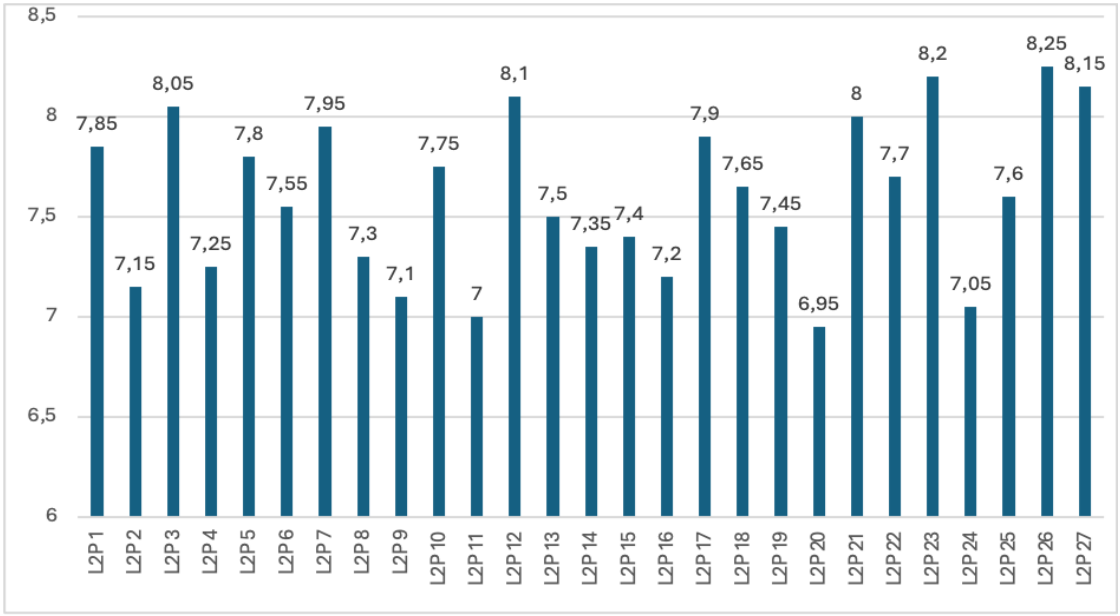

Figure 6. Upper pharyngeal airway measurement values for Group 2

In Group 2, comprising subjects with skeletal Class II and a hyperdivergent growth pattern, the mean upper pharyngeal airway width was 7.60 ± 0.40 mm, with a minimum value of 6.95 mm and a maximum value of 8.25 mm.

When comparing the groups, the mean length of the upper pharyngeal airway in Group 2 was 3.68 mm smaller than in Group 1 ($p<0.001$), indicating that subjects with skeletal Class II and a hyperdivergent growth pattern have significantly more constricted upper pharyngeal airways than those with skeletal Class II and a normodivergent growth pattern.

DISCUSSIONS

The selected lateral cephalograms belonged to subjects aged between 13 and 17 years, who already had a fully erupted permanent dentition but were still in the growth period. These patients had not received any orthodontic treatment with removable appliances during the mixed dentition phase. Some authors suggest that early intervention can reduce the severity of the anomaly or even prevent its occurrence. [10]. Early intervention may reduce the overall need for complex orthodontic treatment, such as permanent tooth extractions or orthognathic surgery. [11]. Furthermore, studies have shown a lower incidence of root resorption and ectopic eruptions when treatment is initiated during the mixed dentition stage. [12].

Although the number of subjects in each group may be considered relatively small, age and sex were well matched between groups. Owing to the retrospective design of the study, a direct assessment of each patient's nasal breathing pattern was not possible, so the selection criteria were based on information from the clinical records at the initial visits regarding pharyngeal pathology, clinical signs and symptoms, and complaints of nasal obstruction, any of which could have been related to adenoidal hypertrophy or enlarged tonsils [13]. The selected patients did not exhibit any of these factors and were therefore considered to have healthy pharyngeal function. This approach excluded patients with severe pathological pharyngeal obstruction, who would have shown some of the aforementioned signs and symptoms; however, it did not allow for the detection of mild or moderate pharyngeal obstructions. [14]. Nevertheless, because these selection criteria were applied to both groups, they were considered comparable. Consequently, since only relatively healthy pharyngeal patients with skeletal Class II malocclusion were included, the pharyngeal widths were expected to reflect solely their natural anatomic conditions, without pharyngeal pathology.

Subjects with Class II malocclusion and a vertical growth pattern presented significantly narrower upper pharyngeal airways than Class II subjects with a normodivergent growth pattern (Figure 5 and Figure 6), confirming previous findings reported in the literature. [15].

By analysing these results, it can be inferred that upper airway width is influenced by the craniofacial growth pattern, as previously suggested. However, some studies have reported weak correlations between growth pattern, facial morphology and nasopharyngeal airway dimensions, probably because they assessed the influence of the nasopharyngeal airway in conjunction with facial form and occlusion.

The present study was conducted on two dimensional radiographs to evaluate only the widths of the pharyngeal airways, not airflow capacity, which would require a more complex three dimensional and dynamic assessment; recent studies have indeed highlighted the value of three dimensional evaluation using magnetic resonance imaging [16] the high cost of this investigation and the lack of standardization of the patient's head position still limit the use of this method in research. According to Muto[17] a 10° change in craniofacial inclination can alter measurements in the upper airway region by approximately 4 mm. Lateral cephalograms were used for this type of assessment as part of the patients' orthodontic records, offering the advantages of low cost and low radiation dose, easy accessibility, and standardized measurements with high reproducibility for diagnostic

purpose [18]. These advantages make this method widely used in research, which supports the methodology adopted in the present study and allows comparison of the results.

The findings do not indicate that subjects with a vertical growth pattern have a lower respiratory flow than those with a normodivergent growth pattern. However, Ricketts [20] și Dunn [21] they observed that nasal obstruction leading to mouth breathing is related to the width of the nasopharynx; the narrower the nasopharyngeal space, the less adenoidal enlargement is required to obstruct the nasopharyngeal airway. This helps explain the higher prevalence of mouth breathing in subjects with vertical growth patterns. Paul și Nanda [22] observed that higher prevalences of mouth breathing and nasopharyngeal airway obstruction have been reported in subjects with Class II malocclusions. The present study included only patients without evident pharyngeal pathology, whereas other investigations have used randomly selected subjects; some contrasting studies have compared nasal breathers with mouth breathers and found a higher proportion of mouth breathers among Class II patients, who consequently had a narrower nasopharynx.

Class II malocclusion can affect patients' daily lives both aesthetically and functionally. One of the most common functional problems is inadequate airflow through the nasal cavities, which leads patients to use the oral cavity to compensate for the impaired nasal function; unfortunately, mouth breathing is considered a detrimental habit associated with two major consequences: reduced cerebral oxygenation and sleep disturbances. Due to chronic under oxygenation, patients experience persistent fatigue and poor concentration, which makes everyday activities more difficult, and in addition they cannot rest properly because sleep is interrupted by apneic episodes and xerostomia related to mouth breathing.

On some lateral cephalograms, an accentuation of the cervical spine curvature can be observed, supporting the findings of Nobili and Adversi, who demonstrated that subjects with Class II malocclusion present a forward displaced posture. These patients tend to tilt the head anteriorly, resulting in greater head extension relative to the vertebral column and, consequently, a more pronounced lordotic curvature of the spine. [24].

This study showed that, in Class II malocclusions without evident pharyngeal pathology, the nasopharyngeal airway is narrower in subjects with a hyperdivergent vertical growth pattern than in those with a neutral growth pattern. However, the prevalence of pharyngeal obstruction across different growth patterns and malocclusions was not evaluated and should be addressed in future studies.

CONCLUSIONS

Vertical growth patterns in the subjects can be defined using at least three correlated cephalometric measurements (FMA, SN-GoGn, and NS-Gn), because the FMA angle alone is insufficient for categorization, as some subjects in Group 2 with a hyperdivergent pattern still showed normal FMA values. Patients with Class II malocclusions and a hyperdivergent vertical growth pattern have significantly narrower upper pharyngeal airways than Class II patients with a neutral growth pattern.

The narrowing of the upper airway is attributed to altered mandibular rotation and maxillo mandibular discrepancy, with the mandible being retruded in most cases. Changes in upper airway width do not depend on the sagittal subdivision of skeletal Class II, but rather on the vertical growth pattern. nitiating orthodontic treatment would modify the cephalometric measurements and mandibular rotation, leading to a reshaping of the upper airway and an improvement in respiratory function.

Conflicts of Interest

The authors declare no conflict of interest.

REFERENCES

[1] Cenzato N, Nobili A, Maspero C. Prevalence of dental malocclusions in different geographical areas: scoping review. Dent J (Basel). 2021;9(10):117. doi:10.3390/dj9100117.

[2] Rathi S, Gilani R, Kamble R, Bhandwalkar S. Temporomandibular joint disorder and airway in Class II malocclusion: a review. Cureus. 2022;14(10):e30515. doi:10.7759/cureus.30515.

[3] Lombardo G, Vena F, Negri P, et al. Worldwide prevalence of malocclusion in the different stages of dentition: a systematic review and meta-analysis. Eur J Paediatr Dent. 2020;21(2):115-122. doi:10.23804/ejpd.2020.21.02.05.

[4] Lee JE, Jung CY, Kim Y, Kook YA, Ko Y, Park JB. Analysis of alveolar bone morphology of the maxillary central and lateral incisors with normal occlusion. Medicina (Kaunas). 2019;55(9):565. doi:10.3390/medicina55090565.

[5] Nowak M, Golec J, Wieczorek A, Golec P. Is there a correlation between dental occlusion, postural stability and selected gait parameters in adults? Int J Environ Res Public Health. 2023;20(2):1652. doi:10.3390/ijerph20021652.

[6] Yadav D, Rani MS, Shailaja A, Anand D, Sood N, & Gothi R. Angle's Molar Classification Revisited. Journal of Indian Orthodontic Society, 2014; 48, 382 – 387

[7] Caroccia F, Lopes C, Pipitone R, D'Addazio G, Moscagiuri F, D'Attilio M. Evaluation of Body Posture during Class II Functional Treatment with Fränkel II: A Longitudinal Study. Applied Sciences. 2022;12(17):8900.

[8] Shioya S & Arai K. Dentoskeletal morphology of adult Class II division 1 and 2 severe deep overbite malocclusions. Orthodontic Waves. 2017; 76. 10.1016/j.odw.2017.01.003.

[9] Ardani IGAW, Sanjaya ML, Sjamsudin J. Cephalometric Characteristic of Skeletal Class II Malocclusion in Javanese Population at Universitas Airlangga Dental Hospital. Contemp Clin Dent. 2018 Sep;9(Suppl 2):S342-S346. doi: 10.4103/ccd.ccd_465_18. PMID: 30294169; PMCID: PMC6169297.

[10] Sencak RC, Benavides E, Cevidanes L, Yatabe M, Koerich L, Souki BQ, Ruellas ACO. Asymmetry in Class II subdivision malocclusion: Assessment based on 3D surface models. Orthod Craniofac Res. 2024 Apr;27(2):267-275. doi: 10.1111/ocr.12723. Epub 2023 Oct 26. PMID: 37882502.

[11] Candida E, Grippaudo FR, Romeo C, Tauro R, Blasi A and Grippaudo C. 3D Facial Analysis in Class II Subdivision Malocclusion. The open dentistry journal. 2022, DOI: 10.2174/18742106-v16-e2110281

[12] Akın M, İleri Z, Polat O, Başçiftçi FA. Evaluation of mandibular asymmetry in class II subdivision malocclusion. Selcuk Dental Journal, 2015; 2: 43-50

[13] Feres MFN, Eissa O, Roscoe MG, El-Bialy T. Comparison of the Condyle Sagittal Position of Class I and Class II Division 2 in Orthodontic Patients. J Contemp Dent Pract. 2020 Sep 1;21(9):977-981. PMID: 33568581.

[14] Di Giacomo P, Ferrara V, Accivile E, Ferrato G, Polimeni A, Di Paolo C. Relationship between Cervical Spine and Skeletal Class II in Subjects with and without Temporomandibular Disorders. Pain Res Manag. 2018 Oct 16;2018:4286796. doi: 10.1155/2018/4286796. PMID: 30410638; PMCID: PMC6206553.

[15] Paul D, Varma S, Ajith VV. Airway in Class I and Class II skeletal pattern: A computed tomography study. Contemp Clin Dent. 2015 Jul-Sep;6(3):293-8. doi: 10.4103/0976-237X.161856. PMID: 26321823; PMCID: PMC4549975.

[16] Aditya T, Jayesh SR, Sanket A, Sonali D, Ravindra M. Relationship between extended head posture and malocclusion. Indian Journal of Orthodontics and Dentofacial Research, January-March, 2018;4(1):35-40. doi: 10.18231/2455-6785.2018.0007

[17] Alsheikho HO, Jomah DH, Younes M, Tizini M, Hassan H, Khalil F. Evaluation of head and cervical spine posture after functional therapy with Twin-Block and Bionator appliances: A pilot randomized controlled trial. Cranio. 2024 Jan;42(1):102-111. doi: 10.1080/08869634.2021.1909455. Epub 2021 Apr 11. PMID: 33843477.

[18] Malik N, Fernandes BA, Ramamurthy PH, Anjum S, Prakash A, Sinha A. Cephalometric evaluation of the cervical spine posture following fixed functional therapy with Forsus™ appliance. J Indian Soc Pedod Prev Dent. 2022 Jan-Mar;40(1):81-85. doi: 10.4103/jisppd.jisppd_173_21. PMID: 35439888.

[19] Farronato G, Rosso G, Giannini L, Galbiati G, Maspero C. Correlation between skeletal Class II and temporomandibular joint disorders: a literature review. Minerva Stomatol. 2016 Aug;65(4):239-47. Epub 2016 Mar 3. PMID: 26938175.

[20] Silva NN, Lacerda RH, Silva AW, Ramos TB. Assessment of upper airways measurements in patients with mandibular skeletal Class II malocclusion. Dental Press J Orthod. 2015 Oct;20(5):86-93. doi: 10.1590/2177-6709.20.5.086-093.oar. PMID: 26560826; PMCID: PMC4644924.

[21] Pothuri A Sr, Pj M, N L, N M, Chinnapan V. New Trend in Treating Class II Division 2 Subdivision: A Case Report. Cureus. 2023 Oct 19;15(10):e47353. doi: 10.7759/cureus.47353. PMID: 38022208; PMCID: PMC10657339

[22] Jadhav PJ, Sonawane SV, Mahajan N, Chavan BG, Korde SJ, Momin NM, Mahale PR. Correlation of Pharyngeal Airway Dimensions with Maxillomandibular Skeletal Relation and Mandibular Morphology in Subjects with Skeletal Class I and Class II Malocclusions and Different Growth Patterns: A Cephalometric Study in Selected Local Population. J Pharm Bioallied Sci. 2021 Nov;13(Suppl 2):S1111-S1114. doi: 10.4103/jpbs.jpbs_349_21. Epub 2021 Nov 10. PMID: 35017940; PMCID: PMC8686866.

[23] Sana S, Kondody RT, Swamy K, Fatima A. Evaluation and Correlation Between Pharyngeal Space, Mandible, and Tongue in Two Different Facial Patterns. Journal of Indian Orthodontic Society. 2022;56(4):351-358. doi:10.1177/03015742221083065

[24] Koletsi D, Makou M, Pandis N. Effect of orthodontic management and orofacial muscle training protocols on the correction of myofunctional and myoskeletal problems in developing dentition. A systematic review and meta-analysis. Orthod Craniofac Res. 2018; 21: 202–215. https://doi.org/10.1111/ocr.12240